Bio-mineral processing of carbonaceous refractory gold ore applying fungal enzymes

コジョ, トワム, コナドウ

https://doi.org/10.15017/2534420

出版情報：Kyushu University, 2019, 博士（工学）, 課程博士
バージョン：
権利関係：

九州大学
KYUSHU UNIVERSITY

Bio-mineral processing of carbonaceous refractory gold ore applying fungal enzymes

By

Kojo Twum KONADU

A thesis submitted to Kyushu University
for the degree of Doctor of Engineering

Department of Earth Resources Engineering
Graduate School of Engineering
Kyushu University
Fukuoka, Japan

September 2019

Abstract

The bio-treatment of carbonaceous matter in double refractory gold ores (DRGO) is one of the most environmentally safe beneficiation routes for improving gold recovery. As a result, many bacterial and fungal species have been studied for their potential application to the gold ore on an industrial scale. A white-rot fungus, *Phanerochaete chrysosporium*, is one of these microbes, and its carbonaceous matter decomposition ability is due to the secretion of extracellular lignin-degrading enzymes. While fungal enzymes have been applied to water treatment in the pulp industry, it has never been successfully utilized for solid substrates in any industry. Several attempts have been made to apply this fungus to the treatment of DRGO in the past 3 decades. In most cases when the real ore was used, the characterization of the effectiveness of the fungus was based only on the gold recovery rather than direct analysis of the carbonaceous matter transformation. Therefore, to improve the understanding of the carbonaceous matter transformation, the cell-free spent medium (CFSM) of *P. chrysosporium* was used to treat DRGO sequentially, and the alteration in the carbonaceous matter is elucidated in this thesis.

It was important to determine the effectiveness of the CFSM as an oxidant for the carbonaceous matter in the DRGO. As such, powdered activated carbon (PAC) was used as a surrogate due to its graphitic structure during the CFSM treatment in **Chapter 3**. It was found that the CFSM treatment decomposed the aromatic C=C bonds in the PAC (confirmed by solid ^{13}C-NMR), which resulted in decreases in the specific surface area and formation of large micron-sized pores on the bio-treated PAC. Additionally, some of the bio-molecules, secreted by the fungus into the CFSM, passivated the surface of the treated PAC and thus increased the surface negativity. Due to these factors, the gold uptake decreased significantly, implying that the CFSM treatment degraded the aromatic carbon as a solid substrate.

In **Chapter 4**, the sequential bio-treatment of the DRGO by sulfide oxidation using a thermophilic archaeon followed by enzymatic degradation of the carbonaceous matter was investigated using a combination of water chemistry, QEMSCAN, TG-DTA, SEM, DNA extraction and cyanidation. When the DRGO was pre-treated by bio-oxidation of sulfides with *Acidianus brierleyi* (DA) and only CFSM (DC), the gold recovery was improved from 24% to 77% and 38%, respectively. This was due to the inability of the CFSM to effectively breakdown the sulfides, which were the major gold-bearing minerals. When sulfide oxidation using *A. brierleyi* was followed by carbonaceous matter degradation using the CFSM (DAC) and vice versa (DCA), the gold recovery was 76% and 45%, respectively. The DCA sequence was judged to have been unsuccessful. The DAC sequence, on the other hand, showed that the CFSM treatment had converted the carbonaceous matter into an alkaline soluble substance which could be removed by washing. After 1 M NaOH washing, the gold recovery for DAC was 92% while 60% was observed for DCA. This result indicates that the sequence utilizing the iron-oxidizing microbe before the CFSM was the ideal way to pre-treat the DRGO.

The transformation of the carbonaceous matter during the DAC sequence was investigated using QEMSCAN analysis, Raman spectroscopy and three-dimensional fluorescence spectroscopy in **Chapter 5**. The results show that the carbonaceous matter was initially hosted in illite and the amount of carbon relative to the amount of illite affected the texture of the carbonaceous illite mineral. The enzymatic decomposition of the carbonaceous matter was found to be accelerated in the DRGO if the sample had undergone a prior treatment to decompose Fe sulfides and arsenopyrite. This is because the enzymes are susceptible to arsenic poisoning and therefore, the oxidative dissolution of arsenopyrite aided the enzymatic reaction. The lignin-degrading enzymes preferentially attacked the defects in the graphitic structure of carbonaceous matter and in the process, produced humic-like substances. The humic-like substances that are produced by the CFSM treatment acted as one of the binding agents in the

agglomeration of the carbonaceous aluminosilicate residue (C-Si-Al). This new C-Si-Al appeared to be the main product of the carbonaceous illite decomposition, and its retention of the humic substances explains why the alkaline washing step was needed to improve gold recovery from DAC from 76% to 92%.

In **Chapter 6**, a preliminary investigation was conducted to determine if enzymatic treatment would be viable for carbonaceous base metal ores like copper or nickel sulfides. Such a beneficiation route would involve having to decompose the carbonaceous matter before the copper or nickel recovery. This means that the DCA sequence would have to be considered and in **Chapter 4**, it was found to be ineffective due to the possible inhibition of *A. brierleyi*. Therefore, it was necessary to determine the leading cause of *A. brierleyi* inhibition after the CFSM treatment. The three main impediments that were identified after the CFSM only treatment were humic-like substances from the decomposition of the carbonaceous illite, biomolecules like carbohydrates and organic acids which aided in the formation of biofilms and large agglomerates, and finally, the fungal biomass. Washing the CFSM-treated solids with 1 M HCl and 1 M NaOH removed biofilms, broke down the aggregates and extracted the humic acids, but sulfide oxidation by *A. brierleyi* was still impeded. Therefore, it was concluded that the fungal biomass itself was the main impediments, and its negative effect became prominent if it made up more than 1wt% of the ore. Based on this information, the application of the *A. brierleyi* to the CFSM-treated carbonaceous base metal ore would not be successful without first reducing the amount of fungal biomass significantly.

In the **Chapter 7**, this work is summarized.

Table of Content

List of Tables

List of Figures

Chapter 1:

Introduction

1.1. Gold ore mineralogy

Gold is a precious metal that has played a significant part in human history for about 6500 years (Higham et al., 2007). It has been used for jewelry (Drost, and Hausselt, 2013), medicinal purposes (Pricker, 1996), monetary policy (Eichengreen, and Fetters, 1991), and material sciences (Akbarian et al., 1996; Bond 2002; Goodman, 2002; Corti et al., 2002; Corti and Holiday 2004). The significant sources of gold can be classified as either primary or secondary ores based on how they are formed; naturally or anthropological activities (Marden and House, 2006; Cui and Zhang, 2008). Primary gold ores are available in several mining regions around the world, and between 2010 and 2018, it accounted for approximately 69.5% of gold production (Goldhub, 2019). These primary ores are found in geographically, and geologically diverse regions of the world and its successful processing is reliant on understanding the composition and mineral interactions in the ore (Marden and House, 2006).

Primary ores can be classified based on the ease of recovery and mineralogy into placers, free-milling, oxide ore, sulfide ore (iron sulfide, arsenic sulfide, copper sulfide and antimony sulfide), tellurides and carbonaceous ores (Cook and Chryssoulis, 1990; Southam and Beveridge, 1994; Deschenes and Prud'homme, 1997; Marsden and House, 2006). The amount of gold in these sample exists at ppm concentration regions, and therefore, the smaller mass gold can usually be found in a larger mass of some other minerals. As such, the gold-mineral interactions and how these minerals respond to the beneficiation method can significantly affect the gold yield. Due to the effect of gold-mineral interactions on recovery, primary ores can be further classified into three main groups based on the degree of difficulty encountered during the beneficiation process.

1.1.1. Placers and Free milling ores

The processing of placer and free milling ores yield a very high gold recovery. Placer deposits are remarkably easy to process because the gold exists in a very liberated state within the mineral matrix (**Fig 1.1c**). It can be formed from wreathing and natural gravity concentration mechanisms (Henley and Adams, 1979; Southam and Beveridge, 1994). As a result of the ore formation mechanism, only a few washing and concentration steps are required to adequately liberate the precious metal (Marsden and House, 2006).

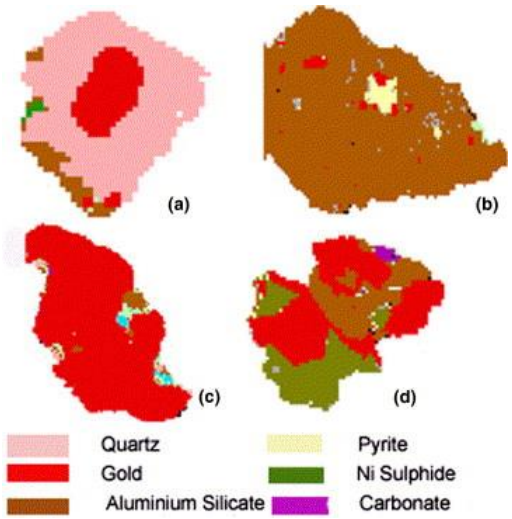

Figure 1. 1 Gold associations in ORE 1 by trace mineral search (TMS) analysis: (a) gold inclusion in quartz, (b) gold and pyrite inclusions in Al silicates, (c) liberated gold particle and (d) gold associated with aluminium silicates and Ni sulfides (Goodall et al., 2005).

Free milling gold ores have a lesser degree of gold liberation compared to placer deposits (**Fig 1.1a**). This particular classification often applies to gold hosted by oxide minerals like silicates, whereby the introduction of a comminution step is often necessary to ensure significant recovery. This ore type can be formed from the amalgamation and metamorphosis of placer deposits or weathering of sulfide ores (La Brooy et al., 1994; Marsden and House, 2006). The stresses and cracks generated by the size reduction process increase the liberations

of the gold, which in turn ensures a high recovery. Ore bodies with this characteristic can be found in several mining regions including Witwatersrand (South Africa), Jacobina (Brazil) and Tarkwa (Ghana). Typically, gold recovery of between 90-100% can be attained for placer and free milling ores with this mineralogy (La Brooy et al., 1994).

1.1.2. Refractory gold ores

Refractory gold ores (RGO) are widely distributed in the world and can be found in several gold mining areas such as, the Prestea, Tarkwa and Ashanti goldfields of Ghana, Sao Bento Mineracao in Brazil, Carlin Gold Mine and California mother lode in USA, Kerr Addison Mines in Canada, Bakyrchik mine in Kazakhstan, Natalkinsk mine in Russia, Shaanxi in China and the Ratatotok district, North Sulawesi in Indonesia, Macraes in New Zealand, Paddington in Western Australia, Stawell in Eastern Australia, Betze-Post in US, Jundee in Western Australia, Penjom in Malaysia (Osseo-Asare et al., 1984; Abotsi and Osseo-Asare, 1986; Afenya, 1991; Turner et al., 1994; Miller et al., 2005; Marsden and House, 2006; Yang et al., 2013). The degree of refractory behavior varies due to the mineralogical composition of the ore, the location of the gold relative to the other gangue minerals and gold recovery. The effect of the ore mineralogy and the gold location on refractoriness will be explained further in the next section on sulfide minerals and carbonaceous gold ores. Generally, gold ores can be grouped into mildly (80-90% recovery) to highly (≤50% recovery) refractory gold ores (La Brooy et al., 1994). The poor leaching efficiency can be attributed to the presence of sulfides and carbonaceous matter (CM) in gold ore matrix.

1.1.2.1. Sulfide minerals

Sulfide minerals can decrease the leaching efficiency of the ore through a number of ways,

two of them are encapsulation of the gold ore and excessive consumption of reagents. Two most common sulfide minerals associated with gold in sulfide ores are arsenian pyrite and arsenopyrite (Fleet and Mumin, 1997; Simon et al., 1999; Chen et al., 2002; Reich et al., 2005; Paktunc et al., 2006). The gold can exist in the iron sulfide in two states as either sub-micron Au(0) inclusions or a chemically bonded Au(I). Simon et al., (1999) reported that the grain size of arsenian pyrite affected the chemical state of the gold, the coarser grains had more of the chemically bonded Au(I) while the finer-grained arsenian pyrite was much more associated with Au(0). Due to the relative stability of pyrite and arsenopyrite in cyanide solution (Sanchez and Hiskey, 1988; Liu and Yen, 1995), the physical location of the imbedded sub-micron sized Au(0) is a dominant factor for determining the ore's refractoriness (Marden and House, 2006). On the other hand, gold resources with a significant amount of chemically bonded Au(I) would be very refractory in spite of the location.

Copper – gold deposits can serve as ores for either gold only or both metals depending on the grade of each metal in the deposit. A trace metal search (TMS) analysis of a sulfidic ore showed that some of the gold was distributed between chalcopyrite, Zn sulfide and Fe oxide (**Fig. 1.2**). Chalcopyrite and some other copper sulfides are unstable in cyanide solution and rapidly dissolves into solution upon interacting with the free cyanide to form various stable complexes ($Cu[CN]_2^-$, $Cu[CN]_3^{2-}$, $Cu[CN]_4^{3-}$) (Marden and House, 2006). This greatly reduces the availability of free cyanide for the complexation of gold. Thus, the required cyanide concentration for gold leaching has to be increased significantly to accommodate the losses. Also, the stability of these copper cyanide complexes in the aqueous phase increases the amount of wasted cyanide discharged from the mine. In cases where the cyanide level is above the accepted environmental safety limit, an additional cyanide treatment process will have to be incorporated into the beneficiation route (Dai et al., 2012). This will further increase the cost of the entire process. In summary, the sulfide minerals can decrease the gold recovery through

encapsulation or excessive reagent consumption.

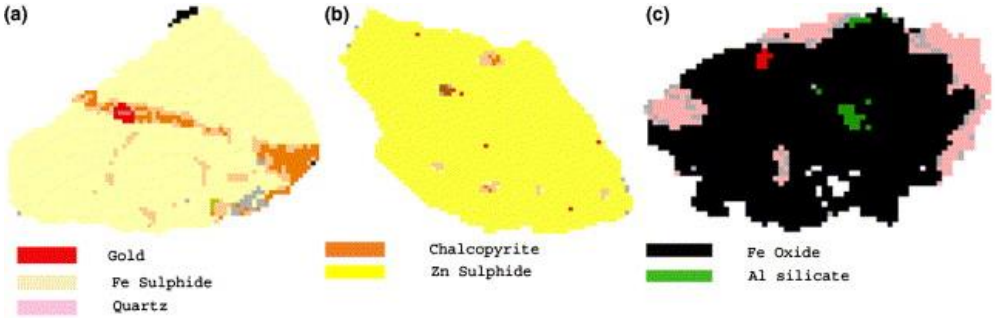

Figure 1. 2 Gold associations in ORE 2 by TMS (a) gold particle in chalcopyrite vein in an Fe sulfide, (b) fine gold association in Zn sulfide and (c) gold inclusion in Fe oxide. Pixel size = 2 μm (Goodall et al., 2005).

1.1.2.2. Carbonaceous gold ores

The carbonaceous matter in gold ores includes aliphatic hydrocarbons, carbonate minerals, humic acids and elemental carbon (Abtosi and Osseo-Asare, 1986; Stenebraten et al., 1999). Out of these substances, the most troublesome are humic acids and elemental carbon because they have displayed the ability to adsorb gold from solution during leaching, leading to recovery losses. The ratio of humic acids to elemental carbon varies from deposit to deposit, although it has been reported that elemental carbon is the most prominent part of the carbonaceous matter found within the Prestea deposit (Abosti and Osseo-Asare, 1986; Afenya, 1991). Humic acids have been proposed to adsorb gold through three possible mechanisms of complexation, ionic interactions and colloidal reactions (Baker, 1978; Wood 1996). However, there is some disagreement about the exact mechanism of Au-humic acid interaction owing to the heterogeneity and insufficient characterization of humic substances (Wood 1996). Elemental carbon exists in a highly disseminated state within the ore, having a particle size distribution ≤ 2 μm (Afenya, 1991). It is able to adsorb aurocyanide through the following

proposed mechanisms, which are strong π- π interactions between the orbitals of the aromatic rings (activated carbon) and $Au(CN)_2^-$ (aurocyanide), ion-pair mechanism and ion exchange (Adams and Fleming, 1989; Adams, 1990; Ibrado and Fuerstenau, 1992; 1995; Yin et al., 2014). The affinity of the elemental carbon for aurocyanide is most likely due to its structural similarities to activated carbon and coal (Abosti and Osseo-Asare, 1986; Afenya, 1991).

Extraction and characterization of the elemental carbon have shown that this is primarily composed of aromatic rings. The organization of these rings gives it the mixed amorphous and crystalline carbon graphite-like phases (Franklin, 1951; Abosti and Osseo-Asare, 1986; Schmalz et al., 1988; Afenya, 1991; Lastoskie et al., 1993; Harris, 2013). The structure of the elemental carbon suggests that it may have been synthesized through a similar process to the coal formation. The problem with having elemental carbon in the ore is its aurocyanide sorption as shown by, Ibrado and Fuerstenau (1992), who determined the gold uptake ability of carbonaceous matter from several sources as a function of their maturity, oxygen content, surface acidic function groups and aromaticity. They found that the higher gold uptakes were observed for the anthracite coals than the lignite and subbituminous coals due to the lower oxygen containing functional groups in anthracite coals and thus ensuring that it had a higher aromaticity. However, this trend of higher maturity leading to higher aurocyanide adsorption did not hold true graphite because the transformation from anthracite to graphite significantly improves the structure and regularity of the graphitic layers, leading to a significant decrease in surface available for adsorption (Ibrado and Fuerstenau, 1992; Tan et al., 2005).

This finding follows a similar trend to the behavior of elemental carbon during the industrial processing carbonaceous ores. Unfortunately, the removal of the $Au(CN)_2^-$ from solution counts as a loss because it is usually not recovered again from the bulky ore (**Fig 1.3**). This unwanted uptake of the $Au(CN)_2^-$ by the elemental carbon in the carbonaceous ore is referred

to as “preg-robbing”. The phenomenon is the reason why carbonaceous ores are categorized with sulfide ores into refractory gold ores. Under some circumstances, some ore bodies have both the problematic sulfide minerals and elementary carbon. This ore type is classified as a double refractory gold ore (DRGO), and a pre-cyanidation step is necessary for gold processing (Marsden and House, 2006). The pre-cyanidation treatments used have evolved, and some of them are discussed below.

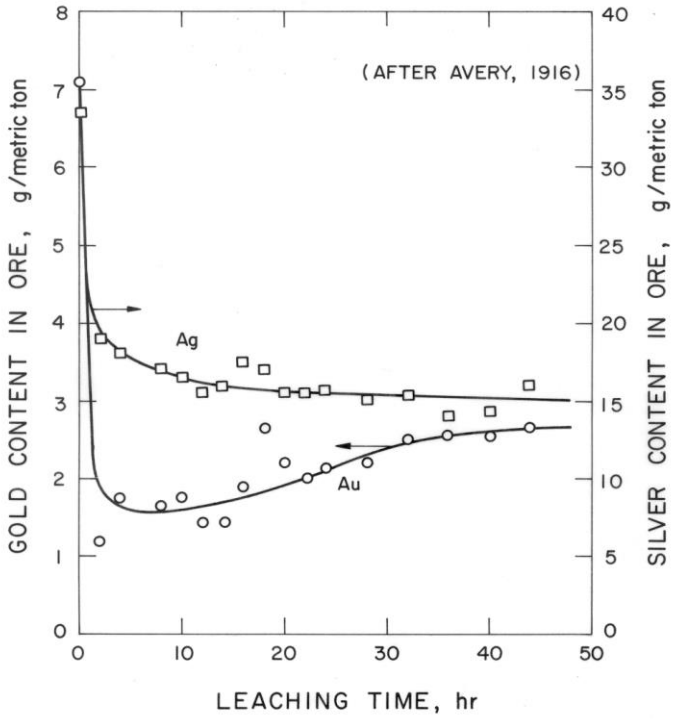

Figure 1. 3 Preg-robbing of gold by a double refractory gold-silver ore (Osseo-Asare et al., 1984).

1.2. Pre-treatment of DRGO

Improving the gold recovery of DRGO can be attained by instituting thermal, chemical or biological pre-treatment before leaching (**Fig. 1.4**). Each processing method has some advantages and drawbacks with respect to DRGO treatment. Thus the selection of a method

must take into account the environmental and economic aspects of the process (Marden and House, 2016).

1.2.1. Thermal pre-treatment

Roasting involves the use of extremely high temperatures for the oxidation of sulfide minerals and carbonaceous matter in all gold ores with refractory components. The working temperature for this method ranges between 600ºC and 800ºC, and it can be accomplished through a traditional oven or by microwave assisted roasting (Haque, 1999; Marsden and House 2006; Nanthakumar et al., 2007; Amankwah and Pickles, 2009). The advantage of the microwave assisted roasting over the conventional roasting is the ability to selective heat the target substance and thus decreasing the energy input (Haque, 1999). This technology would ultimately allow for the processing of low grade using this route. However, the two roasting methods can cause some significant environmental problems through the production of very toxic flue gasses (SO_2 and CO_2) as by-products of sulfide and carbonaceous matter oxidation (Marden and House, 2006) (**Fig 1.4**). In summary, the environmental risks associated with thermal pre-treatment make this process difficult to use effectively.

1.2.2. Chemical pre-treatment

A second option for pre-treatment is the use of aqueous or organic chemical agents under various conditions of pressure and temperature on DRGO. The use of aqueous oxidizing agents has been shown to primarily target sulfide minerals in the ore, leaving behind the more stable carbonaceous matter (Afenya, 1991) (**Fig 1.4**). Some of the aqueous treatments are pressure oxidation (acidic and alkaline), chlorination and nitric acid oxidation (Marsden and House, 2006). Out of these, autoclave pre-treatment is very popular for industrial processing because

of the heightened pressure and temperature aid in relatively fast oxidation of the sulfides (Thomas, 2005). The residual carbonaceous matter in the autoclave product would then have to be either removed or inactivated before recovering the gold.

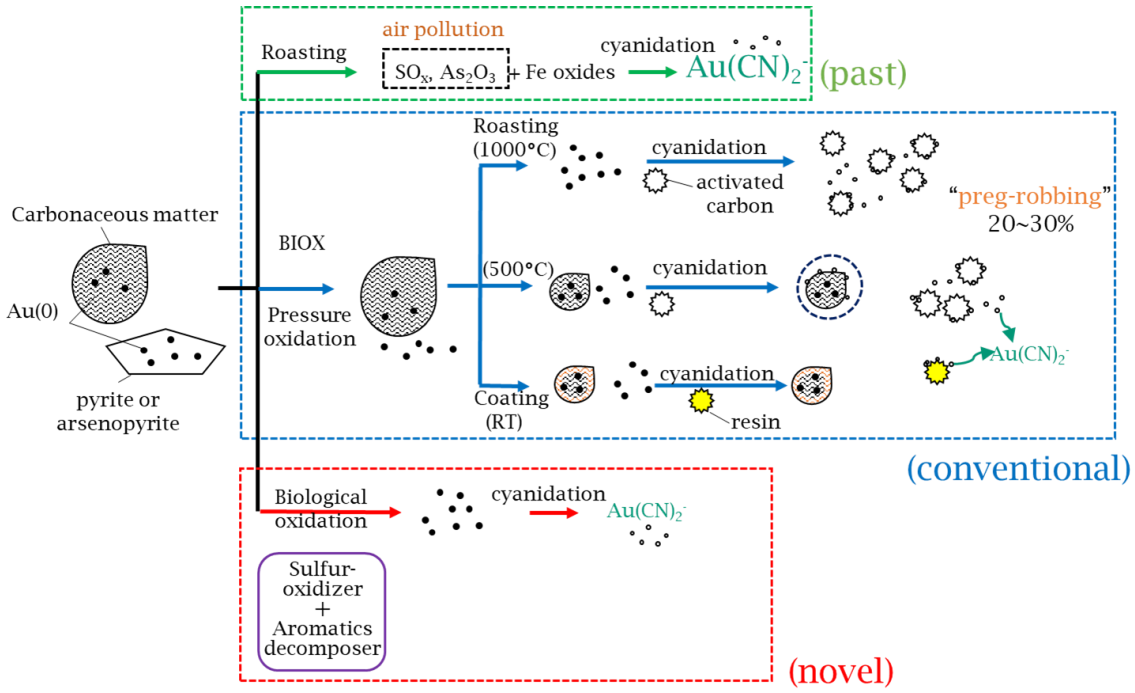

Figure 1. 4 Schematic illustration of past, conventional and the proposed processes for double refractory gold ores (DRGO).

Due to the lack of response by the carbonaceous matter to pressure oxidation and other aqueous treatment, some organic compounds have been used to inhibit preg-robbing (Abotsi, and Osseo-Asare, 1987). This is achieved by; 1) reducing the specific surface area of the carbonaceous matter though blanking with kerosene and machine oil (Ramli and Osman, 2015) or 2) making the ore surface more negatively charged by treating with anionic surfactant (Sodium dodecyl sulfate, SDS and dinonylnaphthalenesulfonic acid, HDNNS) to cause increased repulsion between the solid and the negatively charged $Au(CN)_2^-$ ion (Abotsi, and Osseo-Asare, 1987). However, these surfactants could be transferred to the activated carbon during the cyanidation process, resulting in carbon fouling. A solution to this problem is using

the resin-in-leach (RIL) instead of the traditional carbon-in-leach (CIL) process (Marden and House, 2006; Ramli and Osman, 2015). The RIL process is based on the selective recovery of the $Au(CN)_2^-$ complex from other cyano-complexes of base metals, however, the selectivity of these resins for gold is determined by configuration and distribution of the active groups, and the hydrophobicity of the resin matrix (Riveros, 1993). Thus, the selectivity and cost of the resin can affect the resin loading, unlike the CIL process whereby the activated carbon is produced from cheaper materials (Ioannidou and Zabaniotou, 2007). Despite this, the application of pressure oxidation and RIL processes is one of the ways to improve gold recovery from DRGO.

1.2.3. Biological pre-treatment

Microbial life has diverse structures and functions which make it one of the best avenues for the pre-treatment of DGRO (Bumpus et al., 1985; Lindström, et al., 1992; Bosecker, 1997; Olson et al., 2003; Brierley, 2003; Rawlings, 2013). The use of biological life for mineral processing and particularly, bio-oxidation has gained a significant amount of attention lately due to the continual discovery of beneficial microbes.

Bacterial oxidation (BIOX) is gradually becoming an established part of the beneficiation of sulfide gold ore (Olson et al., 2003) and there currently exist more than 10 operational plants using this technology (**Fig. 1.4**). This procedure is based on the oxidation of sulfur by *Thiobacilius thiooxidans* and iron by *Thiobacilius ferrooxidans* and *Leptospirillum ferrooxidans* at moderate temperature (35°C-45°C) and very acidic conditions (Marsden and House, 2006). These microbes utilize direct and indirect contact mechanisms to break down sulfides, liberating the gold and thus ensuring a higher gold recovery (Amankwah et al., 2005). However, these acidophilic treatment leaves behind the carbonaceous matter mostly unaltered.

To aid the BIOX process in the oxidation carbonaceous matter, Amankwah et al., (2005) proposed the utilization of *Streptomyces setonii* to target and decompose the carbonaceous matter. Alternatively, the DRGO can be treated with anaerobic mixed cultures to convert the carbonaceous matter into methane and CO_2 (Čater et al., 2015). However, both approaches to carbonaceous matter treatment are slightly problematic because its implementation would necessitate a step-wise biological pre-treatment system for sulfides and carbonaceous matter, with the anaerobic system being much more expensive to put in place.

An alternative to the bacterial bio-oxidation is the use of fungal pre-treatment of DRGO. Several fungal species belonging to *Dikarya* subkingdom have shown the ability to produce oxidative enzymes and create an environment suitable for the decomposition of lignin polymers and sulfides (Fakoussa and Hofrichter, 1999, Ofori-Sarpong et al., 2011). As such, fungi in this classification have been used for the bio-treatment of several polycyclic aromatic hydrocarbons (PAH), a heading under which carbonaceous matter falls (Tien and Kirk, 1988). Furthermore, the oxidative conditions established by some of these fungi have been shown to aid in pyrite and arsenopyrite decomposition (Ofori-Sarpong et al., 2011). A deeper understanding of the fungal pre-treatment system and the enzymes involved are presented in the section below.

1.3. Fungal pre-treatment

Some fungal species primarily belonging to the *Basidiomycete* class have shown the ability to undertake a single step degradation of sulfide mineral and carbonaceous matter in DRGO (Ofori-sarpong et al., 2013a). The degradation was accomplished by secreting enzymes with some lignin oxidizing ability (Fakoussa and Hofrichter, 1999; Lange et al, 2013). This is interesting because lignin is the second most abundant natural polymer and it has shown a very resistance to oxidizing microbes. The stability of lignin is due to its relatively high

polymerization and complex 3D structure (Lange et al, 2013). The lignin degrading abilities of these fungi is important to the pre-treatment of DRGO for two reasons; 1) the elemental carbon in DRGO may have been formed from lignin-containing biomass precursors and as such, the lignin-degrading ability of these fungi can be transferred and applied to the carbonaceous matter and 2) dissolution of pyrite and arsenopyrite through a Fenton reaction (Matta et al., 2007). Some of the species that have been identified as producing enzyme include *Phanerochaete chrysosporium* (Tien and Kirk, 1983), *Ganoderma lucidum* (D'souza et al, 1999), *Trametes villosa* (Yaver et al., 1996), *Trametes versicolor* (Bourbonnais et al., 1995) and *Bjerkandera adusta* (Huang et al, 2013).

1.3.1. Phanerochaete chrysosporium

P. chrysosporium is a white rot fungus that can oxidize many polyaromatic hydrocarbons of varying structural and chemical complexity into relatively small compounds. The oxidation process serves a digestive function, i.e. it provides nutrients for the growth and development of the microbe (Pérez, et al., 2002). Consequently, *P. chrysosporium* has been used for the treatment of recalcitrant compounds such as lignin (Kirk and Farrell, 1987; Wariishi et al., 1991), discoloring dyes (Fu and Viraraghavan, 2001) and pre-treatment of carbonaceous refractory gold ores (Ofori-Sarpong et al, 2013a; Ofori-Sarpong et al, 2013b; Liu et.al 2016). To enable the breakdown of aromatic compounds, this fungus produces some digestive enzymes like lignin peroxidase (LiP), manganese peroxidase (MnP), versatile peroxidase (VP), laccase, glucose oxidase and glyoxal oxidase (Kelly and Reddy 1986; Kersten and Kirk, 1987; Kirk and Farrell, 1987; Tien, 1988; Wariishi et al., 1992; Rodriguez et at., 1997; Zeng et al., 2013; Coconi-linares et al., 2014). These biocatalysts accomplish the degradation of polyaromatic hydrocarbons through numerous pathways although they ultimately complement

each other. In summary, *P. chrysosporium* is an important part of the carbon cycle and this ability is dependent on producing enzymes.

1.3.2. Enzymes secreted by P. chrysosporium

Most of the enzymes produced by *P. chrysosporium* work synergistically to catalyze the degradation of polycyclic aromatic carbons. Despite having primarily oxidative characteristics, these biocatalysts' can separate into two groups as oxidase enzymes (laccase, glucose and glyoxal) and peroxidase enzymes (LiP, MnP and VP). The main difference of these between these two groups is their respective dependence oxygen and hydrogen peroxide for catalysis. The currently available structures and reaction pathways of these enzymes are discussed below. Firstly, the laccase enzymes use O_2 as an electron acceptor for the direct oxidation of its substrates (Enguita et al., 2003; Claus, 2004; Riva, 2006; Couto and Herrera, 2006). It accomplishes this through a Cu^{II}/Cu^{I} redox couple formed by the four copper atoms incorporated into the enzyme's active sites as depicted by **Fig. 1.5.** Secondly, O_2 is used by intracellular glucose oxidase and extracellular glyoxal oxidase are among some of the enzymes that manufacture of H_2O_2 to aid in the enzymatic reactions of the peroxidase enzymes (Leonowicz et al., 1999). Glucose oxidase is the more characterized of these two and its H_2O_2 production sequence is shown in **Fig. 1.6** (Magers and Tabb, 1981; Leonowicz et al., 1999)**.** Meanwhile, glyoxal oxidase uses methylglyoxal and glycoaldehyde instead of glucose as the substrate to synthesis H_2O_2 (Kersten and Kirk, 1987).

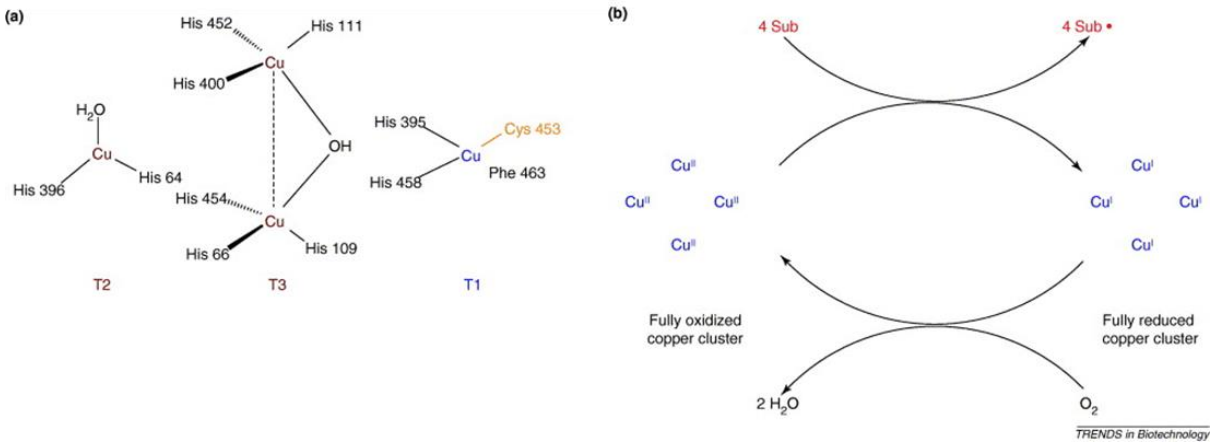

Figure 1. 5 The structure of active site of laccase showing a) the coordination of the copper ions (His- Histidine, and Cys-cysteine amino acids, T1, T2 and T3 refer to the different types of coordination between Cu atoms and amino acids) b) the oxidation of the substrates by the redox couple between CuII/CuI (Riva, 2006).

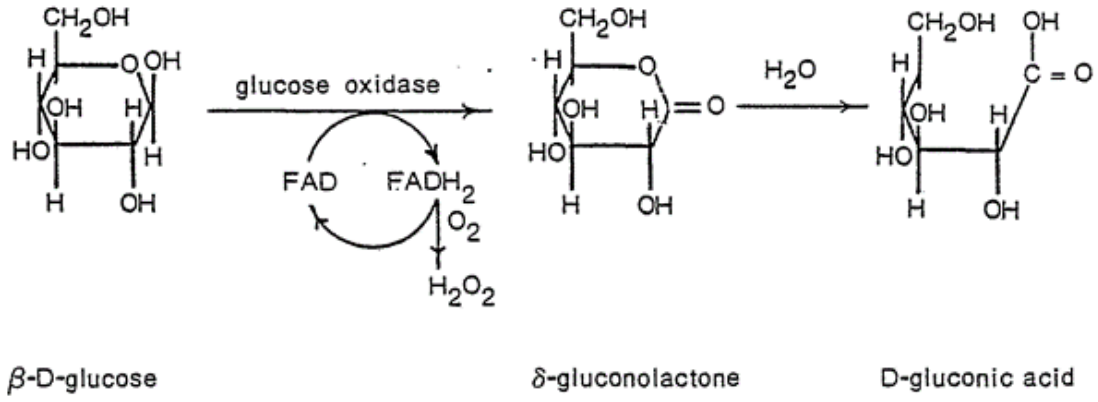

Figure 1. 6 Synthesis of hydrogen peroxide by glucose oxidase and FAD (flavin adenine dinucleotide) from glucose and oxygen (Magers and Tabb, 1981).

Finally, the peroxidase group enzymes (MnP, LiP and VP) use the biological or chemically synthesized H_2O_2 to initiate their catalytic cycles. The structures of these enzymes are shown in **Fig. 1.7 a-c**. For MnP and LiP, it has been observed that the spatial arrangement of amino

acids forms a channel to the active site of the enzyme and this channel is much smaller MnP (Camerero et al, 1999). As such, the resulting stereo-chemical stress in this area might prevent direct access to the active site by large aromatic compounds, and this might be the reason why MnP requires a co-factor (Mn^{3+}/Mn^{2+}) for its reactions. The third enzyme VP is so named because it possesses active sites similar in arrangement and function to both MnP and LiP (Coconi-Linares et.al., 2014). Thus, it has the advantage of being able to oxidize substrates of both enzymes. **Fig. 1. 7d** illustrates the importance of H_2O_2 in initiating the enzymatic reaction with the substrate. This diagram also shows that some peroxidase enzymes can undergo an oxidase cycle (using O_2 instead of H_2O_2); however, the peroxidase cycle is the predominant catalytic route (Berglund et al., 2002). In brief, *P. chrysosporium* produces a significant number of enzymes for its digestive operations, and because most of these are extracellular, it would be possible to design treatments using in vivo or in-vitro methods.

1.4. Objectives and outline of thesis

The bio-decomposition of carbonaceous matter with fungal and bacterial species have been applied over the past 3 decades to improve gold recovery from DRGO (**Table 1.1).** Neutrophilic carbonaceous matter decomposing bacteria and white-rot fungi species have been used alone or in conjunction with iron and sulfur-oxidizing microbes to achieve increased gold recoveries of ranging from 62% - 95% (Brierley and Kulpa, 1992; Amankwa et al.,2005; Yen et al., 2009; Ofori-Sarpong et al., 2013a; Liu et al., 2016). The carbonaceous matter degrading microbes usually employ oxidative enzymes to decompose their substrates and therefore reduce its preg-robbing ability (Pometto et al., 1981, Berglund et al., 2002; Amankwa et al.,2005; Ofori-Sarpong et al., 2010). While the mechanism of carbonaceous matter by fungal treatment

is generally known, knowledge about the transformation of the carbonaceous matter inside the gold ore is still lacking.

Firstly, the effect of the bio-treatment on the carbonaceous matter is usually evaluated based on gold recovery rather than direct characterization of the bio-treated residue (Amankwa et al.,2005; Yen et al., 2009; Ofori-Sarpong et al., 2013a; Liu et al., 2016). Liu et al. (2016) tried to solve this problem by extracting the carbonaceous matter, subjecting it to fungal treatment and then directly characterizing it but the extraction procedure used very strong acids which would have changed the properties of the extracted material compared to the initial material and thus affecting the biodegradation reaction. Therefore, directly analyzing the carbonaceous matter in it's in situ states and after bio-treatment would help improve the understanding of the fungal treatment.

Furthermore, studies about the fungal pre-treatment of DRGO have used the whole cell during the biodegradation reaction and while this has some advantages like 1) the continuous production of enzymes during the treatment period, 2) a relatively short period between inoculation and degradation (Liu et.al 2016), it also has some disadvantages. The significant demerits of using include formation of large agglomerates which might decrease affect the leaching reaction and also, the possible loss of $Au(CN)_2^-$ due to adsorption by the biomass using a similar mechanism to the uptake of Fe(III)-cyanide complexes by *Rhizopus arrhizus* under very alkaline conditions (Aksu et al., 1999; Chatterjee et al., 2010; Chen et al., 2011). Therefore, an investigation using the fungal cell-free spent medium containing the enzymes might be an alternative to the whole cell approach worth studying, and additionally, the absence of the fungal biomass might aid in the direct observation of the carbonaceous matter transformation.

Finally, the bio-treatment systems of DRGO that have used both a sulfide oxidizing bacteria and the fungal treatment have always proceeded with the sulfide decomposition occurring before the carbonaceous matter treatment (Brierley and Kulpa, 1992; Amankwa et al.,2005; Yen et al., 2009; Ofori-Sarpong et al., 2013a; Ofori-Sarpong et al., 2013b). However, it might be interesting to attempt this sequence with the fungal treatment preceding the sulfide decomposition treatment to evaluate its potential applicability to the DRGO sample.

Based on the above stated factors this study selected the in-vitro enzymatic treatment (CFSM) for the degradation of the carbonaceous matter in DRGO to improve gold recovery. The specific goals of this research are:

(1) The enzymatic decomposition of powdered activated carbon (PAC) as a surrogate for the carbonaceous matter in DRGO. The effect of the fungal treatment on the physical, chemical and $Au(CN)_2^-$ uptake ability of the PAC will be determined.

(2) The sequential decomposition of the carbonaceous matter and sulfides to improve gold recovery utilizing the iron oxidizer *Acidianus brierleyi* and the spent medium of the *P. chrysosporium*. The solid residue characterization will be conducted with QEMSCAN analysis and cyanidation was used to evaluate the efficiency of the sequential pre-treatment.

(3) The effect of the spent medium treatment on the transformation of the carbonaceous matter will be determined by QEMSCAN analysis, Raman spectrometry and 3D fluorescence analysis.

(4) The iron oxidizer *A. brierleyi* was found to be inhibited from decomposing sulfides if used sequentially after the fungal spent medium. Therefore, it was necessary to determine the factors responsible for the inhibition as a preliminary step to apply the fungal spent medium treatment to other sulfide ores.

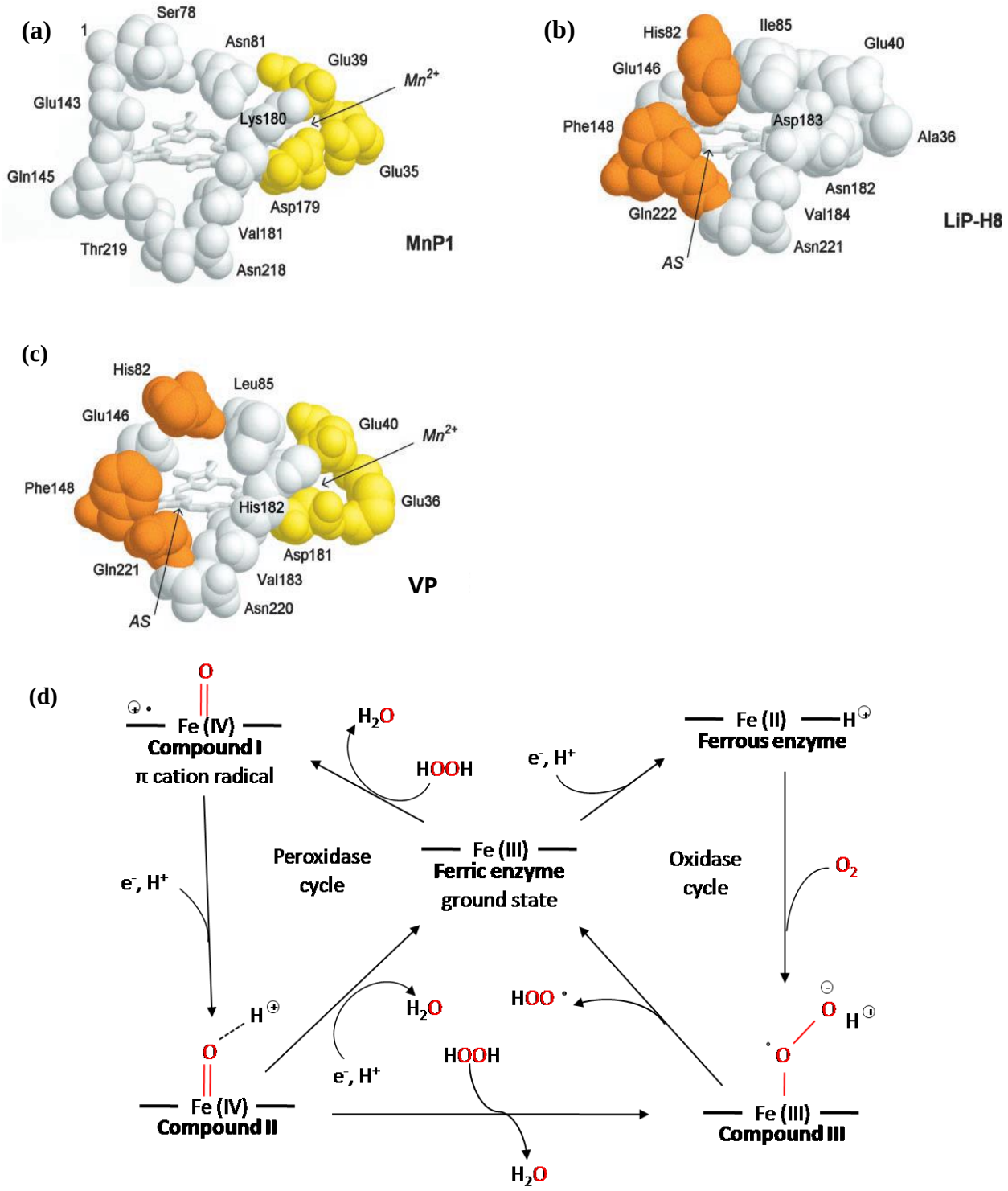

Figure 1. 7 The structure of the active sties in (a) MnP, (b) LiP and (c) VP. The following abbreviations refer to Ala- Alanine, As-aromatic substrate, Asn- Asparagine, Asp- Aspartate, Glu- glutamate, Gln- glutamine, His- Histidine, Ile- Isoleucine, Leu- leucine, Phe- Phenylalanine, Thr- Threonine, Ser- Serine, and Val- Valine (Camerero et al, 1999). (d) The general representation of the catalytic cycles of peroxidases (Berglund et al., 2002).

Table 1. 1 Summary of the previous works regarding of bio-treatment of carbonaceous refractory gold ores (DRGO).

Authors	Au recovery (%)	Remarks (Scientific name of microorganisms, raw ore/ flotation concentrates, aromaticity of carbon in ores, cyanidation)
Ofori-Sarpong et al., (2013b)	94 (from 41%)	The flotation concentrate used in this work contained 30.2 g/t Au and 3.6%C. Au recovery increased from 41% to 78% by bacterial treatment, and then to 94% by fungal treatment with *P. chrysosporium* for 21 days. Cyanidation was conducted at 45% pulp density for 24 h, pH 11 and cyanide strength of 10 kg/t.
Liu et al., (2016)	62 (from 44%)	The carbonaceous matter was extracted from a pre-oxidized carbonaceous gold ore (0.005±0.001% elemental carbon). The extraction procedure followed two steps which were; (1) heated hydrochloric acid and hydrofluoric acid and (2) the metallic sulfide minerals and carbonaceous matter were separated by heavy liquid flotation. 34% of carbon was degraded for 14 days by *P. chrysosporium*. Elemental carbon, fungal degradation residue and water-soluble alkaline precipitate with a content of 0.2% were added to the pre-oxidized gold concentrate (2.18±0.19 g/t Au) to test the cyanidation efficiency. Cyanidation was carried out for 24 h with 0.15% NaCN, a stirring speed of 1050 rpm and a pulp density of 20%.
Konadu et al., (2019)	92 (from 24%)	Flotation concentrate (40.4 g/t Au; 5.86%C) was supplied for sequential bio-treatment using *Acidianus brierleyi* followed by crude enzymes released by *Phanerochaete chrysosporium*. Cyanidation was conducted in 2.5 mM KCN at pH 12 for 24 hrs at 25ºC with the pulp density of 1/20.
Yang et al., (2013)		*Review "*Research status of carbonaceous matter in carbonaceous gold ores and bio-oxidation pretreatment" (*biotreatment using Thiobacillus sp., Phanerochaete chrysosporium, Pseudomonadaceae* and *Streptomyces setonii.)*

Brierley and Kulpa (1992)	74.4	They used *Thiobacillus ferrooxidans* to oxidize sulfides and the gold extraction rate increased from 0 to 55.5% for the untreated control. Afterwards, the carbonaceous matter was deactivated using a microbial consortium, *Pseudomonas maltophilia*,*Pseudomonas oryzihabitans*, *Achromobacter* species and *Arthrobacter* species, and the leaching rate of gold was improved from 55.50% to 74.40%.
Yen et al., (2009)	95.25	Firstly, *Trametes versicolor* culture media (with the fungal agent) were used to deactivate the preg-robbing carbonaceous components, and the gold extraction rate was between 54.10% and 64.50%. Secondly, the refractory sulfides of the ores were decomposed by *Trametes versicolor* culture media (without the fungal agent). Higher gold extraction occurred when the ore samples were treated by a combination of bio-treatment and bio-oxidation with *Trametes versicolor*, resulting in 87.00%_95.25% extraction. The gold leaching rate of carbon-bearing high-arsenic refractory gold concentrate of Guangdong province is only 15.02%.
Yang et al., (2003)	94.41	HYK_2 flora was used to treat this refractory gold ores, and the bacteria could excrete a mass of organic substances when the metal sulfides were oxidized. The bacteria and colloidal phase culture medium could attach to the surface of organic carbon and passivate it, and the leaching rate of gold reached 94.41%. The Dongbeizhai gold mines are typical double refractory ores, and the gold leaching efficiency is almost 0%. This gold ore has a high concentration of harmful elements such as arsenic, sulfur and carbon, and the gold is present as submicroscopic colloidal gold and native gold in the pyrite.
Amankwah et al., (2005)	94.7	*Thiobacillus ferrooxidans* could not oxidize and deactivate carbonaceous matter effectively. It still was preg-robber

		during the cyanide leaching process. They used two-stage bio-oxidation to treat double refractory gold concentrates which contain 65.30 g/t Au, 6.10% C and 11.90% S, and the main sulfide minerals are pyrite and arsenopyrite. In the first stage, chemolithotrophic bacteria were used to oxidize sulfides, and cyanidation resulted in 81.1% gold extraction. The action of *Streptomyces setonii* reduced the carbonaceous matter content in the second stage. The combined effect of the two steps resulted in an overall gold recovery of 94.7% after cyanidation.
Wang et al., (2000)	95	They found that the content of organic carbon was nearly no change before and after bacterium treatment, but the recovery rate of gold was more than 95%. This indicated that *Thiobacillus ferrooxidans* had passivation on organic carbon.
Amankwah and Yen, (2006)		*Streptomyces setonii* to pre-treat lignite, bituminous and anthracite. They found that carbon dioxide was produced in the process of degradation, and the degradation rates of lignite and bituminous were higher than anthracite.
Ofori-Sarpong et al., (2010)		They used lignite, sub-bituminous, bituminous and anthracite as a substitute to study the influence of *Phanerochaete chrysosporium* on the preg-robbing capacity of carbonaceous matter. The results indicated that *Phanerochaete chrysosporium* could decrease the preg-robbing capacity by about 90%. The *Phanerochaete chrysosporium* could secrete enzymes to degrade gold-bearing wood chips, which increased contact between gold and cyanide solution.

References

Abotsi, G. M. K., Osseo-Asare, K., 1987. Surface chemistry of carbonaceous gold ores, II. Effects of organic additives on gold adsorption from cyanide solution. *Int. J. Min. Process.*, 21, 225-239.

Adams, M. D., 1990. The mechanism of adsorption of aurocyanide onto activated carbon, 1. Relation between the effects of oxygen and ionic strength. *Hydrometallurgy*, 25, 171-184.

Adams, M. D., Fleming, C. A., 1989. The mechanism of adsorption of aurocyanide onto activated carbon. *Metall. Trans. B*, 20, 315-325.

Afenya, P.M., 1991. Treatment of carbonaceous refractory gold ores. *Miner. Eng*. 4, 1043-1055.

Akbarian, F., Dunn, B. S., Zink, J. I., 1996. Porous Sol−Gel Silicates Containing Gold Particles as Matrices for Surface Enhanced Raman Spectroscopy. *J. Raman Spectrosc*. 27, 775-783.

Aksu, Z., Calik, A., Dursun, A.Y., Demircan, Z., 1999. Biosorption of iron (III)–cyanide complex anions to *Rhizopus arrhizus*: application of adsorption isotherms. Proc. Biochem. 34, 483-491.

Amankwah, R. K., Pickles, C.A., 2009. Microwave roasting of a carbonaceous sulphidic gold concentrate. *Miner. Eng.,* 22, 1095-1101.

Amankwah, R. K., Yen, W.T., Ramsay, J. A., 2005. A two-stage bacterial pretreatment process for double refractory gold ores. *Miner. Eng.*, 18, 103-108.

Amankwah, R.K., Yen, W.T., 2006. Effect of carbonaceous characteristics on biodegradation and preg-robbing behavior. In Proceedings of 23rd Annual Meeting of International Mineral Processing Conference, Istanbul, Turkey, Vol. 2, 1298-1302.

Baker, W. E., 1978. The role of humic acid in the transport of gold. *Geochimica et Cosmochimica Acta*, 42, 645-649.

Baldrian, M., 2003. Interactions of heavy metals with white-rot fungi. *Enzyme Microb. Tech*., 32, 78-91.

Berglund, G. I., Carlsson, G. H., Smith, A. T., Szöke, H., Henriksen, A., Hajdu, J., 2002. The catalytic pathway of horseradish peroxidase at high resolution. *Nature*, 417, 463-468.

Bond, G. C., 2002. Gold: a relatively new catalyst. *Catalysis Today*, 72, 5-9.

Bosecker, K., 1997. Bioleaching: metal solubilization by microorganisms. FEMS *Microbiol. Rev.*, 20., 591-604.

Bourbonnais, R., Paice, M. G., 1990. Oxidation of non-phenolic substrates. *FEBS Lett.*, 267, 99-102.

Bourbonnais, R., Paice, M. G., Reid, I. D., Lanthier, P., Yaguchi, M., 1995. Lignin oxidation by laccase isozymes from *Trametes versicolor* and role of the mediator 2, 2'-azinobis (3-ethylbenzthiazoline-6-sulfonate) in kraft lignin depolymerization. *App. Environ. Microbial.*, *61*, 1876-1880.

Brierley, J. A., 2003. Response of microbial systems to thermal stress in biooxidation-heap pretreatment of refractory gold ores. *Hydrometallurgy*, 71, 13-19.

Brierley, J.A., Kulpa, C. F. 1992. Microbial consortium treatment of refractory precious metal ores: USA, 5127942 [P].

Bumpus, J. A., Tien, M., Wright, D. Aust, S. D., 1985. Oxidation of persistent environmental pollutants by a white rot fungus. *Science.* 228, 1434-1436.

Calvo, A. M., Wilson, R. A., Bok, J. W., Keller, N. P., 2002. Relationship between secondary metabolism and fungal development. *Microbiol. Mol. Biol. Rev.*, 66, 447-459.

Camarero, S., Sarkar, S., Ruiz-Dueñas, F. J., Martínez, M. J., Martínez, Á. T., 1999. Description of a versatile peroxidase involved in the natural degradation of lignin that has both manganese peroxidase and lignin peroxidase substrate interaction sites. *J. Biol. Chem.,* 274, 10324-10330.

Čater, M., Fanedl, L., Malovrh, Š., Logar, R.M., 2015. Biogas production from brewery spent grain enhanced by bioaugmentation with hydrolytic anaerobic bacteria. *Bioresour. Technol*. 186, 261-269.

Chatterjee, S., Das, S.K., Chakravarty, R., Chakrabarti, A., Ghosh, S., Guha, A.K., 2010. Interaction of malathion, an organophosphorus pesticide with *Rhizopus oryzae* biomass. *J. Hazard. Mater* 174, 47-53.

Chen, G.Q., Zhang, W.J., Zeng, G.M., Huang, J.H., Wang, L., Shen, G.L., 2011. Surface-modified *Phanerochaete chrysosporium* as a biosorbent for Cr (VI)-contaminated wastewater. *J. Hazard. Mater*. 186, 2138-2143.

Chen, T. T., Cabri, L. J., Dutrizac, J.E., 2002. Characterizing gold in refractory sulfide gold ores and residues. *JOM*, 54, 20-22.

Claus, H., 2004. Laccases: structure, reactions, distribution. *Micron*, 35, 93-96.

Coconi-Linares, N., Magaña-Ortíz, D., Guzmán-Ortiz, D. A., Fernández, F., Loske, A. M., Gómez-Lim, M. A., 2014. High-yield production of manganese peroxidase, lignin peroxidase and versatile peroxidase in *Phanerochaete chrysosporium*. *Appl. Microbiol. Biotechnol.*, 98, 9283-9294.

Cook, N. J., Chryssoulis, S. L., 1990. Concentrations of invisible gold in the common sulfides. *Can. Mineral.,* 28, 1-16.

Corti, C. W. Holliday, R. J., 2004. Commercial aspects of gold applications: from materials science to chemical science. *Gold Bulletin*, 37, 20-26.

Corti, C. W., Holliday, R. J., Thompson, D. T., 2002. Developing new industrial applications for gold: gold nanotechnology. *Gold Bulletin*, 35, 111-117.

Couto, S. R., Herrera, J. L. T., 2006. Industrial and biotechnological applications of laccases: a review, *Biotechnol. Adv.*, 24, 500-513.

Cui, J., Zhang, L., 2008. Metallurgical recovery of metals from electronic waste: a review. *J. Hazard. Mater*. 158, 228-256.

D'souza, T. M., Merritt, C. S. Reddy, C. A., 1999. Lignin-modifying enzymes of the white rot basidiomycete *Ganoderma lucidum*. *App. Environ. Microbial*., 65, 5307-5313.

Dai, X., Simons, A., Breuer, P., 2012. A review of copper cyanide recovery technologies for the cyanidation of copper containing gold ores. *Miner. Eng*., 25, 1-13.

Deschenes, G., Prud'homme, P. J. H., 1997. Cyanidation of a copper-gold ore. *Int. J. Min. Process*., 50, 127-141.

Drost, E., Hausselt, J., 2013. Uses of gold in jewellery. *Interdisciplinary Science Reviews*.

Eichengreen, B., Fetters, G., 1991. The Gold Standard and the Great Depression. *NBER Reporter, Spring,* 91, 5-10.

Enguita, F. J., Martins, L. O., Henriques, A. O., Carrondo, M. A., 2003. Crystal structure of a bacterial endospore coat component a laccase with enhanced thermostability properties. *J. Biol. Chem.*, 278, 19416-19425.

Fakoussa, R.M., Hofrichter, M., 1999. Biotechnology and microbiology of coal degradation. *Appl. Microbiol. Biotechnol*. 52, 25-40.

Feng, Y., Xiangbin, X., Junwei, Z., Zelai, L., 2003. Experimental study on bacterial oxidation of carbon-bearing high arsenic refractory gold concentrate [J]. In Gold, 24, 4, 37-39.

Fenn, P., Kirk, T.K., 1981. Relationship of nitrogen to the onset and suppression of ligninolytic activity and secondary metabolism in *Phanerochaete chrysosporium*. *Arch. Microbiol.*, 130, 59-65.

Fleet, M.E., Mumin, A.H., 1997. Gold-bearing arsenian pyrite and marcasite and arsenopyrite from Carlin Trend gold deposits and laboratory synthesis. *Am. Mineral*., 82, 182-193.

Franklin, R.E., 1951. Crystallite growth in graphitizing and non-graphitizing carbons. Proceedings of the Royal Society of London. Series A. *Math. Phys. Sci*. 209, 196-218.

Fu, Y., Viraraghavan, T., 2001. Fungal decolorization of dye wastewaters: a review. *Bioresour. Technol.*, 79, 251-262.

Goldhub, 2019. Gold supply and demand statistics. https://www.gold.org/goldhub/data/gold-supply-and-demand-statistics (accessed 11 April 2019).

Goodall, W.R., Scales, P.J., Butcher, A.R., 2005. The use of QEMSCAN and diagnostic leaching in the characterization of visible gold in complex ores. *Miner. Eng*. 18, 877-886.

Goodman, P., 2002. Current and future uses of gold in electronics. *Gold Bulletin*, 35, 21-26.

Haque, K. E., 1999. Microwave energy for mineral treatment processes—a brief review. *Int. J.Min. Process.* 57, 1-24.

Harris, P. J., 2013. Fullerene-like models for microporous carbon. *J. Mater. Sci.*, 48, 565-577.

Henley, R.W., Adams, J., 1979. On the evolution of giant gold placers. *Trans. Ins. Mining Metallur., Section B, 88, 41-50*.

Higham, T., Chapman, J., Slavchev, V., Gaydarska, B., Honch, N., Yordanov, Y. Dimitrova, B., 2007. New perspectives on the Varna cemetery (Bulgaria)–AMS dates and social implications. *Antiquity*, 81,640-654.

Huang, Z., Liers, C., Ullrich, R., Hofrichter M., Urynowicz, M. A., 2013. Depolymerization and solubilization of chemically pretreated powder river basin subbituminous coal by manganese peroxidase (MnP) from *Bjerkandera adusta*. *Fuel*, 112, 295-301.

Ibrado, A. S., Fuerstenau, D. W., 1992. Effect of the structure of carbon adsorbents on the adsorption of gold cyanide. *Hydrometallurgy*, 30, 243-256.

Ibrado, A. S., Fuerstenau, D. W., 1995. Infrared and X-ray photoelectron spectroscopy studies on the adsorption of gold cyanide on activated carbon. *Min. Eng.*, 8, 441-458.

Ibrado, A.S., Fuerstenau, D.W., 1992. Effect of the structure of carbon adsorbents on the adsorption of gold cyanide. *Hydrometallurgy*, 30, 243-256.

Ioannidou, O., Zabaniotou, A., 2007. Agricultural residues as precursors for activated carbon production—a review. *Renew. Sust. Energ. Rev.* 11, 1966-2005.

Jäger, A., Croan, S., Kirk, T. K., 1985. Production of ligninases and degradation of lignin in agitated submerged cultures of *Phanerochaete chrysosporium*. *App. Environ. Microbiol*., 50, 1274-1278.

Kelly, R. L., Reddy, C. A., 1986. Identification of glucose oxidase activity as the primary source of hydrogen peroxide production in lignolytic cultures of *Phanerochaete chrysosporium*. *Arch. Microbiol,* 144, 248-253.

Kersten, P. J., Kirk, T. K., 1987. Involvement of a new enzyme, glyoxal oxidase, in extracellular H2O2 production by *Phanerochaete chrysosporium*. *J. Bacteriol.*, 169, 2195-2201.

Kirk, T. K., Farrell, R. L., 1987. Enzymatic" combustion": the microbial degradation of lignin. *Annu. Rev. Microbiol.*, 41, 465-501.

Kirk, T. K., Schultz, E., Connors, W.J., Lorenz, L.F., Zeikus, J.G., 1978. Influence of culture parameters on lignin metabolism by *Phanerochaete chrysosporium*. *Arch. Microbiol.*, 117, 277-285.

Konadu, K.T., Huddy, R.J., Harrison, S.T., Osseo-Asare, K., Sasaki, K., 2019. Sequential pretreatment of double refractory gold ore (DRGO) with a thermophilic iron oxidizing archeaon and fungal crude enzymes. Miner. Eng.138, 86-94.

La Brooy, S.R., Linge, H.G., Walker, G.S., 1994. Review of gold extraction from ores. *Miner. Eng.* 1213-1241.

Lange, H., Decina, S., Crestini, C., 2013. Oxidative upgrade of lignin–Recent routes reviewed. *Eur. Polym. J.*, 49, 1151-1173.

Lastoskie, C., Gubbins, K. E., Quirke, N., 1993. Pore size distribution analysis of microporous carbons: a density functional theory approach. *J. Phys. Chem*., 97, 4786-4796.

Leonowicz, A., Matuszewska, A., Luterek, J., Ziegenhagen, D., Wojtaś-Wasilewska, M., Cho, N.S., Hofrichter, M., Rogalski, J., 1999. Biodegradation of lignin by white rot fungi. *Fung. Gene. Biol.* 27, 175-185.

Lindström, E. B., Gunneriusson, E., Tuovinen, O. H., 1992. Bacterial oxidation of refractory sulfide ores for gold recovery. *Crit. Rev. Biotechnol*, 12, 133-155.

Liu, G. Q., Yen, W. T., 1995. Effects of sulfide minerals and dissolved oxygen on the gold and silver dissolution in cyanide solution. *Min. Eng.*, 8, 111-123.

Liu, Q., Yang, H. Y., Tong, L. L., Jin, Z. N., Sand, W., 2016. Fungal degradation of elemental carbon in carbonaceous gold ore. *Hydrometallurgy*, 160, 90-97.

Magers, T. A., Tabb, D. L., 1981. Indicator composition and test device containing amine oxide, and method of use. *U.S. Patent* 4,279,993.

Marsden, J., House, I., 2006. The chemistry of gold extraction. SME, Englewood, USA, 19-358.

Matta, R., Hanna, K. Chiron, S., 2007. Fenton-like oxidation of 2, 4, 6-trinitrotoluene using different iron minerals. *Sc. Tot. Environ*. 385, 242-251.

Miller, J. D., Wan, R. Y., Diaz, X., 2005. Preg-robbing gold ores. *Dev. Min. Process*., 15, 937-972.

Nanthakumar, B., Pickles, C. A., Kelebek, S., 2007. Microwave pretreatment of a double refractory gold ore. *Miner. Eng.*, 20, 1109-1119.

Ofori-Sarpong, G., Tien, M., Osseo-Asare, K., 2010. Myco-hydrometallurgy: Coal model for potential reduction of preg-robbing capacity of carbonaceous gold ores using the fungus, *Phanerochaete chrysosporium*. *Hydrometallurgy*, 102, 66-72.

Ofori-Sarpong, G., Osseo-Asare, K., Tien, M., 2011. Fungal pretreatment of sulfides in refractory gold ores. *Miner. Eng.*, 24, 499-504.

Ofori-Sarpong, G., Osseo-Asare, K., Tien, M., 2013a. Pretreatment of refractory gold ores using cell-free extracts of *P. chrysosporium*: a preliminary study. *Adv. Mater. Res*., 825, 427-430.

Ofori-Sarpong, G., Osseo-Asare, K., Tien, M., 2013b. Mycohydrometallurgy: Biotransformation of double refractory gold ores by the fungus, *Phanerochaete chrysosporium*. *Hydrometallurgy*, 137, 38-44.

Olson, G. J., Brierley, J. A., Brierley, C. L., 2003. Bioleaching review part B. *App. Microbial. Biotechno*, 63, 249-257.

Osseo-Asare, K., Afenya, P. M. Abotsi, G. M. K., 1984. Carbonaceous matter in gold ores: isolation, characterization and adsorption behaviour in aurocyanide solutions. *Prec. Met.: Min. Extrac. Proc.*, 125-144.

Paktunc, D., Kingston, D., Pratt, A., McMullen, J., 2006. Distribution of gold in pyrite and in products of its transformation resulting from roasting of refractory gold ore. *Can. Miner*., 44, 213-227.

Pérez, J., Munoz-Dorado, J., de la Rubia, T. D. L. R., Martinez, J., 2002. Biodegradation and biological treatments of cellulose, hemicellulose and lignin: an overview. *Int. Microbiol.*, 5, 53-63.

Pometto III, A.L., Sutherland, J.B., Crawford, D.L., 1981. *Streptomyces setonii*: catabolism of vanillic acid via guaiacol and catechol. Can. J. Microbial. 27, 636-638.

Pricker, S.P., 1996. Medical uses of gold compounds: past, present and future. *Gold Bulletin*, 29, 53-60.

Ramli, S.C.S. and Osman, R.M., 2015. Meeting the challenge of Penjom Gold Mine's geology in the recovery of fine gold in carbonaceous ores. *Bulletin of the Geological Society of Malaysia*, 61, 1-9.

Rawlings, D.E. ed., 2013. Biomining: theory, microbes and industrial processes. *Springer Science & Business Media*.

Reich, M., Kesler, S., Utsunomiya, S., Palenik, C. ., Chryssoulis, S., ing, R. ., 2005. Solubility of gold in arsenian pyrite. *Geochimica et Cosmochimica Acta*, 69, 2781-2796.

Riva, S., 2006. Laccases: blue enzymes for green chemistry. *Trends Biotechnol.*, 24, 219-226.

Riveros, P.A., 1993. Selectivity aspects of the extraction of gold from cyanide solutions with ion exchange resins. *Hydrometallurgy*, 33, 43-58.

Rodriguez, C. S., Santoro, R., Cameselle, C. Sanroman, A., 1997. Laccase production in semi-solid cultures of *Phanerochaete chrysosporium. Biotechnol. Lett.*, 19, 995-998.

Sanchez, V. Hiskey, J. B., 1988. An electrochemical study of the surface oxidation of arsenopyrite in alkaline media. *Metallur.Trans*.B,19, 943-949.

Schmalz, T. G., Seitz, W. A., Klein, D. J. Hite, G. E., 1988. Elemental carbon cages. *J. Am. Chem. Soc.*, 110, 1113-1127.

Simon, G., Kesler, S. E., Chryssoulis, S., 1999. Geochemistry textures of gold-bearing arsenian pyrite, Twin Creeks, Nevada; implications for deposition of gold in carlin-type deposits. *Econ. Geo.*, 94, 405-421.

Southam, G., Beveridge, T. J., 1994. The in vitro formation of placer gold by bacteria. *Geochimica et Cosmochimica Acta*, 58, 4527-4530.

Stenebråten, J.F., Johnson, W.P., Brosnahan, D.R., 1999. Characterization of Goldstrike ore carbonaceous material. *Mining, Metallur. Explor*. 16, 37-43.

Tan, H., Feng, D., Lukey, G.C., Van Deventer, J.S.J., 2005. The behaviour of carbonaceous matter in cyanide leaching of gold. *Hydrometallurgy*, 78, 226-235.

Thomas, K.G., 2005. Pressure oxidation overview. *Developments in mineral processing*, 15, 346-369.

Tien, M., Kirk, T.K., 1988. Lignin peroxidase of *Phanerochaete chrysosporium*. *Methods Enzymol.*, 161, 238-299.

Tuisel, H., Sinclair, R., Bumpus, J. A., Ashbaugh, W., Brock, B.J., Aust, S.D., 1990. Lignin peroxidase H2 from *Phanerochaete chrysosporium*: purification, characterization and stability to temperature and pH. *Arch. Biochem. Biophys.*, 279, 158-166.

Turner, S. J., Flindell, P. A., Hendri, D., Hardjana, I., Lauricella, P. F., Lindsay, R.P., Marpaung, B., White, G. P., 1994. Sediment-hosted gold mineralisation in the Ratatotok district, North Sulawesi, Indonesia. *J. of Geochem. Explor.*, 50, 317-336.

van Niekerk, J.A., 2009. Recent advances in the BIOX® technology. *Adv. Mater. Res*. 71, 465-468.

Wang, A., Zhang, Y.K., Liu, H.Z., 2000. The property of carboniferous species and its effect on leaching of gold in Dongbeizhai Gold Mine. Multipurpose Utilization of Mineral Resources, 3, 4-8.

Wariishi, H., Valli, K., Gold, M. H., 1991. In vitro depolymerization of lignin by manganese peroxidase of *Phanerochaete chrysosporium*. *Biochem. Biophys. Res. Commun*., 176, 269-275.

Wariishi, H., Valli, K., Gold, M. H., 1992. Manganese (II) oxidation by manganese peroxidase from the basidiomycete *Phanerochaete chrysosporium*: kinetic mechanism and role of chelators. *J. Biol. Chem.*, 267, 23688-23695.

Wood, S. A., 1996. The role of humic substances in the transport and fixation of metals of economic interest (Au, Pt, Pd, U, V). *Ore Geo. Rev.* 11, 1-31.

Yang, F., Xu, X.B., Zhao, J.W., Liang, Z.L., 2003. Experimental study on bacterial oxidation of carbon-bearing high arsenic refractory gold concentrates. Gold, 24, 37-39.

Yang, H. Y., Qian, L. I. U., Song, X. L., Dong, J. K., 2013. Research status of carbonaceous matter in carbonaceous gold ores and bio-oxidation pretreatment. *Trans. Nonferrous Met. Soc. China*, 23, 3405-3411.

Yaver, D. S., Xu, F., Golightly, E. J., Brown, K. M., Brown, S. H., Rey, M. W., Schneider, P., Halkier, T., Mondorf, K., Dalboge, H., 1996. Purification, characterization, molecular cloning, and expression of two laccase genes from the white rot basidiomycete *Trametes villosa*. *App. Environ.Microbiol. 62*, 34-841.

Yen, W.T., Amankwah, R.K., Choi, Y., 2009. Microbial pre-treatment of double refractory: US2009/0158893A1[P]

Yin, C.Y., Ng, M.F., Saunders, M., Goh, B. M., Senanayake, G., Sherwood, A., Hampton, M., 2014. New insights into the adsorption of Aurocyanide Ion on activated carbon surface: electron microscopy analysis and computational studies using fullerene-like models. *Langmuir,* 30, 7703-7709.

Zeng, G. M., Zhao, M. H., Huang, D. L., Lai, C., Huang, C., Wei, Z., Xu, P., Li, N. J., Zhang, C., Li, F. L., Cheng, M., 2013. Purification and biochemical characterization of two extracellular peroxidases from *Phanerochaete chrysosporium* responsible for lignin biodegradation. *Int. Biodeter. Biodegr.*, 85, 166-172.

Chapter 2:

Methodology

2.1. Microbiological experiments

2.1.1. Culture of a white-rot fungus Phanerochaete chrysosporium

P. chrysosporium, a white-rot fungus, was provided for this study by the courtesy of Dr Ming Tien (Penn State University, USA). It is known that *P. chrysosporium* releases lignin peroxidase, Mn-peroxidase and hydrogen peroxidase (Kudo et al., 2017) to decompose cellulose. It was regularly maintained on a solid medium with 0.2% agar including 10 g glucose, 1.18 g succinic acid, 0.2 g ammonium tartrate, 10 mg thiamine, 0.4 mM veratryl alcohol or 10 mg 2,6-dimethoxyphenol, 2 g KH_2PO_4, 0.5 g $MgSO_4.7H_2O$ and 0.1 g $CaCl_2.2H_2O$ per 1 L in addition to 70 mL trace element solution (3 g $MgSO_4.7H_2O$, 1 g NaCl, 0.5 g $MnSO_4.5H_2O$, 0.1 g $FeSO_4.7H_2O$, 0.1 g $CuSO_4$. $5H_2O$, 10 mg boric acid per 1 L) (Tien and Kirk, 1988). 500 mL of liquid mediums with the same composition as above was prepared at pH 4 in 2000 mL Erlenmeyer flasks. The flasks were sterilised at 120°C for 20 mins, afterwards, it was allowed to cool down to room temperature before it was inoculated using a heat-sterilised loop. The flask was incubated at 37°C under stationary conditions. After the growth period, the cell-free spent medium (CFSM) was collected using a 0.22 µm stericup filter (Merck Millipore, USA). It was used immediately for DRGO treatment.

2.1.2. Culture of thermophilic iron-oxidizing archaeon Acidianus brierleyi.

A. brierleyi (DSMZ 1651) was cultured in 500 mL Erlenmeyer flasks with 200 mL solutions containing 4 mL of heterotrophic basal salts (HBS) medium (22.5 g NH_4SO_4; 2.5 g KCl; 2.5 g KH_2PO_4; 25 g $MgSO_4.7H_2O$; 0.7 g $Ca(NO_3)_2$. $4H_2O$; and 7.1 g $NaSO_4$ per litre) and 0.04 % yeast extract. The pH was adjusted to 1.5 and then it was sterilised at 120°C for 20 mins, afterwards, it was allowed to cool down to room temperature, 5 mL of 800 mM $FeSO_4.7H_2O$ stock solution was added as an iron source. The $FeSO_4.7H_2O$ stock solution was sterilised using

a 0.2 µm membrane filter (Advantec, Japan) before being used. The flask was inoculated with an initial cell density of 10^7 cell/mL and the cell growth was monitored periodically using a bacteria counter (SLGC, Japan) and an optical microscope (Olympus BX51, USA).

2.1.3. Genomic analysis

2.1.3.1. DNA extraction

The solid residue collected after CFSM and *A. brierleyi* treatments were analysed for the presence of fungal and archaea genes. Approximately 0.1 g of solid was weighed out into separate sterile microfuge tubes. Total genomic DNA was extracted using the High Pure PCR Template Preparation Kit (Roche Life Science). The cells were lysed using tissue lysis buffer containing 5 µL of lysozyme (10 mg/mL in 20 mM Tris-HCl, pH 8) and 10 µL lyticase (0.5 mg/mL). Extracted genomic DNA was eluted with 50 µL of pre-warmed elution buffer, quantified spectrophotometrically (Nanodrop ND-2000) and stored at 4°C.

The extracted genomic DNA was diluted 1:10 with sterile deionized water, before 1 µL was used as the template in PCR reactions to amplify 16S and 18S rRNA genes as markers for the presence of bacteria and/or fungi, respectively, within the mineral samples. HiFi HotStart ReeadyMix PCR mix (Kapa Biosystems) was used for all PCR reactions. The presence of archaea was assessed using the 16S rRNA gene, as amplified using the oligonucleotide primers 27F and 1492R. *Cupriovidus necator* DSM 531 was used as a positive control. The cycling conditions were as follows: Initial denaturation of 95°C for 3 min, followed by 30 cycles of 98°C for 20 sec, 65°C for 15 sec and 72°C for 75 sec, and a final extension of 72°C for 5 min.

The presence of eukaryotes, including fungi, was assessed using the 18S rRNA gene, as amplified using the oligonucleotide primers Uni18S_566F and Uni18S_1200R. *Saccharomyces cerevisiae* CBS 8803 was used as a positive control. The cycling conditions were as follows: Initial denaturation of 95°C for 3 min, followed by 25 cycles of 98°C for 20

sec, 62°C for 15 sec and 72°C for 30 sec, and a final extension of 72°C for 5 min. Following PCR cycling, 5 µL of 6x Kapa Dye was added to each reaction tube, vortexed briefly and the products separated on a 1% (w/v) Tris-base, acetic acid and EDTA (TAE) agarose gel, against Kapa Express Ladder.

2.1.3.2. Fluorescent in-situ hybridization

Fluorescent In-Situ Hybridization (FISH) is a technique used for qualitative and partially quantitative analysis of microbial ecology. The technique is based on the hybridization of specifically designed oligonucleotide probes with a 18S rRNA sequence in the fungus. 10 mg -100 mg of samples were placed on glass slides with 1.5 mL of a fixative solution containing 25% phosphate buffered saline (PBS; 137 mM NaCl; 2.7 mM KCl; 10 mM Na_2HPO_4; 2 mM KH_2PO_4; pH 7.4) and 4% paraformaldehyde. The glass slide was kept at 4°C for 2 h before begin washed twice with 0.5 mL PBS to remove excess fixatives and unattached mineral grains. Afterwards, the glass slides were kept overnight at 4°C in a solution of 1:1 vol ethanol and PBS. The next step involved dehydrating the slide with an ethanol series for 3 mins each at 50%, 80%, 98% and 99% ethanol. The slides were then stored in ice before being transferred to a 50 mL polypropylene tube containing the hybridization buffer (0.9 M NaCl; 20 mM Tris HCl pH 7.2; 20% formamide; 0.01% sodium dodecyl sulphate; 50 ng/ µL 18S FAM probe) for 2 hr. The glass slides were then removed from the hybridization buffer and placed in a warm wash buffer containing 0.9 M NaCl, 20 mM Tris-HCl, 0.01% SDS and 5 mM EDTA for 10-15 mins at 48°C. Finally, the slide was washed with ice-cold deionized water and then 10 µL of 1 µg/mL 4',6-diamidino-2-phenylindole (DAPI) was added as a general DNA stain for 5 mins. A final washing step with deionized water was conducted before the glass slide was dried in the dark to avoid photo-bleaching of the probe. The glass slides were then analyzed for the fungal DNA using a Ti-E inverted fluorescence microscope (Nikkon, Japan).

2.2. Aqueous analysis

2.2.1. pH and Eh vs SHE

Samples for analysis (1 mL) were usually taken from the flask with sterilized pipette tips and then the solution pH and Eh vs SHE (redox potential) were determined using electrodes from a MM-43X benchtop analyzer (TOADKK, Japan).

2.2.2. Inductively coupled plasma-optical emission spectrometry (ICP-OES) and mass spectrometry (ICP-MS)

The bio-treatment of DRGO decomposed the sulfide minerals and produced soluble iron and arsenic species. Samples for analysis were filtered through a 0.2 µm before being diluted 10-50 times with 0.1 M HCl. The amount of dissolved iron and arsenic were determined by inductively coupled plasma-optical emission spectrometry (ICP-OES, Perkin Elmer Optima 8300).

The aurocyanide ($Au(CN)_2^-$) adsorption ability of activated carbon (preg-robbing) and cyanidation of the DRGO were two of the methods used to evaluate the effectiveness of the bio-treatments. Thus in the case of the preg-robbing test, the $Au(CN)_2^-$ concentration after adsorption was determined by ICP-OES under similar conditions as described above. On the other hand, gold released by cyanidation was assayed using induced coupled plasma-mass spectrometry (ICP-MS, Agilent 7500c). The ICP-MS method was selected over the ICP-OES method for analysing the cyanidation results due to its sensitivity at lower concentrations.

2.2.3. Dissolved total organic carbon

The total dissolved organic carbon (TOC) was determined using a Shimadzu VCSH analyser (Kyoto, Japan) in triplicate.

2.2.4. Three dimensional fluorescence spectrometry

3D fluorescence spectrometry was used to characterize the bio-residue after the CFSM treatment of the gold ore to find the humic acid signature (Senesi et al., 1991; Plaza et al., 2006; Zhang et al., 2013). All the liquid samples were filtered through a 0.2 µm sieve and put in a clear quartz cuvette. The excitation wavelength (Ex) and emission wavelength (Em) used for the measurements were 300 nm - 450 nm and 350 nm to 600 nm, respectively. The analysis was conducted on a JASCO FP-6600 fluorescence spectrometer (Japan).

2.3. Mineralogical analysis

2.3.1. X-ray diffraction (XRD)

X-ray diffraction (XRD) patterns were collected on an Ultima IV diffractometer (RIGAKU, Akishima, Japan) using Cu Kα radiation (40 kV, 40 mA) at a scanning speed of 2° min^{-1} and scanning step of 0.02°.

2.3.2. X-ray fluorescence (XRF)

The elemental composition of the DRGO and bio-treated residues were determined by XRF analysis using ZSX Primus II (Rigaku). Measurements were conducted under vacuum using the oxide mode.

2.3.3. Quantitative evaluation of minerals by scanning electron microscopy (QEMSCAN)

The elemental and mineralogical composition of the gold ore samples before and after treatment were determined by QEMSCAN analysis (FEI 650F, USA). This technique utilizes backscattered electron imaging (BSE), scanning electron microscopy and energy dispersive x-ray spectroscopy (EDS) to differentiate minerals into groups by composition and texture (Pirrie et al., 2004; Goodall et al., 2005; Liu et al., 2005; Pascoe et al., 2007). The samples for analysis were screened through 53 µm and 10 µm sieves, and then the oversize and undersize of the 10 µm were collected and dried overnight at 70-80 °C. Sample blocks were prepared by adding 0.25 g of each screened sample to ca. 2 mL heated and melted carnauba wax and then allowed to solidify before the block was covered with epoxy resin. These wax and epoxy blocks were then polished by silicon carbide paper to provide for QEMSCAN observation. Each block was analysed for 2 to 4 hrs at 20-25 kV, 10 nA and field step of 0.5 -4 µm.

The accuracy of the QEMSCAN observation for a sample was based on using a comprehensive species identification program (SIP) to classify all the observed mineral grains (**Fig 2.1**). The SIP was initially developed based on the mineral phases observed in XRD and XRF. After which, the as-received sample pellet was scanned by QEMSCAN and the data was analyzed by SIP. New mineral phases that were not identified by the SIP were investigated by determining its composition by EDS and morphological characteristics with the SEM in the QEMSCAN. These new minerals were then identified by the Ruff Mineral Database and other references after which these new minerals were added to the SIP. The sample block was then reclassified by the improved SIP. This procedure was repeated until a comprehensive SIP was developed to analyzed ≥ 99% of all the mineral grains for each sample. An arbitrary upper size limit of 1000 µm was used for the analysis because particles larger than this size made up less than 0.02% of any of the samples.

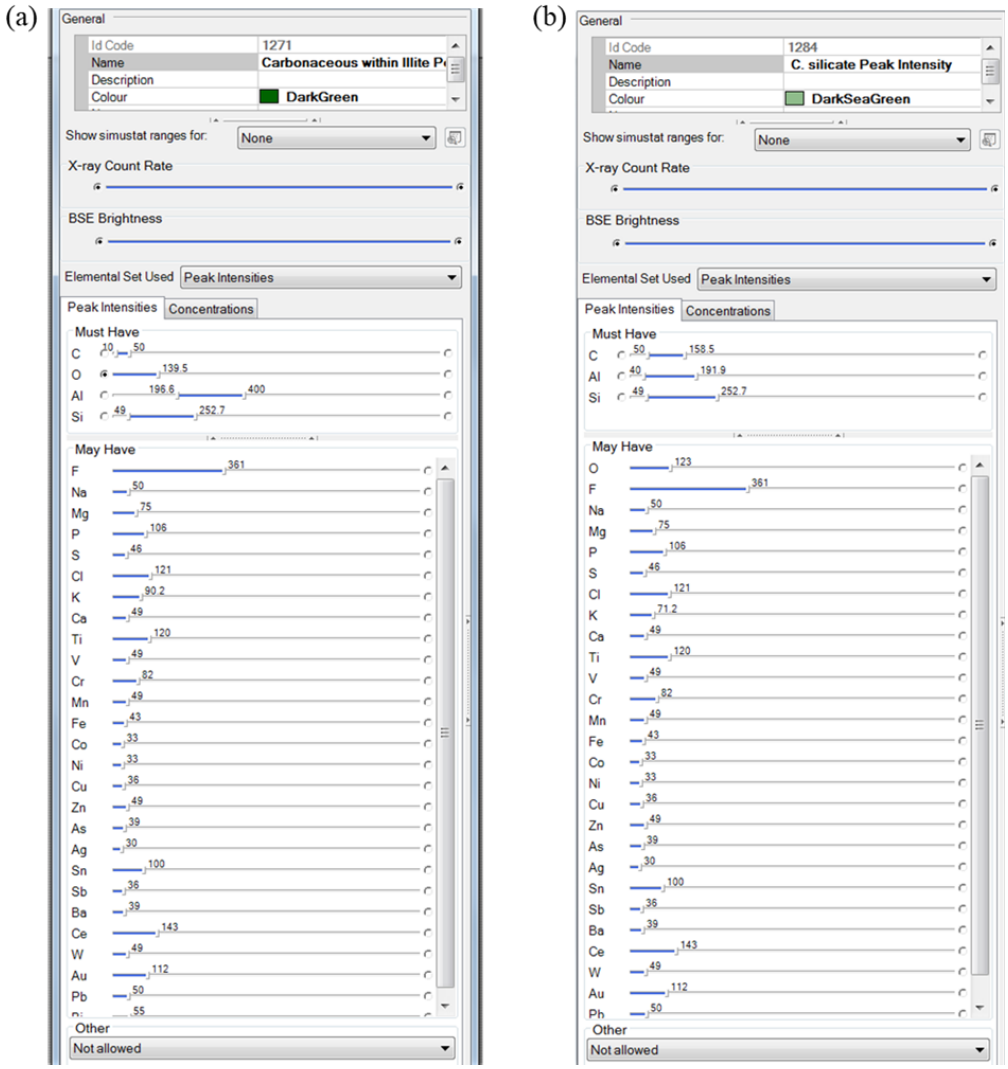

Figure 2. 1 Species identification program (SIP) list requirement for the identification of new carbon-bearing mineral (a) carbonaceous illite which is the main host of carbonaceous matter in the as-received sample and (b) carbonaceous aluminosilicate (C-Si-Al) which is the residue after CFSM treatment in DC and DAC.

2.3.4. Specific surface area measurement by N_2 adsorption

The samples for specific surface area analysis were pre-treated in two steps: vacuum degassing for 90 min at 150°C and finally vacuum pre-treatment for 15 hrs at 150°C. The measurement was conducted by N_2 (99.99%) adsorption using a BELSORP-max porosimeter

(JAPAN BELL, Osaka, Japan). Finally, the data were analyzed by BEL master software in version 6.3.0.0 (JAPAN BELL, Osaka, Japan) based on the non-local density functional theory (Lastoskie et.al 1993).

2.3.5. Scanning electron microscopy

The sample morphology was observed by VE-9800 (Keyence, Japan), UHR FE-SEM SU8000 (Hitachi Co. Ltd., Tokyo, Japan) and NOVA NANOSEM 230 (FEI, USA) at accelerated voltages between 5 kV to 25 kV. VE-9800 and UHR FE-SEM SU8000 were used to observe the changes in the morphology of the CFSM-treated PAC while the NOVA NANOSEM 230 was used to observe bimolecular features like fungal hyphae and biofilm in the sequentially treated DRGO.

2.3.6. Raman spectroscopy

Raman analysis of the carbonaceous matter in the gold ore was determined using DXR Smart Raman (Thermo Scientific) at 532 nm, 10 mW. The spectra collected was the aggregate of 10 measurements at 3 sec laser exposure.

2.3.7. Carbon-13 NMR (^{13}C-NMR)

Solid ^{13}C-CPMAS NMR spectra were collected on an ECA400 (JEOL, Akishima, Tokyo, Japan) equipped with a 3.2-mm CPMAS probe. The experiments were carried out using a standard 4 mm double resonance MAS probe spinning at 15 kHz, π/2-pulse length of 3.2 µs, and a recycle delay of 5 s. Resonance frequency and magnetic field strength used were 100.53 MHz and 9.39 T, respectively. The pristine powdered activated carbon (super special grade,

Wako) was used as a standard for ^{13}C-NMR. Chemical shifts were referenced externally to tetramethyl silane (TMS) at 0 ppm using the methyl signal of hexamethyl benzene at 17.36 ppm as the secondary standard.

2.3.8. Fourier-transform infrared spectroscopy (FTIR)

FTIR spectra were collected in DRIFT method by a FT/IR-670 Plus spectrometer (JASCO, Tokyo, Japan) in the transmission mode using 0.5wt% sample in KBr crystal (spectacle grade, JASCO Corporation, Tokyo, Japan) under the following conditions: accumulation, 100 times; resolution, 16 cm^{-1}; detector, triglycine sulfate (TGS); range of wavenumbers, 4000–400 cm^{-1}.

2.3.9. Zeta potential measurements

The zeta potential was measured in the pH range of 3 to 12 by a Malvern Zetasizer Nano-ZS analyser (Malvern, UK). 5 mg of the solid was suspended in 50 ml of 5 mM NaCl solution and allowed to equilibrate for 2 hrs. The pH was adjusted by dropwise addition of either 50 mM HCl or 50 mM NaOH and the zeta potential was immediately measured afterwards.

2.3.10. Thermogravimetric- differential thermal analysis (TG-DTA)

The thermal decomposition properties of the double refractory gold ore were determined using Bruker 2000SA. 5 – 10 mg of sample was decomposed at a heating rate of 5°C/min in an air atmosphere from room temperature to 800°C.

References

Afenya, P.M., 1991. Treatment of carbonaceous refractory gold ores. *Miner. Eng.* 4, 1043-1055.

Goodall, W.R., Scales, P.J., Butcher, A.R., 2005. The use of QEMSCAN and diagnostic leaching in the characterization of visible gold in complex ores. *Miner. Eng*. 18, 877-886.

Kudo, S., Harada, A., Kubota, H., Sasaki, K., Kaneta, T., 2017. Simultaneous determination of manganese peroxidase and lignin peroxidase by capillary electrophoresis enzyme assays. ACS Omega, 2, 7329-7333.

Lastoskie, C., Gubbins, K. E., Quirke, N., 1993. Pore size distribution analysis of microporous carbons: a density functional theory approach. *J. Phys. Chem.*, 97, 4786-4796.

Liu, Y., Gupta, R., Sharma, A., Wall, T., Butcher, A., Miller, G., Gottlieb, P., French, D., 2005. Mineral matter–organic matter association characterisation by QEMSCAN and applications in coal utilisation. *Fuel*, 84, 1259-1267.

Pascoe, R.D., Power, M.R. and Simpson, B., 2007. QEMSCAN analysis as a tool for improved understanding of gravity separator performance. *Miner. Eng*. 20, 487-495.

Pirrie, D., Butcher, A.R., Power, M.R., Gottlieb, P., Miller, G.L., 2004. Rapid quantitative mineral and phase analysis using automated scanning electron microscopy (QemSCAN); potential applications in forensic geoscience. *Geol. Soc*. 232, 123-136.

Plaza, C., Brunetti, G., Senesi, N., Polo, A., 2006. Fluorescence characterization of metal ion–humic acid interactions in soils amended with composted municipal solid wastes. *Anal. Bioanal. Chem*. 386, 2133-2140.

Senesi, N., Miano, T.M., Provenzano, M.R., Brunetti, G., 1991. Characterization, differentiation, and classification of humic substances by fluorescence spectroscopy. *Soil Sci.* 152, 259-271.

Tien, M., Kirk, T.K., 1988. Lignin peroxidase of *Phanerochaete chrysosporium*. *Methods Enzymol.*, 161, 238-299.

Wariishi, H., Valli, K., Gold, M. H., 1991. In vitro depolymerization of lignin by manganese peroxidase of *Phanerochaete chrysosporium. Biochem. Biophys. Res. Commun.,* 176, 269-275.

Zhang, Y., Liu, X., Osburn, C.L., Wang, M., Qin, B., Zhou, Y., 2013. Photobleaching response of different sources of chromophoric dissolved organic matter exposed to natural solar radiation using absorption and excitation–emission matrix spectra. PLoS One, 8, 77515-77528.

Chapter 3:

Characterization of cell free spent medium (CFSM) treated powdered activated carbon

3.1. Introduction

Characterization of the CM is central to defining its interactions with *P. chrysosporium*. DRGO may contain up to 7wt% of CM which usually exists as finely disseminated particles in the ore (Osseo-Asare et al., 1984; Abotsi and Osseo-Asare, 1986; Afenya, 1991; Marsden and House, 2006; Yang et al., 2013). Extraction of CM and the subsequent gold adsorption experiments indicated that elemental carbon and organic acids were most responsible for preg-robbing (Abotsi and Osseo-Asare, 1986). These components of DRGO may have been formed from precursors such as ligninolytic biomass by processes similar to coal formation (Hauck, 1975). Lignin can be actively metabolized by *P. chrysosporium* into smaller organic molecules (Tien and Kirk, 1984; Kirk and Farrell, 1987; Kersten and Cullen, 2007) and this ability of the microbe could be related to the observed reduction in preg-robbing by DRGO and carbon materials like anthracite and activated carbon (Ofori-Sarpong et al., 2013a). This is, however, mostly qualitative understanding and there is the need to determine the prominent pathways leading to reduction in $Au(CN)_2^-$ uptake.

Fundamental understanding of the mechanisms associated with the interaction between DRGO and CFSM derived from *P. chrysosporium* is necessary for designing an effective pre-treatment method. It has been proposed that the microbe affects gold uptake by carbonaceous matter through a combination of aromatic bond cleavage by enzymes, surface passivation by extracellular polymeric substances (EPS) and pore blockage by spores (Ofori-Sarpong et al., 2013a). These digestive enzymes may, however, be significantly influenced by factors like substrate specificity, pH, temperature, metal toxicity and immobilization (Tien and Kirk, 1984; Kirk and Farrell, 1987; Tien, 1988; Wariishi et al., 1991; Fu and Viraraghavan, 2001; Mielgo et al., 2003; Kersten and Cullen, 2007; Zeng et al., 2013). For example, enzyme selectivity for activated carbon can be either reduced, enhanced or unaffected over the time course of

treatment. The current l ack of such information necessitates this investigation on the products formed via PAC biodegradation.

3.2. Experimental

3.2.1. Materials

All reagents and powdered activated carbon (PAC) used were of special grade and supplied by Wako Chemicals, Japan. PAC was selected as a surrogate for natural carbonaceous matter due to its amorphous crystal structure, which shares some resemblance with the elemental carbon in RGO (Afenya, 1991). Additionally, activated carbon has been extensively applied on the industrial scale for the adsorption of $Au(CN)_2^-$ after cyanidation. Screening analysis of as-received PAC revealed a particle size distribution of 97% below 57 μm. Gold foil with approximately 94% purity (94.3% Au and 5.6% Ag) was provided by Imai Kinpaku Co., Ltd., Japan. Ultra-pure water produced by Millipore synergy unit was used throughout the experiment.

3.2.2. Growth culture and CFSM harvesting

Phanerochaete chrysosporium was cultured under the conditions previously described in section 2.1.1. Briefly, *P. chrysosporium* was cultured in a medium composed of 10 g glucose, 1.18 g succinic acid, 0.2 g ammonium tartrate, 1 mg thiamine, 0.4 mmol veratryl alcohol, 2 g KH_2PO_4, 0.5 g $MgSO_4$ and 0.1 g $CaCl_2.2H_2O$ per 1 L in addition to 70 mL trace element solution (3 g $MgSO_4.7H_2O$, 1 g NaCl, 0.5 g $MnSO_4.5H_2O$, 0.1 g $FeSO_4.7H_2O$, 0.1 g $CuSO_4$, 10 mg boric acid per 1 L) (Tien, 1988) at pH 4.0. All flasks were covered by porous caps to allow for aeration and incubated at 37°C under a stationary condition. After 7 days of fungal

growth, the fungal mass and spores were separated from the CFSM by a sterilized 0.22 µm stericup filter unit. The enzymatic activities of lignin peroxidase (LiP) and Mn peroxidase (MnP) in the filtrate were determined by veratryl alcohol (Tien, 1988) and Mn^{2+} assay (Wariishi et al., 1991). One unit (1U) of enzyme activity is defined as the amount of enzyme required to convert 1 µmol of substrate per minute. CFSM was used within a day of harvesting for PAC treatment. The total dissolved organic carbon (TOC) in the CFSM was determined using a Shimadzu VCSH analyser (Kyoto, Japan) in triplicate.

3.2.3. Enzymatic treatment

25 mg and 250 mg of PAC were separately added to 100 mL flasks with a porous cap and then sterilised by autoclave before enzyme treatment. Hereafter, they are named as PAC 5 and PAC 50, respectively. 50 mL of fresh CFSM was added to respective flasks and the pH was adjusted to 4.0 using either 1 M HCl or 1 M NaOH. After pH adjustment, the mixtures were shaken for enzymatic reaction at 30°C and 120 rpm for 14 days.

Separately, 50 ml of CFSM was autoclaved at 120 ºC, 1 bar for 20 min and then allowed to cool down. Afterwards, its MnP and LiP activities were determined before it was used to react with 25 mg PAC for observation of the physicochemical effects of CFSM on PAC. Hereafter the solid residue of this PAC sample is named as control PAC 5.

All experiments of bio-degradation with CFSM were conducted in duplicates. The filtrate and bio-modified PAC residue were collected periodically for characterization. The residual enzyme activity and total dissolved organic matter concentration of were also determined. The bio-modified solid was subjected to washing with ultrapure water assisted by ultra-sonication prior to solid analysis. Afterward, a portion of these bio-modified solids were supplied for various washing techniques using simple alcohols to remove the bio-chemicals on the surface

of PAC after CFSM treatment. The optimal procedure was washing with 2-propanol at 50°C for 5 min under ultra-sonication.

3.2.4. Characterization of pristine and bio-modified PAC

The chemical alterations in CFSM-treated PAC following the enzyme treatment were examined using X-ray diffraction (XRD), Fourier transformed infrared spectroscopy (FTIR) and ^{13}C-nuclear magnetic resonance spectroscopy (^{13}C-NMR), and measurement of zeta potential. The physical changes in the solid were determined by N_2 adsorption and scanning electron microscopy (SEM). Detailed information about these analytical techniques can be found in section 2.3.

3.2.5. Adsorption of $Au(CN)_2^-$

The Imai Kinpaku gold foil was used to prepare a stock solution of $Au(CN)_2^-$. 85.1 mg of gold foil was completely dissolved in 0.5 mL aqua regia with 1:2 volume ratio of 70% HNO_3 : 35% M HCl. After that, 5 mL of 28% ammonium hydroxide solution was added dropwise to precipitate gold oxide (Au_2O_3). The precipitate formed was washed with 500 mL of ultrapure water and subsequently dissolved in a 50 mL solution containing 0.08 g of KCN at pH 13 for 72 hrs to obtain $Au(CN)_2^-$ solution. The Au concentration was determined by a Perkin Elmer Optima 8300 ICP-OES (Massachusetts, USA). In this KCN treatment, the following ligand-promoted dissolution is expected:

$$Au_2O_3 + 4\ CN^- + 2\ H^+ = 2\ Au(CN)_2^- + H_2O + O_2 \qquad [3.1]$$

For adsorption experiments of $Au(CN)_2^-$, the original PAC, PAC after bio-treatment, and PAC after bio-treatment and washing were provided as adsorbents. 10 mg of PAC powder

samples were suspended in 4.0 mL of 0.254 mM $Au(CN)_2^-$ at pH 11.5, and then the mixture was shaken at 120 rpm and 25˚C using BR-40LF bio-shaker (Taitec Corporation, Saitama, Japan) in triplicate. This experiment was completed in 24 hrs and the remaining liquids were subsequently separated by filtration, and supplied for determination of the residual $Au(CN)_2^-$ concentrations by ICP-OES.

3.3. Results and Discussion

3.3.1. Enzyme activity in CFSM

Over the incubation period, *P. chrysosporium* secreted small quantities of the enzymes LiP and MnP. The fungal mycelium grew into a single mat-like body in 4 days of growth and the solution pH showed insignificant variation. The CFSM harvested after the incubation period of the fungus contained approximately 3.74 g/L of water-soluble organic carbon. This might have been derived from the organic reagents in the growth medium, bio-chemicals and metabolites produced by the fungal culture. Furthermore, these microbial secretions included very low enzymatic activities of 11.7 mU/mL for LiP and 68.3 mU/mL for MnP. This may have been due a limitation in the availability of oxygen to the microbe during the incubation period, which might have been caused by the volume of growth medium used for the cultivation (Tien, 1988). After determination of enzymatic activity in CFSM, biodegradation experiments were conducted and the changes in chemical and physical properties of PAC are presented in the next section. Autoclaved CFSM at 120 °C for 20 min, which was used in control biodegradation of PAC, revealed no enzymatic activity (Zeng et al., 2013).

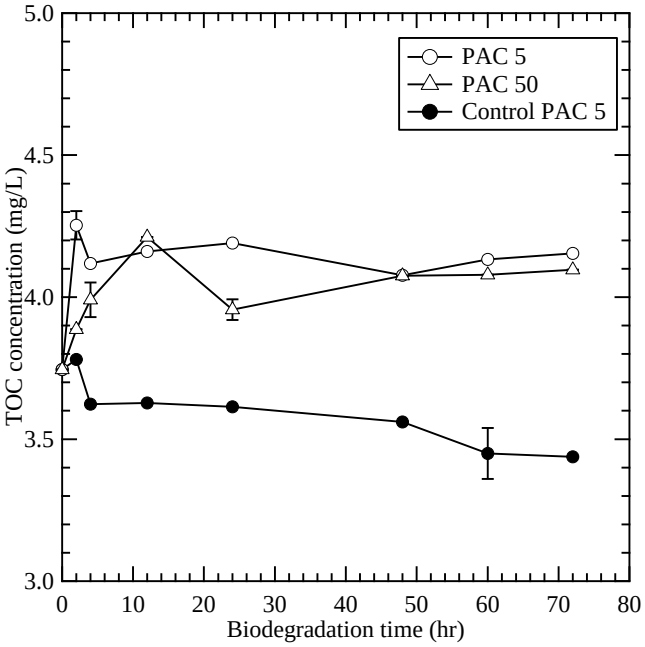

Figure 3. 1 Variation in TOC concentrations of PAC 5, PAC 50 and Control PAC 5 over 72 hrs. The vertical bars represent the standard error of three measurements.

3.3.2. Changes in TOC concentration after CFSM treatment of PAC

Fig. 3.1 presents the variations in TOC concentration during the degradation of PAC by CFSM. The Control PAC 5, which was treated with autoclaved CFSM, shows a steady decrease in the TOC concentration from 3.74 g/L to 3.45 g/L in 72 hrs. Compared with PAC 5, this trend may suggest that the enzymes in CFSM were essential for PAC degradation. Thus in the experiments using functional enzymes in CFSM (PAC 5 and PAC 50), there was an increase in the TOC concentrations over time. Comparatively, PAC 5 produced the highest TOC of 4.25 g/L and attained a faster equilibrium than PAC 50; nonetheless, the TOC concentration of both appears to be similar after 72 hrs regardless of the initial mass of PAC. The most likely products of this treatment would be smaller aromatic hydrocarbons, organic acids and other products (Huang et al, 2013).

3.3.3. Chemical alterations in PAC

FTIR spectra for bio-degraded PACs are shown in **Fig. 3.2.** As expected, the most prominent peak was observed around 1560 cm^{-1} in pristine PAC, which is assigned to the vibration mode of C=C bonding in aromatic carbons (Biniak et al., 1997). In the spectra of control PAC 5 and PAC 50 (3 and 14 days), this peak was quite unchanged from the pristine PAC. Also in the PAC 5 series, it did not disappear, but slightly shifted to the left side after 3 ~ 14 days, whereas a distinctive peak at 1265 cm^{-1}, assigned to aliphatic C-C bond was observed (Biniak et al., 1997; Shin et al., 1997). Additionally, there was a contrast between the PAC 5 series against the PAC 50 series and control PAC 5 with respect to a small shoulder peak at around 1750 cm^{-1}. This functional group which was ascribed to the lactonic C=O bond (Shin et al., 1997), gradually disappeared from the PAC 5 series with time. These results imply that biodegradation of aromatic carbons bonds and C=O bonding into aliphatic carbons had occurred in the PAC 5 series and this was due to the oxidizing conditions prevailing in CFSM. A definitive peak at 1695-1670 cm^{-1}, beside the shoulder peak assigned to lactonic C=O bond and attributed to carbonyl C=O bond (Shin et al., 1997), was not significantly changed after reaction with CFSM in any conditions.

According to ^{13}C-NMR analysis, degradation of aromatic C=C bond was clearly observed already after 3 days with PAC 5, as shown in **Fig. 3.3**. PAC 50 retained most of its aromatic C=C bonds after this time period while PAC 5 transitioned from aromatic C=C bonds to a mixture of aromatic and aliphatic C-H bonds (Mursito et al., 2010). Although, the ^{13}C-NMR data corroborated the findings of the FTIR spectra **(Fig. 3.2)** in the case of aliphatic functional groups**,** there was a disagreement with respect to the FTIR peak assigned to aromatic C=C bonds in PAC 5. This difference was most likely due to the limited natural abundance of ^{13}C, thus reducing the possibility of coupling between adjacent ^{13}C atoms (Mcmurry, 2012).

Altogether, FTIR and ^{13}C-NMR indicate that the extensive aromatic bonding in PAC was disturbed by CFSM treatment.

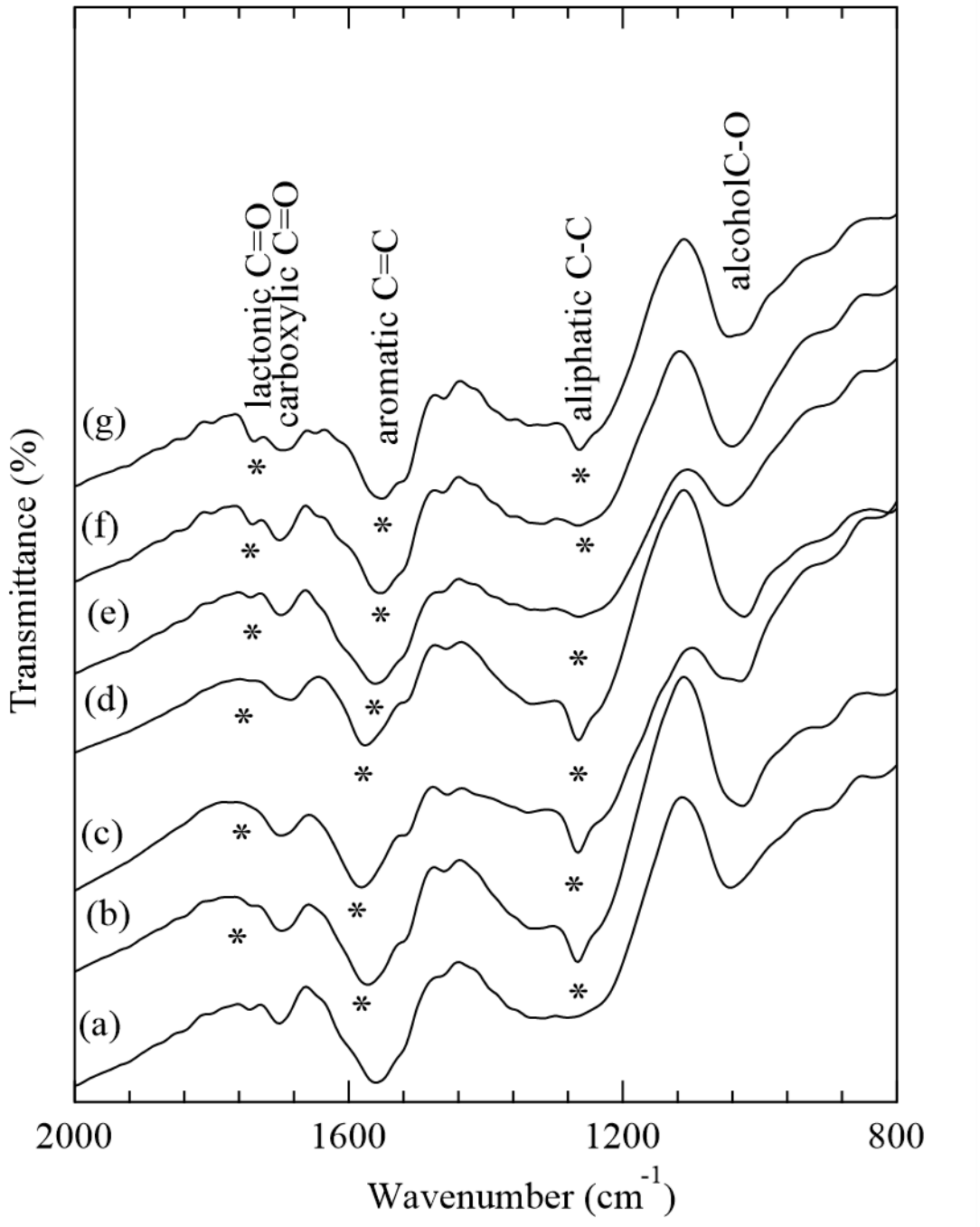

Figure 3. 2 FTIR spectra of (a) pristine PAC, (b) PAC 5 after 3 days, (c) PAC 5 after 7 days, (d) PAC 5 after 14 days, (e) PAC 50 after 3 days, (f) PAC 50 after 14 days, (g) Control PAC after 3 days.

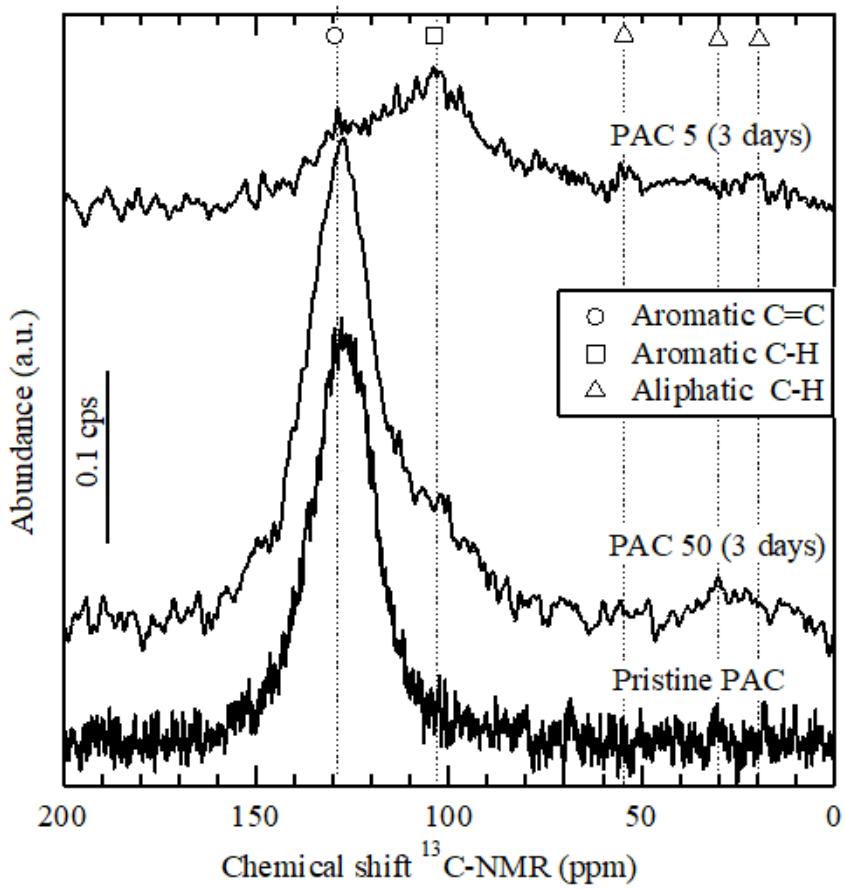

Figure 3. 3 ^{13}C-NMR spectra of the pristine PAC, PAC 50 after 3 days and PAC 5 after 3 days of bio-treatment.

3.3.4. Physical alterations in PAC

Physical characteristics of PAC after enzymatic treatment were investigated using N_2 adsorption for powdery characteristics, FE-SEM observation of surface morphologies and zeta potential measurements for surface charge. There was a steady decrease in BET specific surface area and pore volume of PAC 5 with increase in bio-treatment days (**Table 3.1**). The pristine PAC had a surface area of 1430 m^2/g and pore volume of 1.28 cm^3/g and 14 days of bio-treatment reduced it to 697 m^2/g and 0.69 cm^3/g respectively. Oxidative treatments are

generally known to reduce the surface area of PAC by collapsing pore walls and/or removing the crosslinks between aromatic rings (Huang et al., 2013).

The pores in PAC were comprised of micropores and relatively smaller mesopores **(Fig. 3.4(a), (b))**. The distribution of these pores illustrated that the highest frequency of pore volume and pore area existed at approximately 3 nm and 1.5 nm respectively. The size of the smallest measurable pore (0.6-0.7 nm) is comparable to the pores created by nano-sized crystallites of graphite (Lillo-Ródenas, et al., 2004; Beyssac and Rumble, 2014; Buseck and Beyssac, 2014). In some cases, the order and arrangement of these units produced the larger pores (mesopores and macropores) in carbon materials. All the PAC samples in **Fig. 3.4** displayed a decrease in intensity of frequency (in y-axis) without an increase in pore width (in x-axis) with increase in biodegradation time. This further shows that the aromatic bond cleavage was extensive.

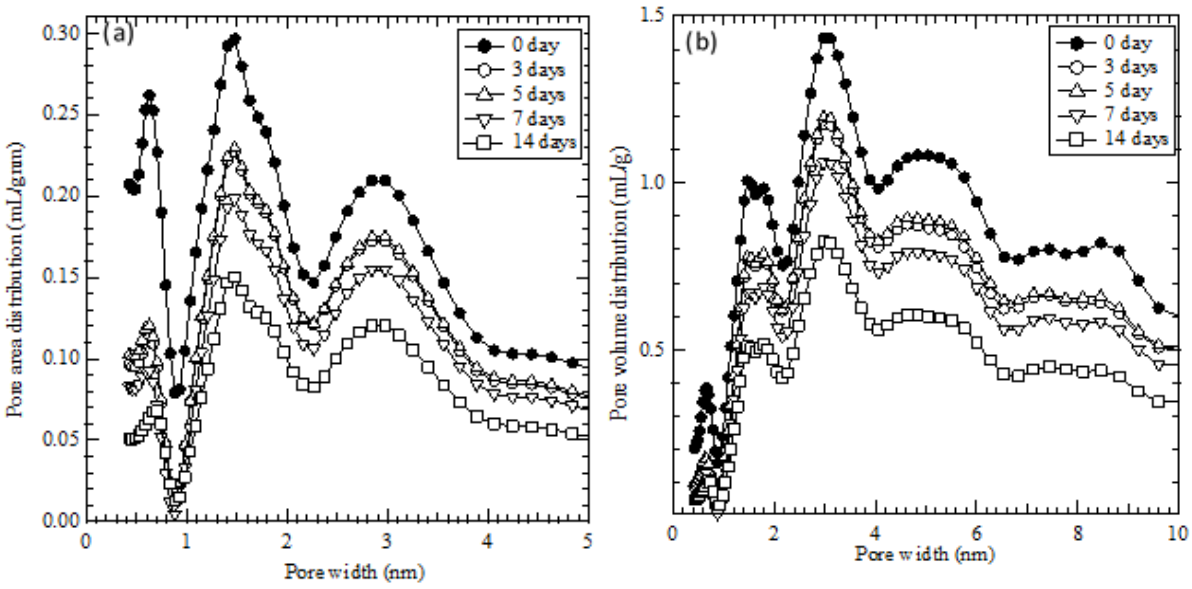

Figure 3. 4 Distribution of (a) pore area and (b) pore volume of PAC and PAC 5 after 3~14 days treatment with the cell-free spent medium (CFSM).

The SEM images of the pristine PAC sample seem to be quite smooth with this magnification (**Fig. 3.5(a, b**)). However, considering the specific surface area (**Table 3.1)** and pore size distribution **(Fig. 3.4(a))**, the pristine PAC should have very fine pores, which are invisible with this magnification (Lillo-Ródenas, et al., 2004). After biodegrading of PAC 5 for 3 days, the surface morphology was relatively unaffected **(Fig. 3.5(c, d))** despite the decrease in surface area (**Table 3.1).** Within 7~14 days of treatment, the solid surface became significantly porous and developed micrometer sized pores **(Fig. 3.5(e) ~ (h))**. Combining the results of N_2 adsorption (**Fig. 3.4** and **Table 3.1)** and FE-SEM observation, it can be concluded that increasing the enzymatic treatment time resulted in the collapse of the nano-sized pores which resulted in the formation of micron-size pores.

Table 3. 1 Changes in specific surface area and pore volume of PAC 5.

Treatment period (day)	**BET specific surface area (m^2/g)**	**Pore volume (cm^2/g)**
0	1430 ± 1.10	1.28 ±0.039
3	1050 ± 2.47	0.97± 0.004
5	1060 ± 2.21	0.99 ± 0.004
7	911 ± 2.13	0.87 ± 0.007
14	697 ± 1.89	0.69± 0.008

The bio-degradation of PAC may have proceeded through the immobilisation of the enzymes on the solid surface during the treatment. The initial zeta potential of PAC was slightly positive (3.1 mV) at pH 4.0, however, it decreased with time to approximately to -11.8 mV after 5 days of bio-degradation (**Fig. 3.6** right y-axis). This change may have been due to the presence of some negatively charged functional groups on the surface of CFSM-treated PAC, the most likely being some carboxylic groups (Chingombe et al, 2005). This interpretation is also consistent with the previous finding that adsorption of the anionic surfactants sodium dodecyl

sulfate (SDS) and dinonylnaphthalene sulfonic acid (HDNNS) on Prestea carbonaceous gold ore resulted in a more negatively charged solid/aqueous interface (Abotsi and Osseo-Asare, 1987).

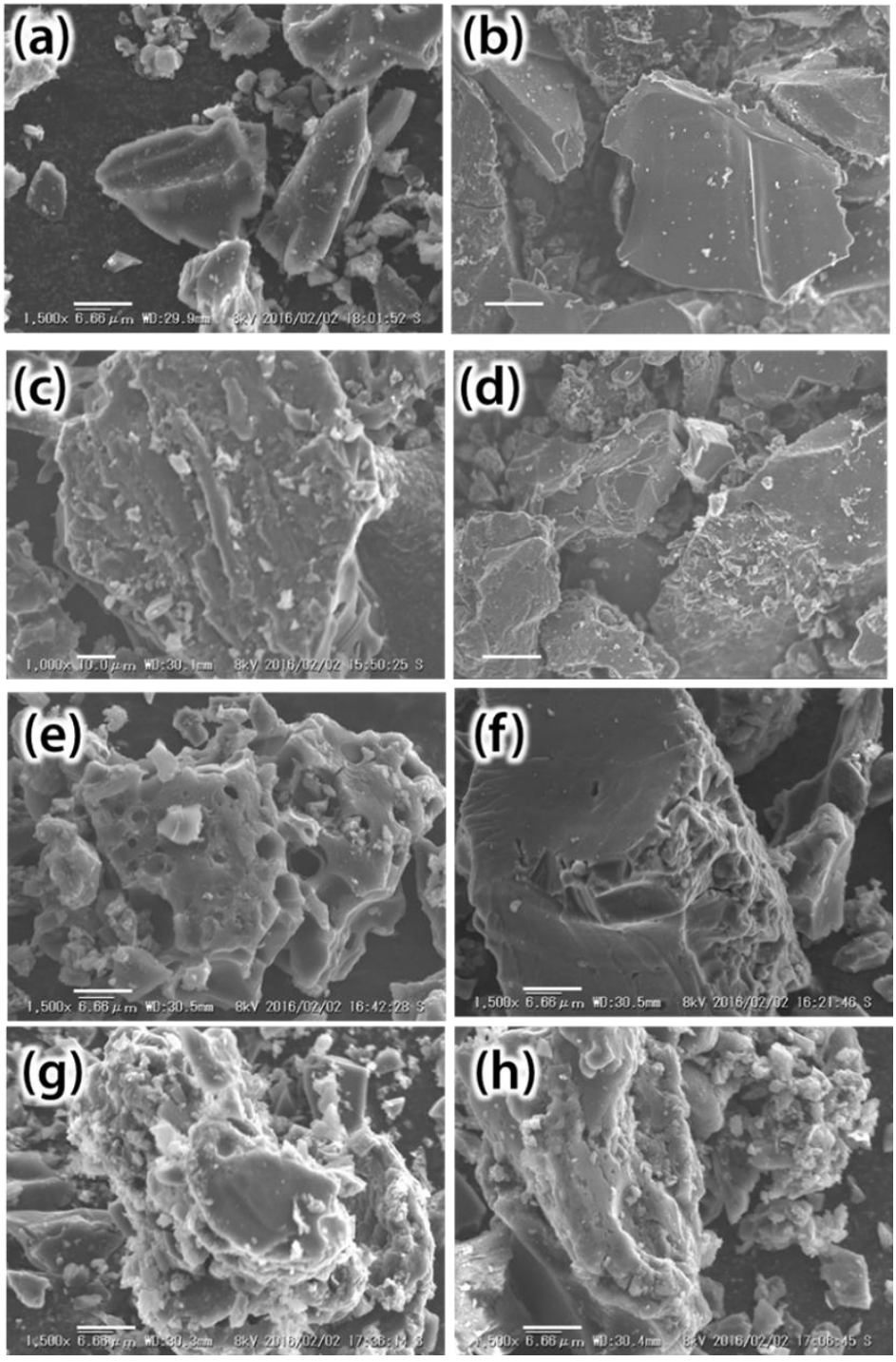

Figure 3. 5 SEM images for (a) and (b) the pristine PAC, (c) and (d) PAC 5 after 3 days, (e) and (f) PAC 5 after 7 days, (g) and (h) PAC 5 after 14 days. Horizontal bars indicate 10 μm.

Considering the point of zero charge of LiP and MnP which is between pH 3.3 to 4.7 (Tien and Kirk, 1984; Farrell et al., 1989; Glumoff et al., 1990), the electrostatic repulsion between negatively charged PAC and these enzymes might have been low enough for the immobilisation to occur through some non-covalent interactions (Li and Wen, 2009). This might explain the absence of MnP and LiP activity in the reaction mixture after 24 hrs of treatment. An alternative explanation for the loss in activity is that the enzymes were denatured during the PAC treatment and thus rendered inactive. This situation requires more study to be able to make a definitive determination.

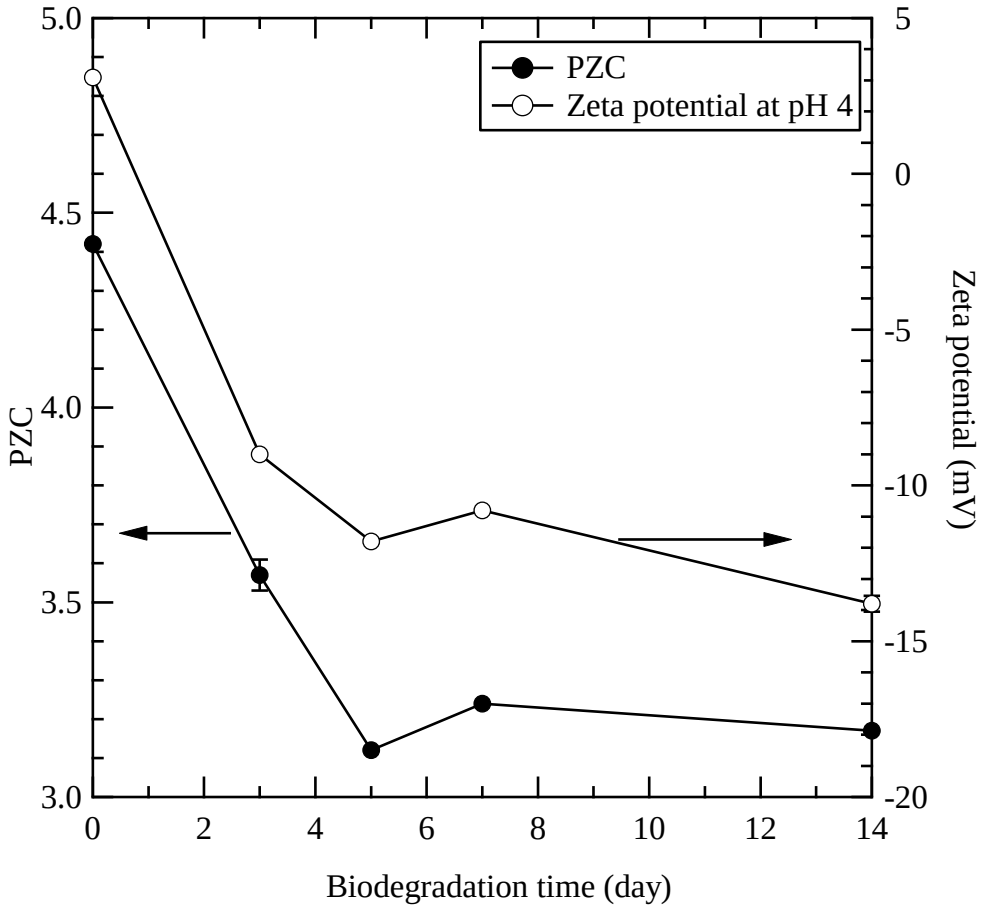

Figure 3. 6 The pH of zero charge (PZC) and zeta potential at pH 4 of pristine PAC and PAC 5 after 3~14 days treatment with CFSM depending on degradation time. The vertical bars represent the standard error of three measurements.

3.3.5. $Au(CN)_2^-$ adsorption

CFSM treatment of PAC was able to decrease $Au(CN)_2^-$ uptake through the cleavage of the aromatic C=C bonds and surface passivation by bio-chemicals in the filtrate. In the $Au(CN)_2^-$ uptake experiments, the possible effects of both factors should be taken into consideration to explain adsorption results. In preliminary experiments, a washing procedure to remove adsorbed bio-chemicals on PAC 5 was established using control PAC 5 with either ethanol or 2-propanol. The success of this procedure was evaluated by $Au(CN)_2^-$ uptake after washing (data are not shown). The control PAC 5 reduced $Au(CN)_2^-$ uptake by 25%. As previously mentioned, the autoclaved filtrate had no enzyme activity, so the possible reason for the decrease in adsorption of $Au(CN)_2^-$ is surface coverage by organic carbon present in the CFSM. These compounds reduced the sorption sites on PAC and thus, lessening its affinity for $Au(CN)_2^-$ when compared to the pristine PAC. To remove these substances, washing with 2-propanol for 5 min at 50℃ was chosen, since this procedure caused the least damage to $Au(CN)_2^-$ uptake behaviour of the pristine PAC.

The contribution of enzyme activity and/or surface passivation in $Au(CN)_2^-$ uptake by bio-treated PAC is illustrated by **Fig. 3.7**. The $Au(CN)_2^-$ uptake was significantly reduced within 12 hrs of enzyme treatment before it attained equilibrium after 3 days. According to the FTIR results (**Fig. 3.8)**, the washing procedure relatively reduced the peak intensities of aromatic C=C and C=N bonds at 1580 cm^{-1} (Biniak et al., 1997), of protein C-N bond at 1520 cm^{-1} (Shin et al., 1997) and of aliphatic C-C bond at 1270 cm^{-1} (Biniak et al., 1997) in all the 2-propanol washed solids that had previously undergone enzymatic treatment. After washing, the subsequent $Au(CN)_2^-$ uptake was comparatively higher for the 2-propanol washed solids than the unwashed solids up to 1 day. However, there was a reversal in this trend within 3-7 days of biodegradation. This change could be the result of the large fluctuation in the adsorption of $Au(CN)_2^-$ onto the washed PAC despite measurements in triplicate. This finding suggests that

within 3~7 days, the treatment produced a heterogeneous mixture of easily removable and less easily removable hydrocarbons on the surface of PAC. Since the CFSM did not have LiP activity after 0.5 day and MnP activity after 1 day, this process of biodegradation might have proceeded in the solid phase of microporous PAC. Further treatment continued until the 14th day and this resulted in an additional breakdown of the PAC which corresponded with a decreased $Au(CN)_2^-$ uptake. However, the surface was easily cleaned by 2-propanol, resulting in the similar $Au(CN)_2^-$ uptake to 0.5~ 1 day after washing.

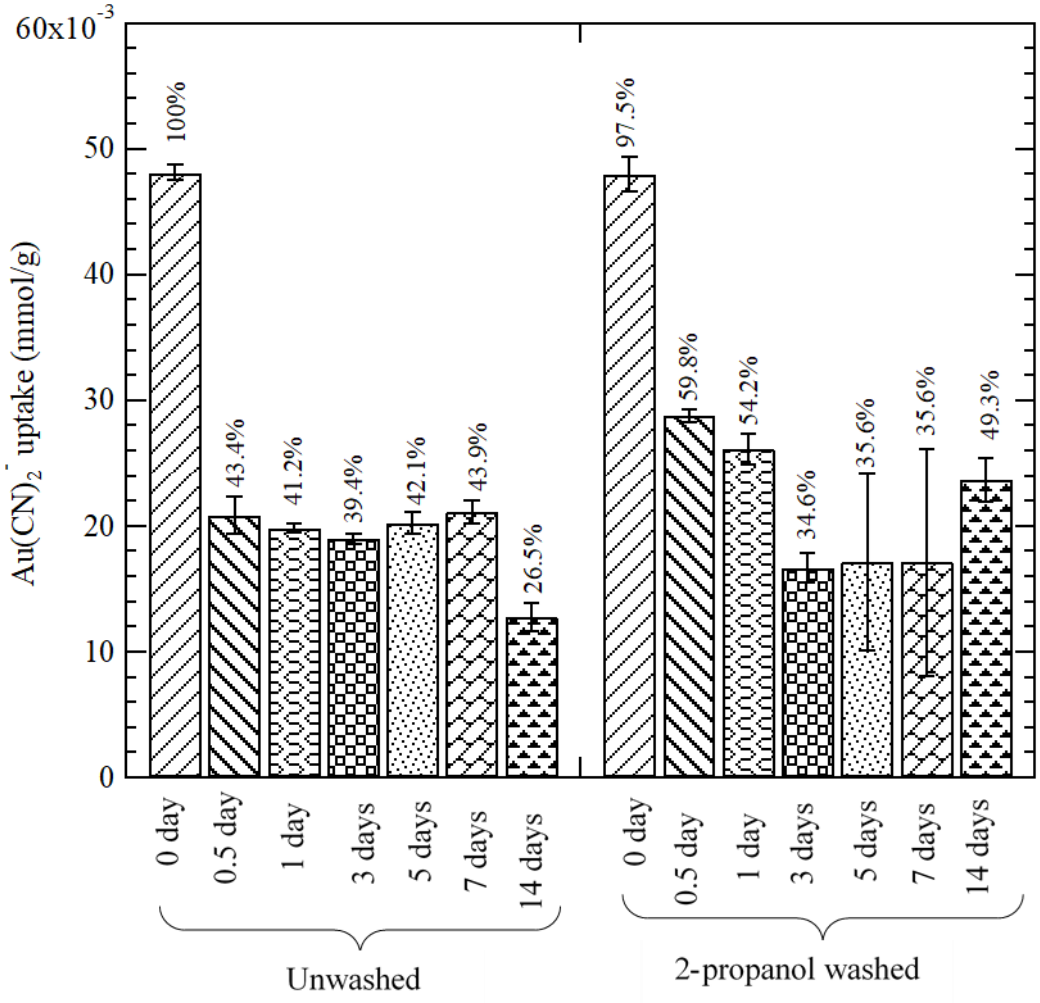

Figure 3. 7 Uptake of $Au(CN)_2^-$ on PAC and PAC 5 after different degradation days before and after washing with 2-propanol. The vertical bars represent the standard error of three measurements.

The combined effects of surface passivation of PAC by CFSM and washing with 2-propanol can be schematically illustrated as shown in **Fig. 3.9**. The original PAC is a very porous material and can significantly adsorb $Au(CN)_2^-$. Soon after contact with CFSM, the surface is intensively covered with the bio-chemicals in CFSM, for example the enzymatic proteins and sugars, leading to decrease in $Au(CN)_2^-$ uptake to 41-43%. Bearing in mind that even after removal of these bio-chemicals $Au(CN)_2^-$ uptake was still around 54-60%, it is apparent that the cleavage of aromatic C=C bonds happened to reduce the affinity with $Au(CN)_2^-$. Within 1 day of the biodegradation time, the specific surface area decreased and aromatic C=C bonds were cleaved. After several additional days of treatment, the more bio-degraded products were probably formed on the surface of PAC and partially removed along with bio-chemicals by washing with 2-propanol. However, the washing was not perfect, so the remaining substances inhibited $Au(CN)_2^-$ uptake (~35%). After 14 days, more bio-degradation products were gained, which resulted in a further reduction of $Au(CN)_2^-$ uptake to 26%, but these substances were more susceptible to 2-propanol washing probably due to their more fragile state. Finally, they were mostly washed out, recovering $Au(CN)_2^-$ uptake around 50%.

In summary, the biodegradation of carbonaceous matter may contribute to reducing $Au(CN)_2^-$ uptake in at least the following four aspects: (1) decrease in the specific surface area, (2) adsorption of bio-chemicals derived from CFSM, for example proteins and sugars, which have lower affinity for $Au(CN)_2^-$ than the original carbonaceous matter, (3) enzymatic degradation of aromatic C=C and C=N bonds, which are responsible for adsorption of $Au(CN)_2^-$, (4) bio-degraded products, for example aliphatic hydrocarbons, which have a lower affinity for $Au(CN)_2^-$ ions compared with aromatic hydrocarbons.

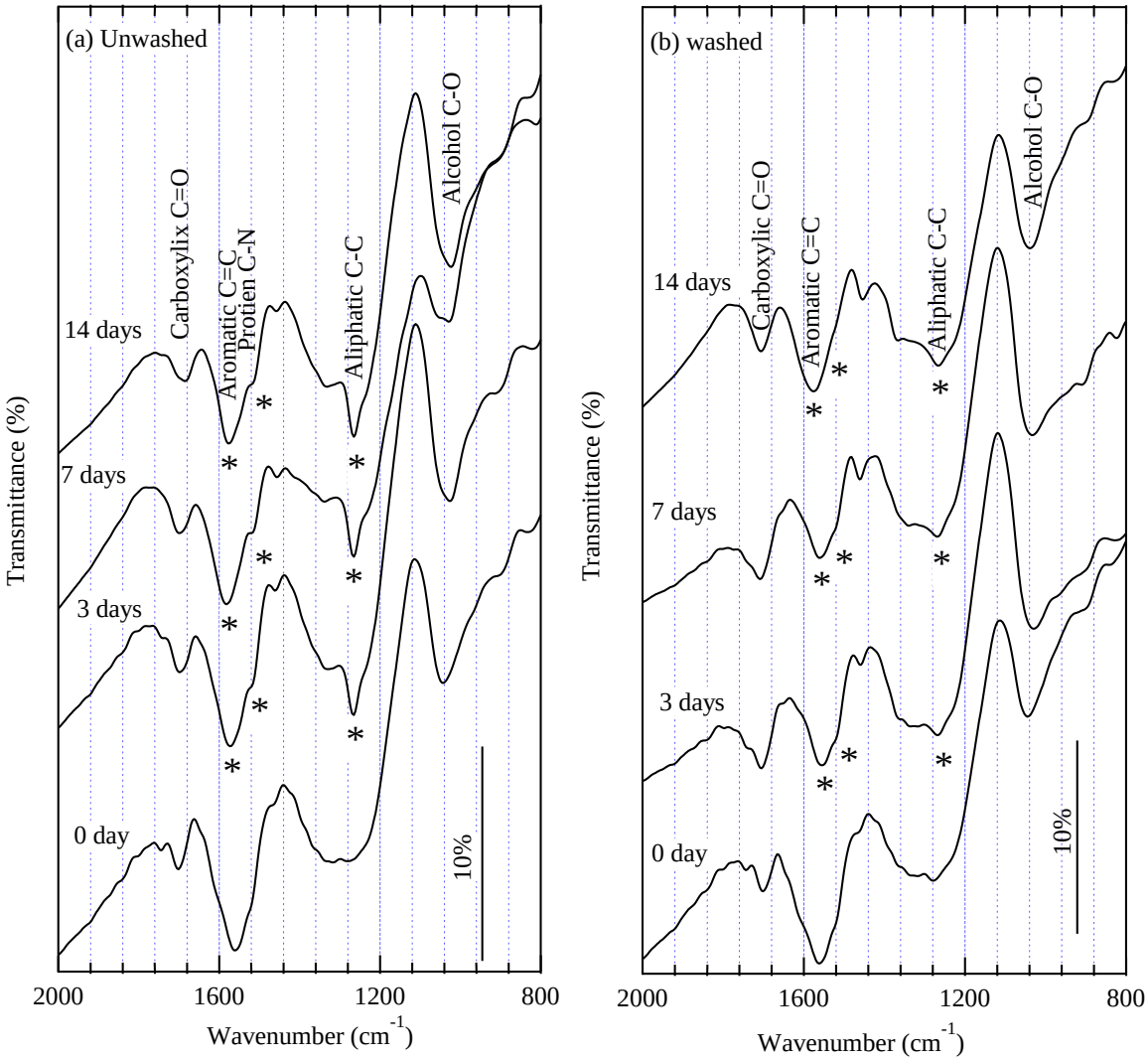

Figure 3. 8 FTIR spectra of pristine PAC and PAC 5 after 3~14 days treatment with CFSM. (a) before and (b) after washing with 2-propanol.

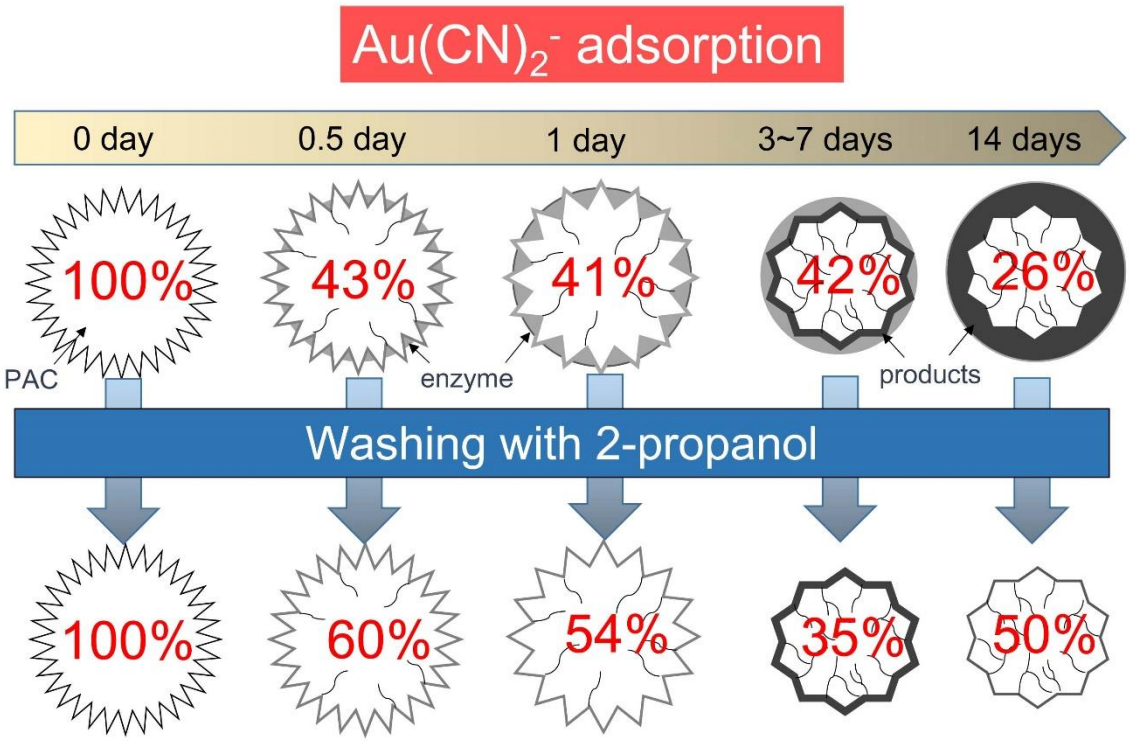

Figure 3. 9 Schematic illustration of biodegradation effects and washing effects of PAC on $Au(CN)_2^-$ uptake.

3.4. Conclusions

CFSM from *P. chrysosporium*, which includes the enzymes LiP and MnP at least, was prepared for degradation of powdered activated carbon (PAC) as a surrogate for carbonaceous matter in gold ores. The characterization results showed that enzyme treatment clearly affected the chemical stability of aromatic C=C bonds, the pore area distribution, and the specific surface area. The adsorbed amount of $Au(CN)_2^-$ on PAC after treatment with CFSM significantly decreased, possibly due to enzyme activity and surface passivation, while the heat-killed CFSM achieved a reduction in $Au(CN)_2^-$ uptake through surface passivation only. Thus, it can be concluded that CFSM released from *P. chrysosporium* is able to degrade the aromatic carbons including carbonaceous matter in refractory gold ores, leading to the reduction of $Au(CN)_2^-$ uptake, and there is negligible contribution of bio-chemicals to

adsorption of $Au(CN)_2^-$. However, the structurally transformed products from aromatic to aliphatic hydrocarbons might have contributed to reduce $Au(CN)_2^-$ uptake on the surface of PAC.

References

Abotsi, G. M. K., Osseo-Asare, K., 1986. Surface chemistry of carbonaceous gold ores I. Characterization of the carbonaceous matter and adsorption behaviour in aurocyanide solution. *Int. J. Min. Process.*, 18, 217-236.

Abotsi, G. M. K., Osseo-Asare, K., 1987. Surface chemistry of carbonaceous gold ores, II. Effects of organic additives on gold adsorption from cyanide solution. *Int. J. Min. Process.* 21, .225-239.

Afenya, P. M., 1991. Treatment of carbonaceous refractory gold ores. *Miner. Eng.*, 4, 1043-1055.

Amankwah, R. K., Yen, W.T., Ramsay, J. A., 2005. A two-stage bacterial pretreatment process for double refractory gold ores. *Miner. Eng.*, 18, 103-108.

Baldrian, M., 2003. Interactions of heavy metals with white-rot fungi. *Enzyme Microb. Tech.*, 32, 78-91.

Beyssac, O., Rumble, D., 2014. Graphitic carbon: a ubiquitous, diverse, and useful geomaterial. *Elements*, 10, 415-420.

Biniak, S., Szymanski, G., Siedlewski, J., Swiatkowski, A., 1997. The characterization of activated carbons with oxygen and nitrogen surface groups. *Carbon*, 35, 1799-1810.

Buseck, P. R., Beyssac, O., 2014. From organic matter to graphite: graphitization. *Elements*, 10, 421-426.

Chingombe, P., Saha, B., Wakeman, R. J., 2005. Surface modification and characterisation of a coal-based activated carbon. *Carbon*, 43, 3132-3143.

Farrell, R. L., Murtagh, K. E., Tien, M., Mozuch, M. D., Kirk, T. K., 1989. Physical and enzymatic properties of lignin peroxidase isoenzymes from *Phanerochaete chrysosporium*. *Enzyme Microb. Tech.*, 11, 322-328.

Fu, Y., Viraraghavan, T., 2001. Fungal decolorization of dye wastewaters: a review. *Bioresour. Technol.*, 79, 251-262.

Glumoff, T., Harvey, P. J., Molinari, S., Goble, M., Frank, G., Palmer, J. M., Smit, J. D. G., Leisola, M. S. A., 1990. Lignin peroxidase from *Phanerochaete chrysosporium*. Eur. J. Biochem., 187, 515-520.

Hauck, R. D., 1975. The genesis and stability of nitrogen in peat and coal. *Prepr. Div. Fuel Chem. American Chem. Soc,*. 20 (1975), 85-93.

Huang, Z., Liers, C., Ullrich, R., Hofrichter M., Urynowicz, M. A., 2013. Depolymerization and solubilization of chemically pretreated powder river basin subbituminous coal by manganese peroxidase (MnP) from *Bjerkandera adusta*. *Fuel*, 112, 295-301.

Kersten, P., Cullen, D., 2007. Extracellular oxidative systems of the lignin-degrading basidiomycete *Phanerochaete chrysosporium*. *Fungal Genet. Biol.*, 44, 77-87.

Kirk, T. K., Farrell, R. L., 1987. Enzymatic" combustion": the microbial degradation of Lignin. *Annu. Rev. Microbiol.*, 41, 465-501.

Li, J., Wen, X., 2009. Noncovalent immobilization of manganese peroxidases from *P. chrysosporium* on carbon nanotubes. *Frontiers Environ. Sci. Eng. China,* 3, 294-299.

Lillo-Ródenas, M. A., Cazorla-Amorós, D., Linares-Solano, A., Béguin, F., Clinard, C., Rouzaud, J. N., 2004. HRTEM study of activated carbons prepared by alkali hydroxide activation of anthracite. *Carbon*, 42, 1305-1310.

Marsden, J., House, I., 2006. The chemistry of gold extraction. SME, Englewood, USA, 147-224.

McMurry, J. E., 2012. Organic chemistry. Brooks/Cole Cengage Learning, Boston USA, 8th ed., 441-476.

Mielgo, I., Palma, C., Guisan, J. M., Fernandez-Lafuente, R., Moreira, M. T., Feijoo, G., Lema, J. M., 2003. Covalent immobilisation of manganese peroxidases (MnP) from *Phanerochaete chrysosporium* and *Bjerkandera sp*. BOS55. *Enzyme Microb. Tech.*, 32, 769-775.

Mursito, A. T., Hirajima, T., Sasaki, K., 2010. Upgrading and dewatering of raw tropical peat by hydrothermal treatment. *Fuel*, 89, 635-641.

Nanthakumar, B., Pickles, C. A., Kelebek, S., 2007. Microwave pretreatment of a double refractory gold ore. *Miner. Eng.*, 20, 1109-1119.

Ofori-Sarpong, G., Amankwah R. K. Osseo-Asare, K., 2013a. Reduction of preg-robbing by biomodified carbonaceous matter–A proposed mechanism. *Miner. Eng.*, 42, 29-35.

Ofori-Sarpong, G., Osseo-Asare, K., Tien, M., 2013b. Pretreatment of refractory gold ores using cell-free extracts of *P. chrysosporium*: a preliminary study. *Adv. Mater. Res*., 825, 427-430.

Ofori-Sarpong, G., Tien, M., Osseo-Asare, K., 2010. Myco-hydrometallurgy: Coal model for potential reduction of preg-robbing capacity of carbonaceous gold ores using the fungus, *Phanerochaete chrysosporium*. *Hydrometallurgy*, 102, 66-72.

Osseo-Asare, K., Afenya, P. M., Abotsi, G. M. K., 1984. Carbonaceous matter in gold ores: isolation, characterization and adsorption behavior in aurocyanide solutions. *Prec. Met.: Min. Extrac. Proc., Metallurgical society of AIME*, Englewood, USA, 125-144.

Shin, S., Jang, J., Yoon, S. H., Mochida, I., 1997. A study on the effect of heat treatment on functional groups of pitch based activated carbon fiber using FTIR. *Carbon*, 35, 1739-1743.

Tien, M., Kirk, T. K., 1984. Lignin-degrading enzyme from *Phanerochaete chrysosporium*: purification, characterization, and catalytic properties of a unique H_2O_2-requiring oxygenase. *Proc. Natl. Acad. Sci. USA, 81*, 2280-2284.

Tien, M., Kirk, T.K., 1988. Lignin peroxidase of *Phanerochaete chrysosporium*. *Methods Enzymol.*, 161, 238-299.

Wariishi, H. Valli, K., Gold, M. H., 1992. Manganese (II) oxidation by manganese peroxidase from the basidiomycete *Phanerochaete chrysosporium*: kinetic mechanism and role of chelators. *J. Biol. Chem.*, 267, 23688-23695.

Yang, H. Y., Qian, L. I. U., Song, X. L., Dong, J. K., 2013. Research status of carbonaceous matter in carbonaceous gold ores and bio-oxidation pretreatment. *Trans. Nonferrous Met. Soc. China*, 23, 3405-3411.

Zeng, G. M., Zhao, M. H., Huang, D. L., Lai, C., Huang, C., Wei, Z., Xu, P., Li, N. J., Zhang, C., Li, F. L., Cheng, M., 2013. Purification and biochemical characterization of two extracellular peroxidases from *Phanerochaete chrysosporium* responsible for lignin biodegradation. *Int. Biodeter. Biodegr*., 85, 166-172.

Chapter 4:

Sequential pre-treatment of double refractory gold ore (DRGO) with a thermophilic iron oxidizing archaeon and fungal crude enzymes

4.1. Introduction

The heterogeneous composition of naturally occurring gold ores has a significant impact on the metal yield during ore processing. Consequently, the ease of gold recovery has been adopted as a tool for classifying ore bodies in hydrometallurgical processing. The type of ores, in order of increasing difficulty, are alluvial ores, free milling ores and refractory ores (Lunt and Weeks, 2016). Currently, refractory gold ores make up about one-third of the total gold production from natural ores, and they typically yield about <50% of gold in average during direct cyanidation regardless of gold grade (Ofori-Sarpong et al., 2013; Yang et al., 2013). Refractory behavior can result from several factors, including the locking of gold in metal sulfides like pyrite and arsenopyrite, and preg-robbing by carbonaceous matter (Cook and Chryssoulis, 1990; Ofori-Sarpong et al., 2013; Chen et al., 2014). In cases where the ore contains both of these components, a very low gold recovery may be observed and as such, it is classified as a double refractory gold ore (DRGO). In some cases, gold recovery from such types of ore was abandoned.

Recovering gold from DRGO necessitates the use of some ore pre-treatment techniques prior to cyanidation to remove or minimize the effects of the sulfides and carbonaceous matter. Methods like bio-oxidation or pressure oxidation of sulfides and blanking followed by Resin-in-leach have already been established to treat these refractory components (Afenya, 1991; Miller and Brown 2005; Thomas, 2005). Recent studies have shown that pyrite, arsenopyrite and carbonaceous matter can be decomposed by the white-rot basidiomycetes *Phanerochaete chrysosporium* (Ofori-Sarpong et al., 2011; 2013; Liu et al., 2013; Konadu et al., 2017). It is accomplished by producing lignin-degrading enzymes such as lignin peroxidase and manganese peroxidase for the degradation of carbonaceous matter (Tien and Kirk 1988; Wariishi et al., 1991; Fujian et al., 2001). Additionally, the microbe synthesizes hydrogen peroxide for the activation of the peroxidase enzymes. A beneficial side effect of the presence

of hydrogen peroxide is that it is a highly oxidizing agent capable of degrading sulfide minerals (Kersten and Kirk, 1987; Ofori-Sarpong et al., 2013).

Despite its usefulness, the major drawback of using *P. chrysosporium* is that the biomass often attaches directly onto the ore during its growth. This is problematic because the fungal biomass might aggregate individual particles in the ore, which would reduce the available particle surface for cyanidation and result in gold recovery losses (Marsden and House, 2006). To avoid this problem, the cell-free spent medium (CFSM) of the *P. chrysosporium* was used to treat the DRGO. Previous research using the CFSM to treat activated carbon, as a surrogate for the carbonaceous matter, showed that the preg-robbing ability of the activated carbon could be decreased significantly (Konadu et al., 2017). However, preliminary tests conducted with CFSM in the presence of activated carbon and sulfides showed a minimal impact, on either pyrite decomposition or reducing gold uptake. This might have been due to the increased competition for the finite amounts of secreted enzymes and hydrogen peroxide in the CFSM. Therefore, the thermo-acidophilic iron-oxidizing archaeon, *Acidianus brierleyi*, was selected to aid in the fast decomposition of sulfide so that the CFSM could primarily decompose the carbonaceous matter.

This work is aimed at determining the treatment sequence that would significantly increase gold recovery. Furthermore, an in-depth analysis of the ore mineralogy was conducted by quantitative evaluation of minerals by scanning electron microscopy (QEMSCAN) (Goodall et al., 2005; Pascoe et al., 2007). This will help to expand the current understanding of the changes that occur especially during the bio-oxidation of refractory components by the CFSM. This study would thus help to generate interest in the processing of very refractory gold ores.

4.2. Experimental

4.2.1. Sample preparation and characterization

The sample used in this work was part of the flotation concentrate obtained from a mine in the Prestea Bogoso gold mining region in Ghana. Two kilograms of double refractory gold ore (DRGO) was split manually with a riffle to obtain 1 kg of samples, one of which was washed twice with 2 L of warm ultra-pure water and finally washed with 700 mL of 70% ethanol to remove surfactants used for sulfide flotation. The solid was collected by filtration and then dried under a continuous vacuum at room temperature before being subsequently split into smaller portions by a centrifugal separator. The sample had a P_{80} of 75µm.

The flotation concentrate was subsequently subjected to characterization prior to the following bio-treatments without sieving. Major elemental compositions were determined by X-ray fluorescence spectrometry (XRF, ZSX Primus II), and minor and trace elements were determined by inductively coupled plasma-optical emission spectrometry (ICP-OES, Perkin Elmer Optima 8300) after acid digestion. Carbon contents and carbonaceous compounds were evaluated by CHN analysis (Yanaco CHN MT-5) and thermogravimetric- differential thermal analysis (TG-DTA, Bruker 2000SA), respectively. Morphological characteristics were observed by field emission scanning electron microscopy (FE-SEM, FEI NOVA NANOSEM 230 with field emission). Mineralogical compositions were determined by XRD (Rigaku Ultima IV; Cu Kα 40 kV, 40 mA), and QEMSCAN (FEI 650F; 25 kV, 10 nA and field step of 0.5 -4 µm).

The gold content of the original DRGO was determined as follows: roasting 0.4 g of the sample in air at 800°C for 6 hrs, followed by the microwave digestion of about 50 mg of sample in a solution of 6 mL 35% HCl, 2 mL 99.9% HF and 2 mL 60% HNO_3 for 45 min at 180°C, and then determination of the dissolved gold by induced coupled plasma-mass spectrometry (ICP-MS, Agilent 7500c). The Au content in the original DRGO was determined to be 40.4 g/t; such a high grade is to be expected (Ofori-Sarpong et al., 2013) since the sample under investigation is a sulfide flotation concentrate.

4.2.2. Bio-treatment of DRGO

The flotation concentrate was treated by four routes in order to decompose sulfides and carbonaceous matter as shown in **Fig 4.1**. These treatments were: (i) sulfide decomposition by *A. brierleyi* only (DA); (ii) Carbonaceous matter and sulfide decomposition by CFSM only (DC); (iii) *A. brierleyi* followed by CFSM (DAC); and (iv) CFSM followed by *A. brierleyi* (DCA). The sections below show typical *A. brierleyi* and CFSM treatment procedures.

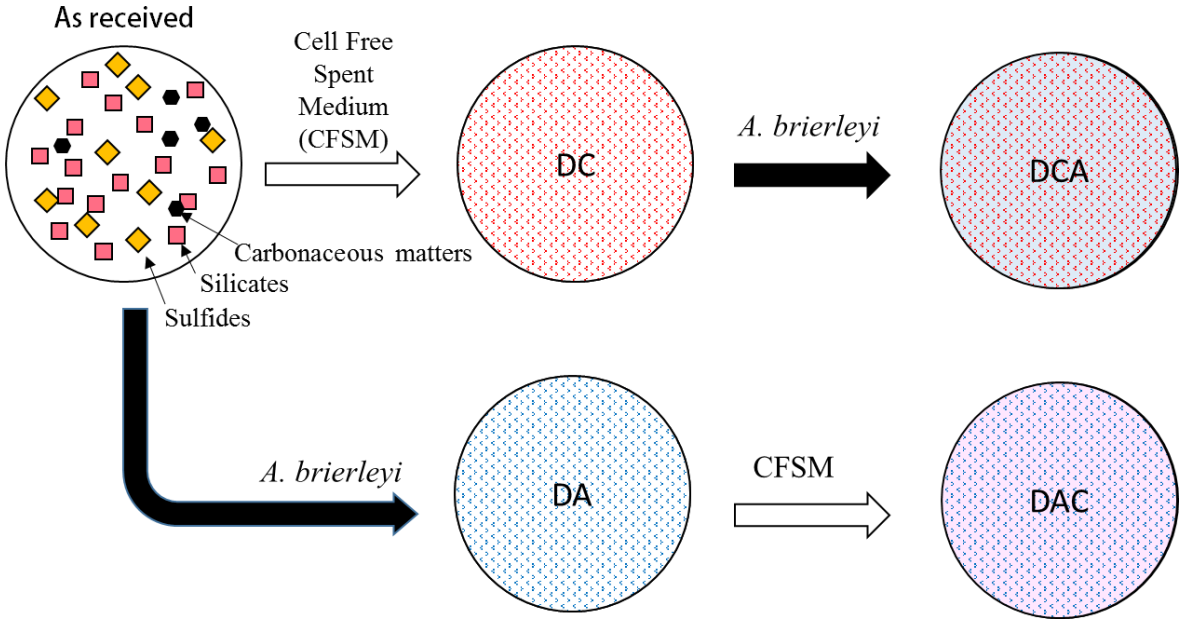

Figure 4. 1 Two pathways of sequential bio-treatment and nomenclature of the solid residues after bio-treatment.

4.2.2.1. Treatment of sulfides in DRGO by A. brierleyi *(DA)*

A. brierleyi (DSMZ 1651) was cultured in 500 mL Erlenmeyer flasks with the same composition as previously stated in section 2.1.2. To summarise, 200 mL of medium was prepared containing 4 mL of heterotrophic basic salts, 5 mM $FeSO_4.7H_2O$, 0.04% yeast extract. The pH was adjusted to 1.5 using 1 M H_2SO_4, and then the flasks were incubated at 70°C and 120 rpm in a shaker. These conditions were maintained throughout the *A. brierleyi* treatment unless stated otherwise. The archaeon was preliminarily adapted to the 50 g/L DRGO, 5 mM

$FeSO_4.7H_2O$ in 200 mL for 8 days. The cells were separated and collected by two-step centrifugation at 2000 rpm for 10 min and 10000 rpm for 15 min. The cells were re-suspended in sterilized pure water and then used as an inoculate for the DRGO treatment.

40 g of DRGO was added to 800 mL of the HBS medium including 0.04% yeast extract and 5 mM of $FeSO_4.7H_2O$ at pH 1.4 in 2 L Erlenmeyer flasks in triplicate, where 10^7 cell/ml of *A. brierleyi* was inoculated. The flasks were kept at 70°C and 120 rpm for 14 days and supernatants were regularly taken to monitor pH, Eh (vs SHE), total Fe concentrations and cell density. The pH, Eh and dissolved Fe concentrations were determined, respectively by electrodes and ICP-OES. Cell densities were directly counted under microscopic observation. A sterilized control experiment was conducted in parallel under the same conditions without inoculation of the archaea cells. This process is named as DA.

4.2.2.2. Treatment of DRGO with cell-free spent medium (CFSM) for P. chrysosporium *(DC)*

Liquid cultures of *P. chrysosporium* for CFSM production were prepared with the same composition as the solid agar cultures in section 2.1.1. This microbe was grown in 500 mL of the above medium at pH 4.0 ± 0.1 in a 2 L-flask. All flasks were covered by porous plugs to allow for aeration and incubated at 37°C under stationary conditions. After 3 days of fungal growth, CFSM was recovered to separate from the fungal tissues and spores by a sterilized 0.22 µm stericup filter unit. Since manganese peroxidase (MnP) and lignin peroxidase (LiP) activities in CFSM were confirmed by simultaneous determination using a capillary electrophoresis assay elsewhere (Kudo et al., 2017), CFSM can be regarded as the crude enzyme including MnP and LiP. The liquid (CFSM) was immediately used for biodegradation of DRGO. The fungal growth and harvesting process was repeated four times to provide fresh enzymes for the treatment of DRGO.

25 g of DRGO was added to 500 mL of CFSM in four 2 L-flasks. The flasks were covered by porous plugs and kept at pH 4.0, 30°C and 128 rpm for 3 days. After that, the solid was collected by centrifugation before being re-suspended in a fresh batch of CFSM. This process was repeated five times. After the final step, the solid residues were collected and washed with ultra-pure water before being dried under vacuum. This process is named as DC.

4.2.3. Gold recovery

0.4 g of the as-received sample and treated residues were suspended in 8.5 mL of 1 M NaOH to remove alkaline soluble by-products of the CFSM treatment of the carbonaceous matter. The washing was conducted for 24 hrs at 120 rpm and room temperature. Afterwards, the solid mass was collected, washed thrice with ultrapure water before being dried under vacuum overnight. Each bio-treatment was evaluated by the gold recovered in triplicate (n =3). 0.1 g samples of solid residues from DA, DC, DAC and DCA were suspended in 2 mL of 2.5 mM KCN at pH 12 (adjusted by 0.01 M NaOH) for 24 hrs at 125 rpm. The solid was allowed to settle, and then the supernatant was collected by filtration. The gold concentrations were determined by ICP-MS.

4.3. Results and Discussion

4.3.1. Bio-oxidation of sulfides by A. brierleyi

The oxidation of sulfides in DRGO by *A. brierleyi* was monitored by pH, Eh, dissolved Fe and cell density over 14 days on DA and DCA as shown in **Fig. 4.2**. **Figure 4.2a** generally showed that the pH increased from 1.4 to 1.5-1.7 within 2 days for all samples except for DCA, in which it took 4 days. The pH increase was probably due to decomposition of small amounts of alkaline oxides and hydroxides present in the DRGO. After this period, pH either steadied

or started to reduce due to acid production resulting from sulfide decomposition (**Fig. 4.2a**). The Eh, cell density and total Fe concentration (**Fig. 4.2b-d**) clearly showed that *A. brierleyi* was able to decompose Fe-bearing sulfides dominated by pyrite and arsenopyrite in as-received concentrate (DA), while the growth of the *A. brierleyi* appears to have been inhibited on DCA, possibly due to sulfide surface being covered by some biomolecules and/or secondary formed Fe-oxide phases derived from the CFSM treatment. Also, it was observed that Fe oxidation attained equilibrium between 10 and 14 days. The results of further investigations on the solid residue of the sequential treatments are presented below.

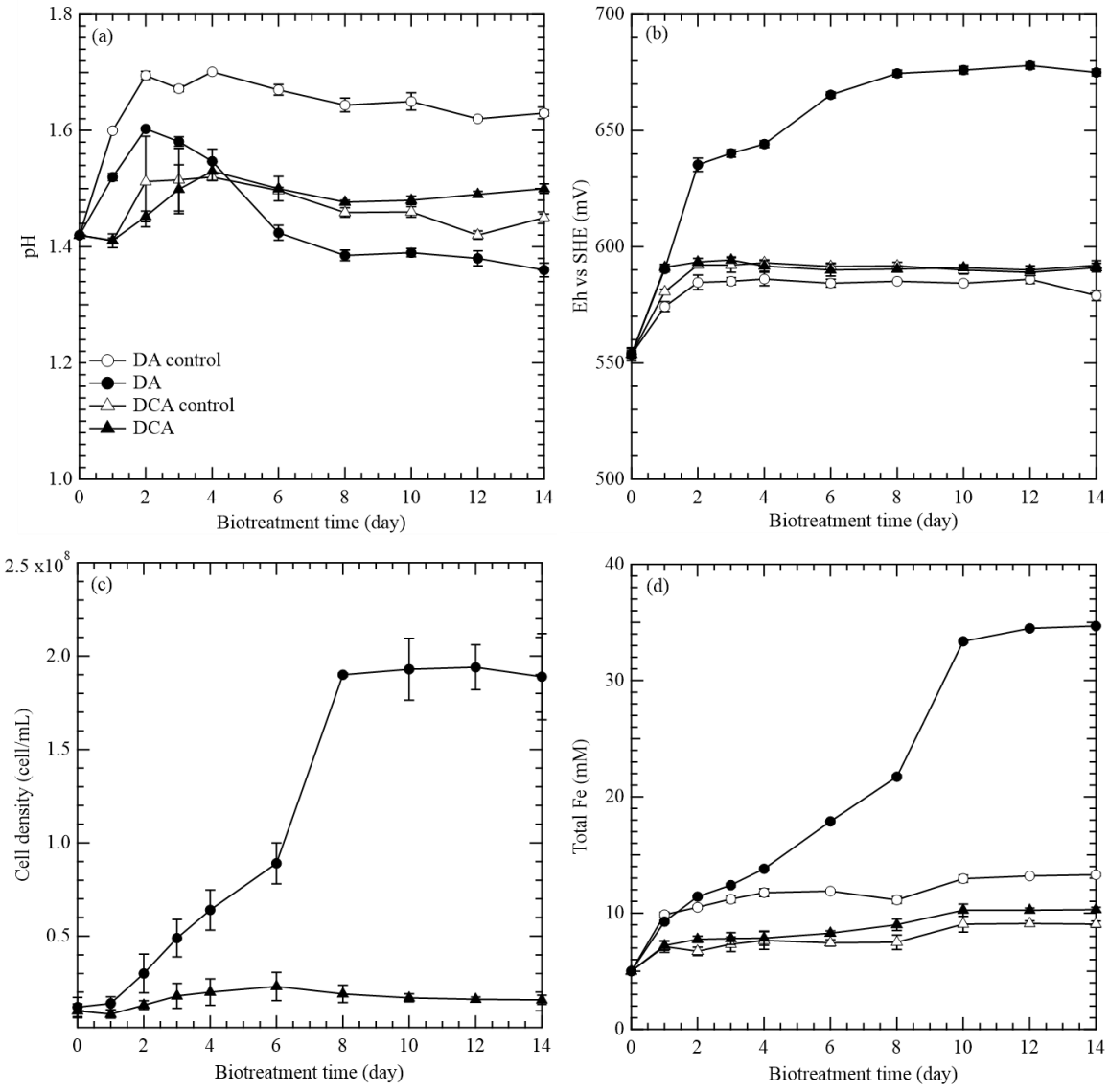

Figure 4. 2 Changes in (a) pH, (b) Eh vs SHE, (c) cell density, and (d) Fe concentrations with time of biooxidation by A. brierleyi. Symbols: ○, DA control; ●, DA; △, DCA control; ▲, DCA (n=3).

4.3.2. Bio-oxidation of sulfides and carbonaceous matter by CFSM

Sulfide and carbonaceous matter decomposition by the CFSM were determined by TG-DTA for the samples that were collected before and after the various bio-treatment options, and the results are presented in **Fig. 4.3**. The as-received (DRGO) and the DA sample showed a gradual weight loss of 1.97% and 2.97% respectively from room temperature to 430°C, and this change was most likely due to the release of physically adsorbed water and the interlayer water molecules from clay minerals (Shvarzman et al., 2003). A further weight loss of 12.6% and 10.3% was observed between 430°C and 800°C, which can be ascribed to the exothermic oxidation of sulfides and carbonaceous matter (CM1) (**Fig. 4.3a** and **4.3b**). **Fig. 4.3c** shows that the sulfides and carbonaceous matter decomposition at 460°C and 580°C respectively occurred at a relatively equal rate in the as-received sample. On the other hand, carbonaceous matter decomposition occurred at a higher rate than sulfide decomposition in the DA sample. This indicates that the sulfide content in the as-received sample was lowered after the DA treatment, which supports the results in **Fig. 4.2**.

Comparatively, treating the as-received and the DA sample with CFSM resulted in the DC and DAC residues decomposing in three temperature regions of room temperature to 200°C, 200°C to 430°C and 430°C to 800°C. Additionally, the weight loss ensued at a very rapid rate in the range of 200°C - 430°C for DC and DAC compared with the as-received sample (**Fig. 4.3a**). This change was not due to the removal of water because the DTA result shows that the reaction was exothermic in nature (**Fig. 4.3b**). It can be supposed that the oxidative CFSM treatment of the as-received sample (DC) and the DA residue (DAC) might have introduced

some new by-products (CM2 in **Fig. 4.3c**), which were much less stable than either carbonaceous matter (CM 1 in **Fig. 4.3c**) or pyrite. The possible products of the CFSM treatment are fungal biomass (Yu et al., 2013), organic by-products, and iron hydroxides; however, the exothermic DTA profile discounts iron oxides indicating that this new substance might be organic in nature (Balek and Subrt, 1995), therefore, it labelled as CM2. Finally, in the high-temperature region of 430°C - 800°C, it was observed that the relative amount of carbonaceous matter had decreased in the DC compared to the as-received sample, which was the result of the CFSM treatment (**Fig. 4.3c**). Furthermore, the DAC sequence also showed that the CFSM treatment had decomposed the carbonaceous matter while also improving upon the sulfide removal by *A. brierleyi*.

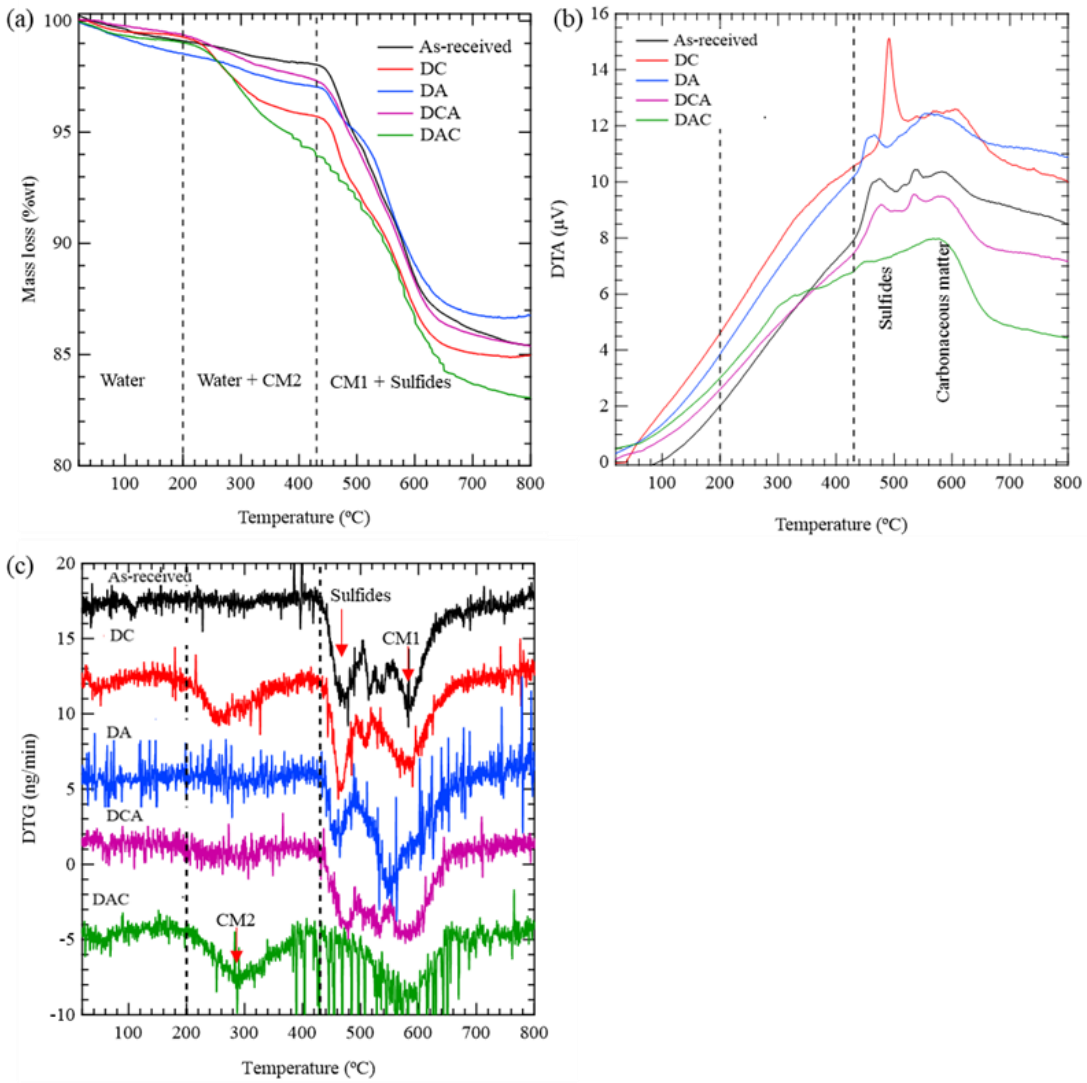

Figure 4. 3 Thermal decomposition characteristics of the as-received sample (DRGO) and the bio-treated residues of DA, DC, DCA and DAC showing (a) mass loss, (b) DTA and (c) DTG. CM1; Carbonaceous matter in the as-received sample and CM2; an organic by-product of CFSM treatment.

4.3.3. Bulk mineralogy by QEMSCAN

The XRD pattern for the flotation concentrate indicates the presence of silicates such as quartz, muscovite, and illite as the major mineral phases and pyrite as a minor phase (**Fig. 4.4**). Furthermore, these silicate phases appeared not to have been affected by either the CFSM or archaea treatment. The XRD patterns for the residues after bio-treatment DA and DAC showed some decreases in the intensity of XRD peaks assigned to pyrite, and this phenomenon was not observed for DC and DCA. This is consistent with the water chemistry results in **Fig. 4.2d**, showing that the oxidative dissolution of Fe-bearing sulfides was caused by *A. brierleyi* in DA and was not observed in DCA. Additionally, it revealed that the CFSM was unable to significantly decompose the sulfides (DC) when it was used directly on the as-received sample. However, the opposite result was observed when the CFSM treatment was conducted after using *A. brierleyi* (DAC), with the predominant peak for pyrite at 2θ 33.8˚disappearing entirely. Quantification of the remaining pyrite in DAC was not readily available in XRD, so QEMSCAN was applied to determine the elemental and mineralogical compositions of the DRGO and bio-treated samples, based on the XRD (**Fig 4.4**), XRF (not shown) and size analysis (**Fig 4.5**). **Fig. 4.5** shows that all the samples were separated into three size fractions using 53 µm and 10 µm sieves. The -10 µm size fraction constitute about half of the as-received sample, and this percentage was not significantly changed after any of the bio-treatments. This illustrated that most of the non-reactive silicates might have been in the size fraction under 10 µm. The most significant alteration in the size analysis was observed for DAC, where the +53 µm size fraction decreased significantly with an accompanying increase in the -53 µm + 10 µm

fraction. Combining this result with pyrite decomposition observed in **Figs. 4.2** and the decrease in the +53 size fraction observed in **Fig. 4.5** for DA and DAC, it indicated that the sulfides might make up a significant portion in +53 µm size fraction.

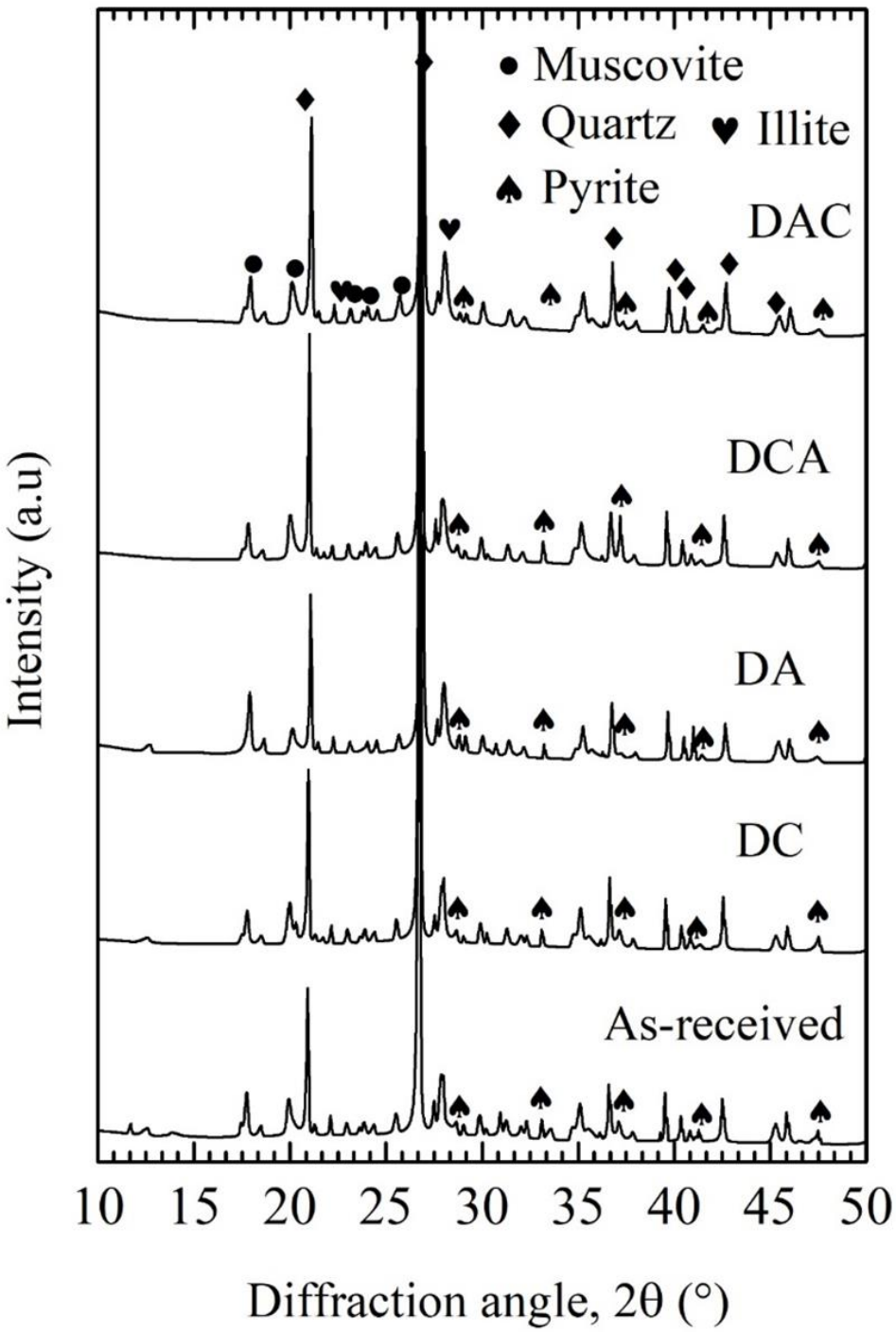

Figure 4. 4 XRD diffraction patterns for the as-received ore, and the solid residues after treated by CFSM (DC), *A. brierleyi* (DA), CFSM followed by *A. brierleyi* (DCA), and *A. brierleyi* followed by CFSM (DAC)

The elemental compositions of the as-received sample and the bio-treated residues is presented in **Table 4.1**. The results for Fe, As, and S contents in the DRGO by QEMSCAN (-1000 μm/+10 μm) and acid digestion were compared and they appear to be consistent with each other. This indicates that the majority of the sulfides were present in the -1000 μm /+10 μm size fraction, therefore, the significant particle aggregation in the -10 μm size fraction shown in the QEMSCAN scan map for the as-received sample (**Fig. 4.6**) and bio-treated residues should not significantly affect the sulfides contents. The mineralogical analysis shows that the major sulfide phases consist of 15.04% pyrite (FeS_2) and 2.45% arsenopyrite (FeAsS) (**Table 4.2**). The data also identified the major silicates and clay minerals as illite ($(K,H_3O)(Al,Mg,Fe)_2(Si,Al)_4O_{10}[(OH)_2,(H_2O)]$), kaolinite ($Al_2Si_2O_5(OH)_4$), quartz ($SiO_2$) and carbonaceous illite, which is a mineral formed by the association of carbonaceous matter with illite during the earliest stages of crystallization (Ahn et al., 1999). The other minor silicates included muscovite ($KAl_2(Si_3Al)O_{10}(OH,F)_2$), potassium feldspar ($KAlSi_3O_8$) and a carbonaceous alumino-silicate, which was designated as C-Si-Al because its chemical formula is yet unknown. The results show that the relative amount of these silicates generally increased in the residues regardless of the treatment used. This is unsurprising since these bio-treatments were aimed at decomposing some specific parts of the sample (Fe-sulfides and carbonaceous matter) and therefore, the amount of the unreactive silicate and clay minerals will accordingly be expected to increase relatively. The data also shows the presence of calcite ($CaCO_3$) and dolomite ($CaMg(CO_3)_2$) in the flotation concentrate, which might have been decomposed by produced acid during bio-oxidation of sulfides by *A. brierleyi* to release HCO_3^- leading to the slight increase in pH observed in **Fig. 4.2a**. The pyrite and arsenopyrite grains in DRGO mostly existed as completely liberated and/or associated with silicates like quartz and carbonaceous illite (**Fig. 4.6**).

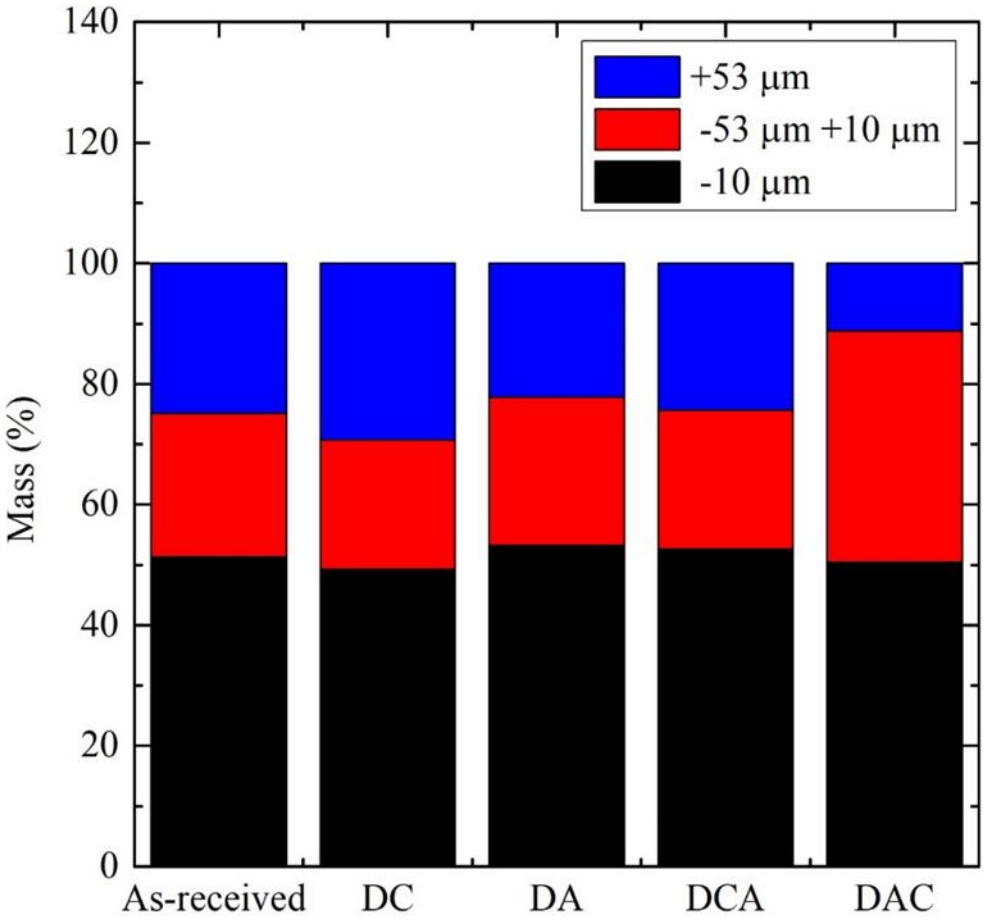

Figure 4. 5 Size analysis of as-received ore, and the solid residues after treatment by CFSM (DC), *A. brierleyi* (DA), CFSM followed by *A. brierleyi* (DCA), and *A. brierleyi* followed by CFSM (DAC).

Table 4. 1 Elemental composition (wt%) of as-received ore, and the solid residues after treated by CFSM (DC), *A. brierleyi* (DA), CFSM followed by *A. brierleyi* (DCA), and *A. brierleyi* followed by CFSM (DAC). QEMSCAN results is only for the -1000 µm/ +10 µm region because -10 µm size fraction could not be analysed due to extensive agglomeration of the fine particles.

Samples	**Elements (wt%)**								
	Fe	S	As	C	Si	Al	Na	Mg	Others
As-received	10.19[*1]	8.56[*1]	1.60[*1]	5.86[*2]	19.32[*3]	7.59[*3]	0.38[*3]	0.078[*3]	
	11.09[*4]	8.42[*4]	1.14[*4]	0.51[*4]	8.55[*4]	1.8[*4]	0.17[*4]	0.13[*4]	16.86
DC	12.23[*1]	7.21[*1]	1.82[*1]	-[*5]	-[*5]	-[*5]	-[*5]	-[*5]	-[*5]
	12.11[*4]	9.73[*4]	1.77[*4]	0.49[*4]	8.43[*4]	1.86[*4]	0.11[*4]	0.16[*4]	16.05
DA	7.05[*1]	5.86[*1]	0.84[*1]	-[*5]	-[*5]	-[*5]	-[*5]	-[*5]	-[*5]
	8.23[*4]	7.31[*4]	0.36[*4]	0.63[*4]	9.52[*4]	2.19[*4]	0.12[*4]	0.2[*4]	18.18
DCA	10.16[*1]	7.96[*1]	1.17[*1]	-[*5]	-[*5]	-[*5]	-[*5]	-[*5]	-[*5]
	10.92[*4]	9.76[*4]	1.6[*4]	0.5[*4]	7.9[*4]	1.63[*4]	0.1[*4]	0.15[*4]	14.84
DAC	3.84[*1]	1.76[*1]	0.29[*1]	-[*5]	-[*5]	-[*5]	-[*5]	-[*5]	-[*5]
	4.67[*4]	0.26[*4]	0.01[*4]	1.41[*4]	11.39[*4]	0.05[*4]	0.17[*4]	5.71[*4]	25.83

[*1] acid digestion, [*2] CHN analysis, [*3] XRF analysis and [*4] QEMSCAN analysis. [*5] not determined.

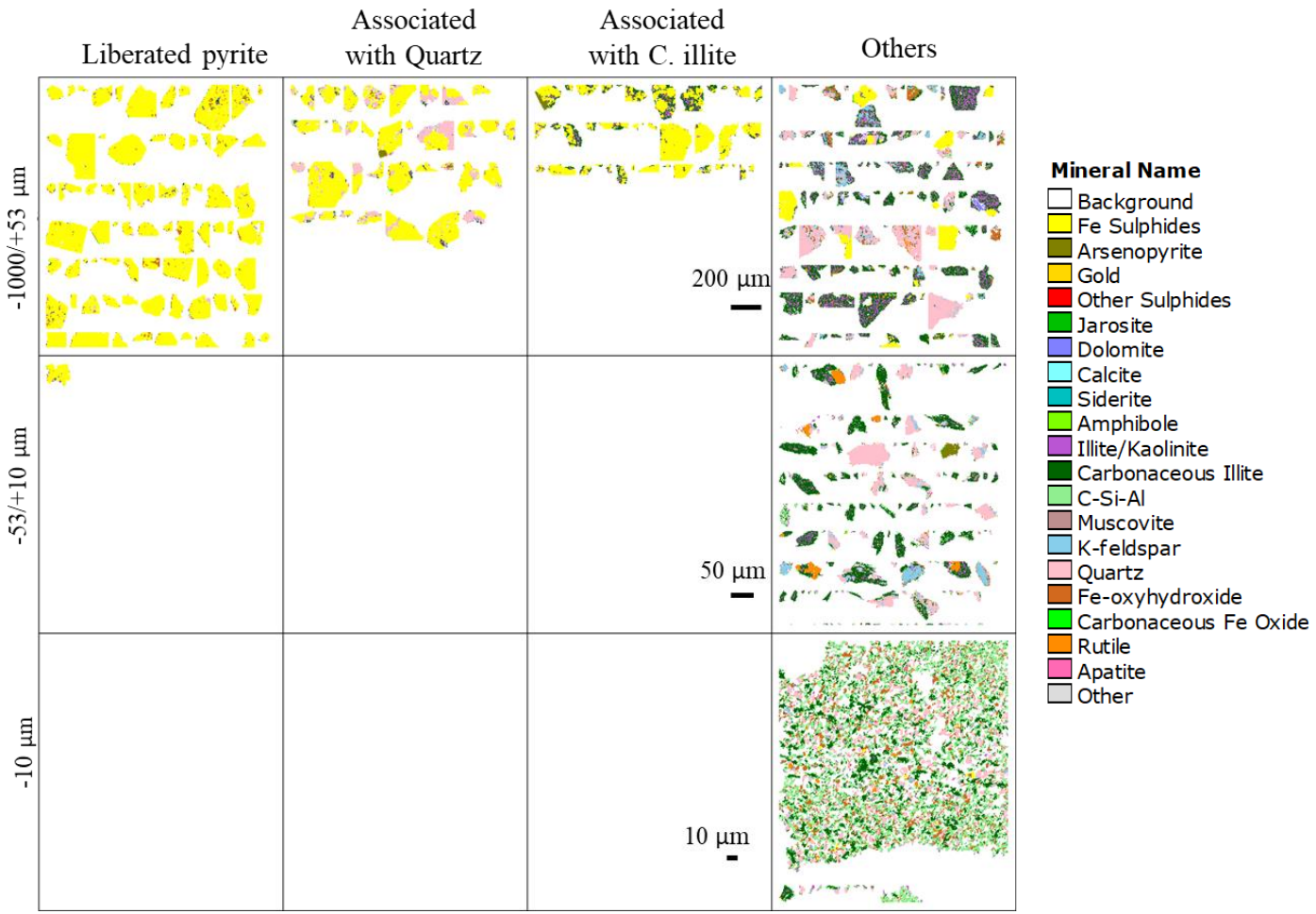

Figure 4. 6 QEMSCAN maps of liberated pyrite, pyrite associated with quartz and carbonaceous illite, and others in the as-received ore depending on size fractions (µm). Severe agglomeration in the -10/+0 µm range made the results in the region inconclusive. Scales of 200 µm, 50 µm and 10 µm was used for the -1000 µm /+53 µm and -53 µm/+10 µm and -10 µm respectively.

Table 4. 2 Mineralogical composition (wt%) of -1000 µm/+10 µm size fraction determined by QEMSCAN for the as-received ore, and the solid residues after treated by CFSM (DC), *A. brierleyi* (DA), CFSM followed by *A. brierleyi* (DCA), and *A. brierleyi* followed by CFSM (DAC). The total mass of the -10 µm size fraction is also given because agglomeration in this region impeded the QEMSCAN analysis.

Mineral	As-received (wt%)	After bio-treatment (wt%)			
		DC	DA	DCA	DAC
Fe sulfides	15.04	17.04	13.55	17.23	0.49
arsenopyrite	2.45	3.81	0.77	3.45	0.02
other sulfides	0.14	0.10	0.04	0.07	0.03
jarosite	n.d.	n.d.	n.d.	n.d.	n.d.
dolomite	0.09	n.d.	n.d.	n.d.	n.d.
calcite	0.03	0.01	0.01	0.03	0.03
amphibole	0.07	0.04	0.04	0.10	0.08
illite/kaolinite	3.44	3.40	3.40	2.38	5.65
carbonaceous illite	7.62	6.83	9.66	7.81	8.44
C-Si-Al	1.61	2.59	2.78	1.84	19.48
muscovite	0.54	0.59	0.60	0.39	0.72
K-feldspar	2.74	2.20	2.59	1.76	1.61
quartz	9.62	9.78	10.48	9.55	6.62
Fe-oxyhydroxide	3.56	3.18	1.94	1.84	5.79
carbonaceous Fe oxide	0.48	0.32	0.10	0.16	0.12
rutile	1.08	0.74	0.78	0.71	0.41
apatite	0.14	0.07	0.07	0.07	0.01
others	0.02	0.01	0.02	0.01	n.d.
Total -1000 µm/+10 µm	48.67	50.71	46.83	47.40	49.50
Total -10 µm	51.33	49.29	53.17	52.60	50.50

n.d., not detected.

The false color map of the DRGO after bio-oxidation by *A. brierleyi* (DA) is shown in **Fig. 4.7**. It can be clearly seen that pyrite was still one of the dominant phases in this sample but compared to the as-received sample in **Fig. 4.6**, the particles were relatively less numerous and slightly smaller. The effect of the archaea on sulfide oxidation can be quantified effectively by elemental composition determined by acid digestion in **Table 4.1** and to a less degree by mineralogical analysis by QEMSCAN in **Table 4.2**. The reason for the discrepancy between the two quantification methods is caused by the fact that the bio-treatment might produce smaller residual sulfide particles than 10 μm which could not be analyzed for mineralogy by QEMSCAN. Therefore, based on acid digestion, it was observed that the DA treatment reduced the amount of iron, sulfur and arsenic by 30.8%, 31.5% and 47.5%, respectively. Most of the iron, sulfur and arsenic in the DA residue after the treatment were divided into 13.6% pyrite, 0.77% arsenopyrite and 1.94% Fe-oxyhydroxides. Using the amount of these same Fe-minerals (pyrite, arsenopyrite and Fe-oxyhydroxides) in the as-received concentrate as the standard, it was determined that *A. brierleyi* treatment probably decreased each of the minerals by 10.0%, 68.6% and 45.5%, respectively (**Table 4.1**). This clearly shows that these three minerals, especially pyrite and arsenopyrite, were the sources of iron dissolved by *A. brierleyi* (**Fig. 4.2d**) and the process did not appear to form any appreciable amounts secondary mineral phases such as potassium jarosite ($KFe_3(OH)_6(SO_4)_2$). It is interesting to note that the dissolved iron concentrations became stagnant within 12-14 days despite the pyrite being a significant component of the DA sample (**Fig. 4.7**).

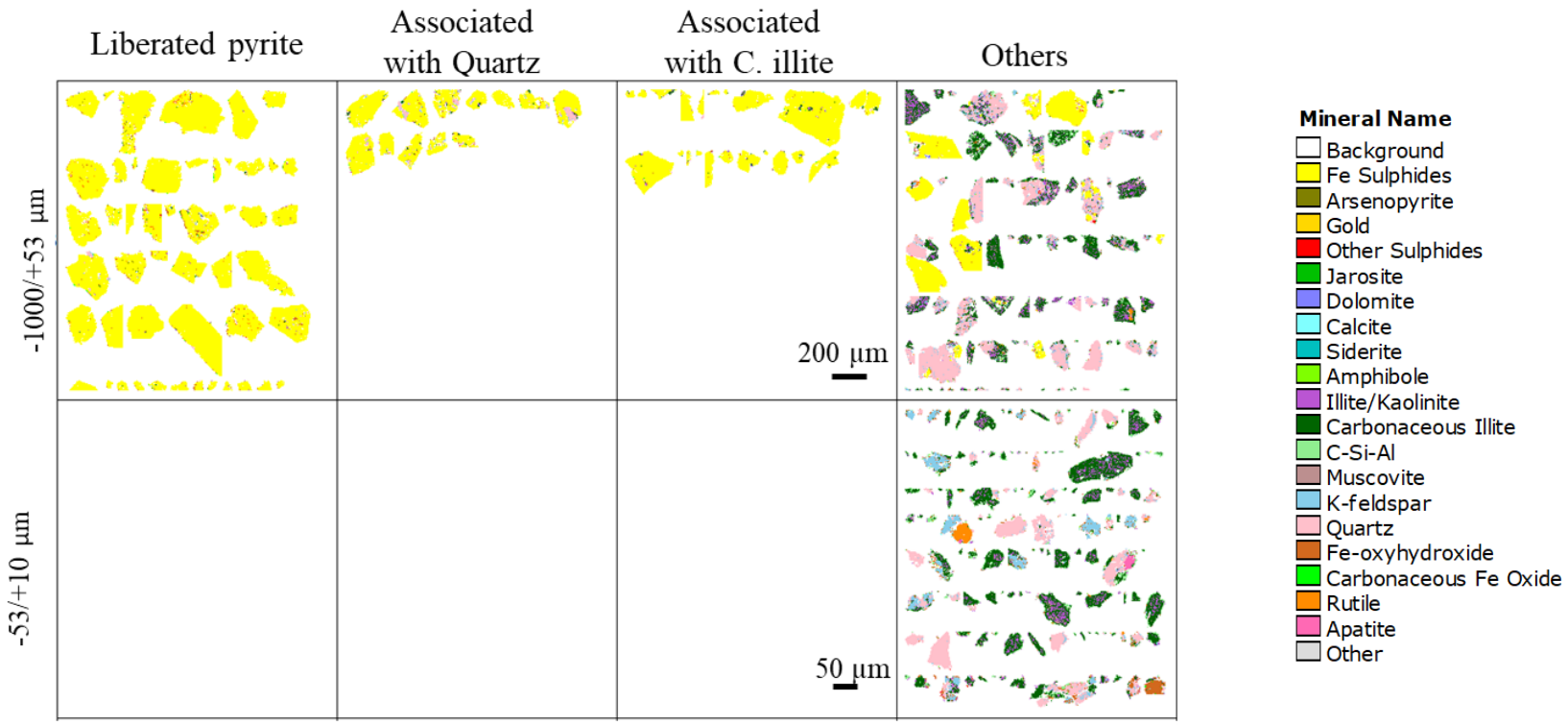

Figure 4. 7 QEMSCAN maps of liberated pyrite, pyrite associated with quartz and carbonaceous illite, and others in the solid residues of DRGO after 14 days-treated by *A. brierleyi* (DA) depending on size fractions (µm). Scales of 200 µm and 50 µm was used for the -1000 µm /+53 µm and -53 µm/+10 µm respectively.

Mineralogical compositions for DC and DCA (before and after sulfide oxidation by *A. brierleyi*) can be compared in **Table 4.2** based on QEMSCAN results. The result for DC showed that the CFSM treatment did not appear to have any significant effect on the sulfide oxidation. Therefore, it was hoped that the introduction of *A. brierleyi* would ensure the effective oxidation of sulfides after CFSM treatment. However, QEMSCAN results conclusively proved that sulfide oxidation did not significantly occur in DCA as shown in **Fig. 4.9**. This might have been due to the surface of the individual grains being covered by some bio-molecular substances during the CFSM treatment, which prevented the archaea cells from gaining direct access to the surface of the liberated pyrite (Larsson et al., 1993). The QEMSCAN analysis did not show that the surface of the pyrite was passivated after the CFSM treatment (**Fig. 4.8**). This further indicates that the surface passivation was probably not caused by secondary formed minerals like jarosite **(Table 4.2**), but rather thin layers of some biomolecules derived from fungal metabolic products, which is not well detectable by QEMSCAN. The detection limit in the present apparatus of QEMSCAN is 4 μm. Generally, the oxidative dissolution of pyrite takes place through an indirect contact mechanism (Sasaki et al., 1996). It is not always necessary for *A. brierleyi* to directly access pyrite grains, however, ferric ions (Fe(III)), which are produced through oxidation of ferrous ion (Fe(II)) by planktonic cells of *A. brierleyi*, are needed to attack the surface of pyrite. **Fig. 4.9** indicates that a robust surface must be formed on the pyrite after fungal treatment, probably due to physically electrostatic interaction and (bio-)chemical interaction. The surface of pyrite should be negatively charged around pH 4-5 because of pH_{zpc}~ 2 (Sasaki et al., 1996; Wei and Osseo-Asare, 1996) and proteins as biomolecules are positively charged at lower pH values than their iso-electrostatic points.

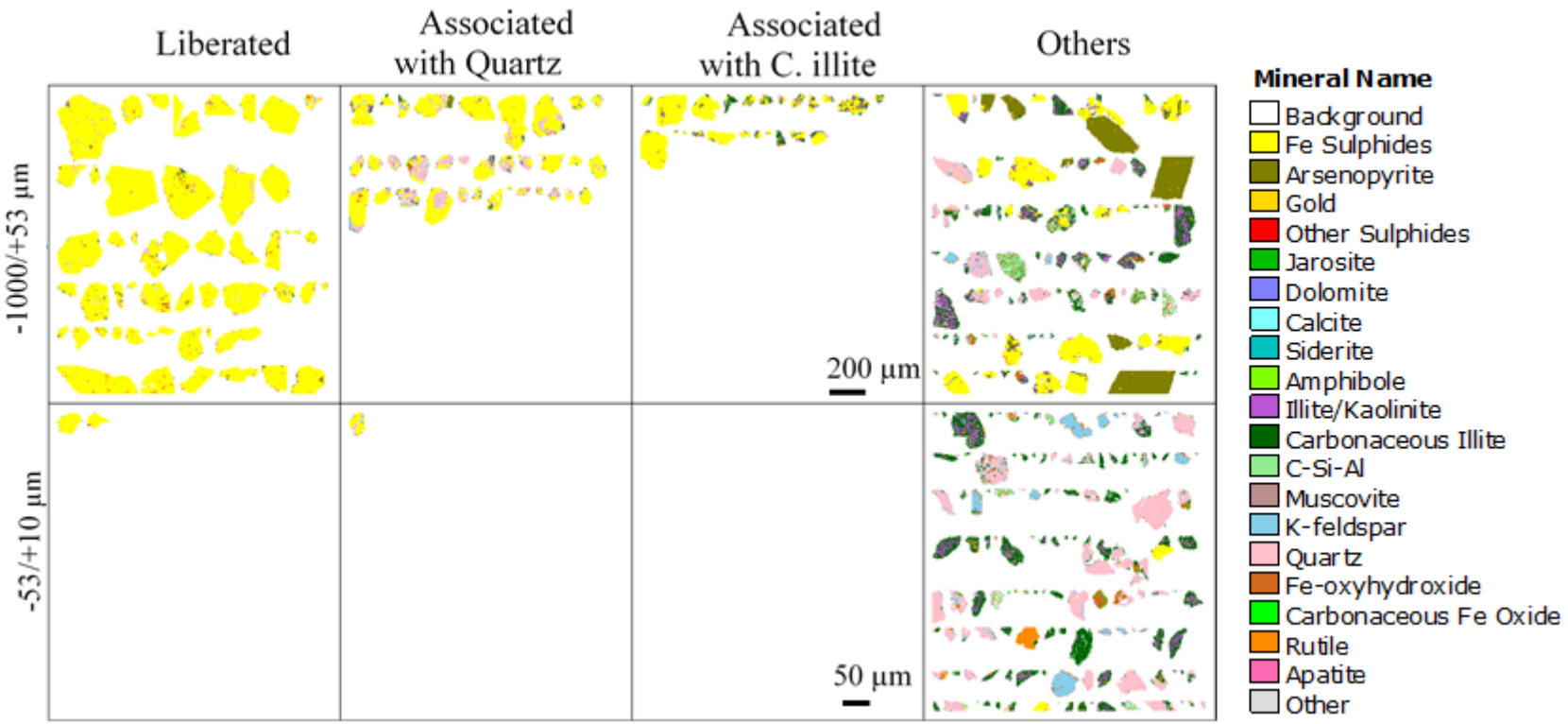

Figure 4. 8 QEMSCAN maps of liberated pyrite, pyrite associated with quartz and carbonaceous illite, and others in the solid residues after the treatment by CFSM (DC) for 15 days depending on size fractions (µm). Scale of 200 µm and 50 µm was used for the -1000 µm /+53 µm and -53 µm/+10 µm respectively.

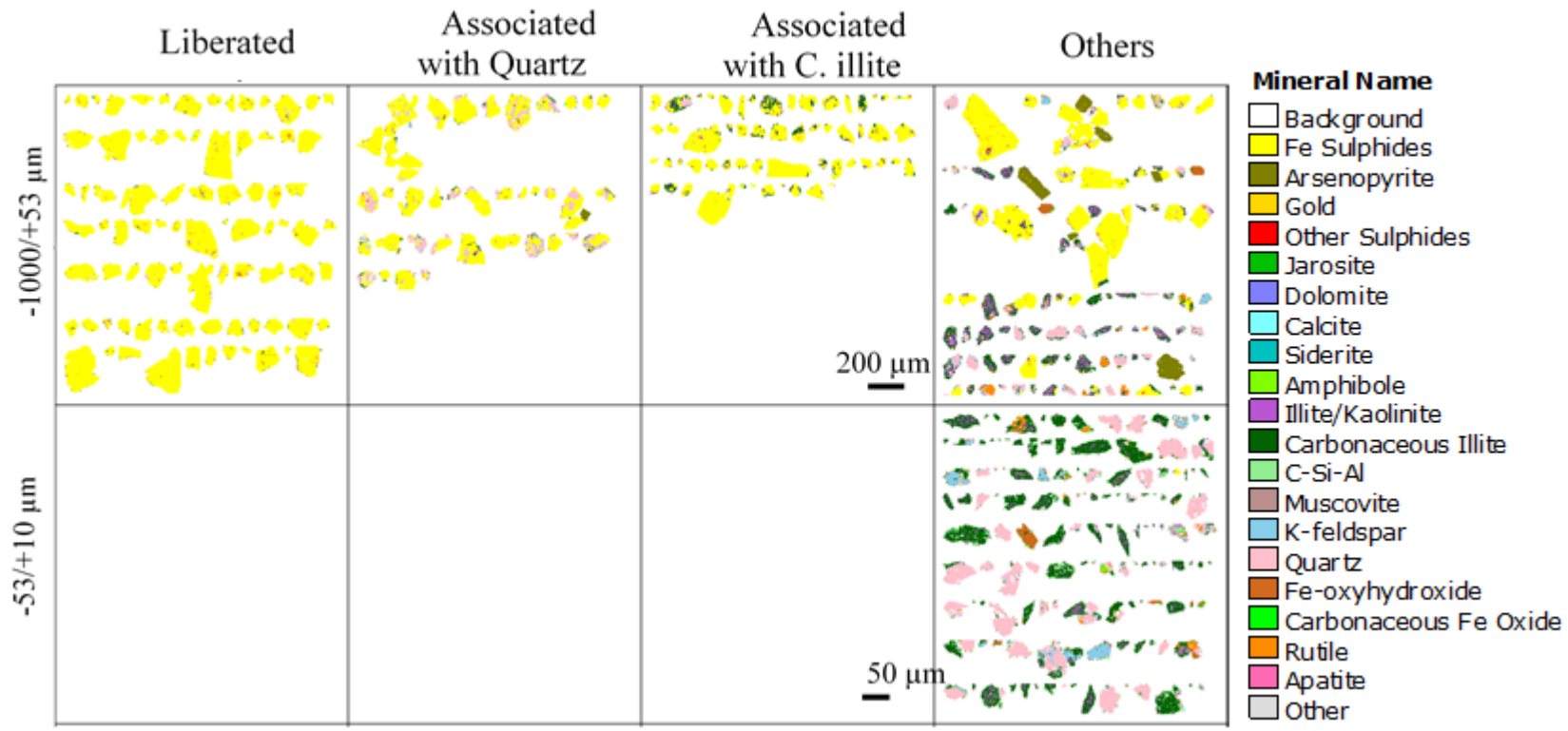

Figure 4. 9 QEMSCAN maps of liberated pyrite, pyrite associated with quartz and carbonaceous illite, and others in the solid residues after the treatment of the sample in **Fig. 4.8** followed by *A. brierleyi* treatment for 14 days (DCA) depending on size fractions (µm). Scale of 200 µm and 50 µm was used for the -1000 µm /+53 µm and - 53 µm/+10 µm respectively.

Conversely, when these two bio-treatment processes were combined in the reverse order, with *A. brierleyi* before CFSM (DAC), there was a dramatic disappearance of the major sulfides in QEMSCAN (**Fig. 4.10**). Based on the acid digestion findings in **Table 4.1**, the progressive removal of iron, sulfur and arsenic can be seen to follow the trend of as-received (0% Fe, 0% S and 0% As) < DA (30.8%Fe, 31.5%S and 47.5%As) < DAC (62.3%Fe, 79.4%S and 81.9%As). Additionally, **Table 4.2** shows that the amount of Fe-oxyhydroxides in DAC corresponds to a three-fold increase compared with DA. This can be expected because the CFSM treatment was conducted at pH 4, where iron precipitation would be prevalent. The main reason for the increased sulfide decomposition by the CFSM in DAC compared with DC might have been caused by an increase in the accessibility of the enzymes to both the carbonaceous matter and the sulfides. In addition, the inhibitory effect of arsenic on enzyme activity decreased after the reduction of the major arsenic species by the oxidative dissolution of arsenopyrite by *A. brierleyi* in DAC. It has been already shown that some heavy metals can adversely affect the activity of white-rot fungi and some peroxidases (Mascher et al., 2002; Baldrian 2003). Therefore, it is possible that the presence and release of heavy metals from the DRGO prevented the CFSM treatment from being effective in DC. Consequently, when the bio-oxidation of sulfides by *A. brierleyi* preceded the CFSM treatment, it was able to reduce the arsenic and heavy metal contents significantly and therefore allow the responsible enzymes in CFSM to effectively attack and decompose the carbonaceous matters. The enzyme reaction products were not always easily soluble in weakly acidic solutions. Finally, it appears that the DAC treatment resulted in a significant increase in the amount and size of the carbonaceous alumino-silicate (C-Si-Al) compared with the as-received sample and the other residues. It was observed that the C-Si-Al in DAC had irregularly shaped, highly porous sediment-like structure compared to the carbonaceous illite. These features are reminiscent of the products formed from the decomposition of the aromatic carbon in the carbonaceous illite by the CFSM and

then agglomeration of smaller particles. In this step, the tiny gold grains might possibly be involved in the agglomerates, leading to it being locked up. To the best of our knowledge, this is the first direct observation of the by-product after the CFSM treatment of carbonaceous matter in gold ores. The factors responsible for the significant carbonaceous matter and sulfide decomposition by the CFSM resulting in the increased formation of C-Si-Al, were further investigated by DNA extraction and SEM observation.

4.3.4. DNA extraction and SEM

The genomic analysis indicated the presence of archaeon by the amplification of an approximately 1600 bp DNA fragment from the sample DAC (**Fig. 4.11a**). This obviously shows that the archaeon was attached to the surface or entrapped in the solid residue during the DA treatment. However, the amount present was probably below the detection limit and only after the CFSM treatment further altered the solid that it could be detected. What was far more interesting was the detection of fungal DNA on the DC and DAC samples and its absence on DCA (**Fig. 4.11b**). For DC and DAC, the data shows that the fungus *P. chrysosporium* might have flowered from the spores in the CFSM. This was confirmed by the presence of long strands of fungal hyphae as shown by SEM observations in **Fig. 4. 12b and 4. 12e,** and the increased thermal decomposition between 200-430°C (**Fig. 4.3**)**.** The growth of the fungus directly on the sample would have enhanced enzyme production resulting in the increased decomposition of sulfides and carbonaceous matter. The fungus would have also produced binding agents to help its attachment to the particle surface. This indicates that the C-Si-Al might be the product of the carbonaceous matter biodegradation bound together to form larger structures.

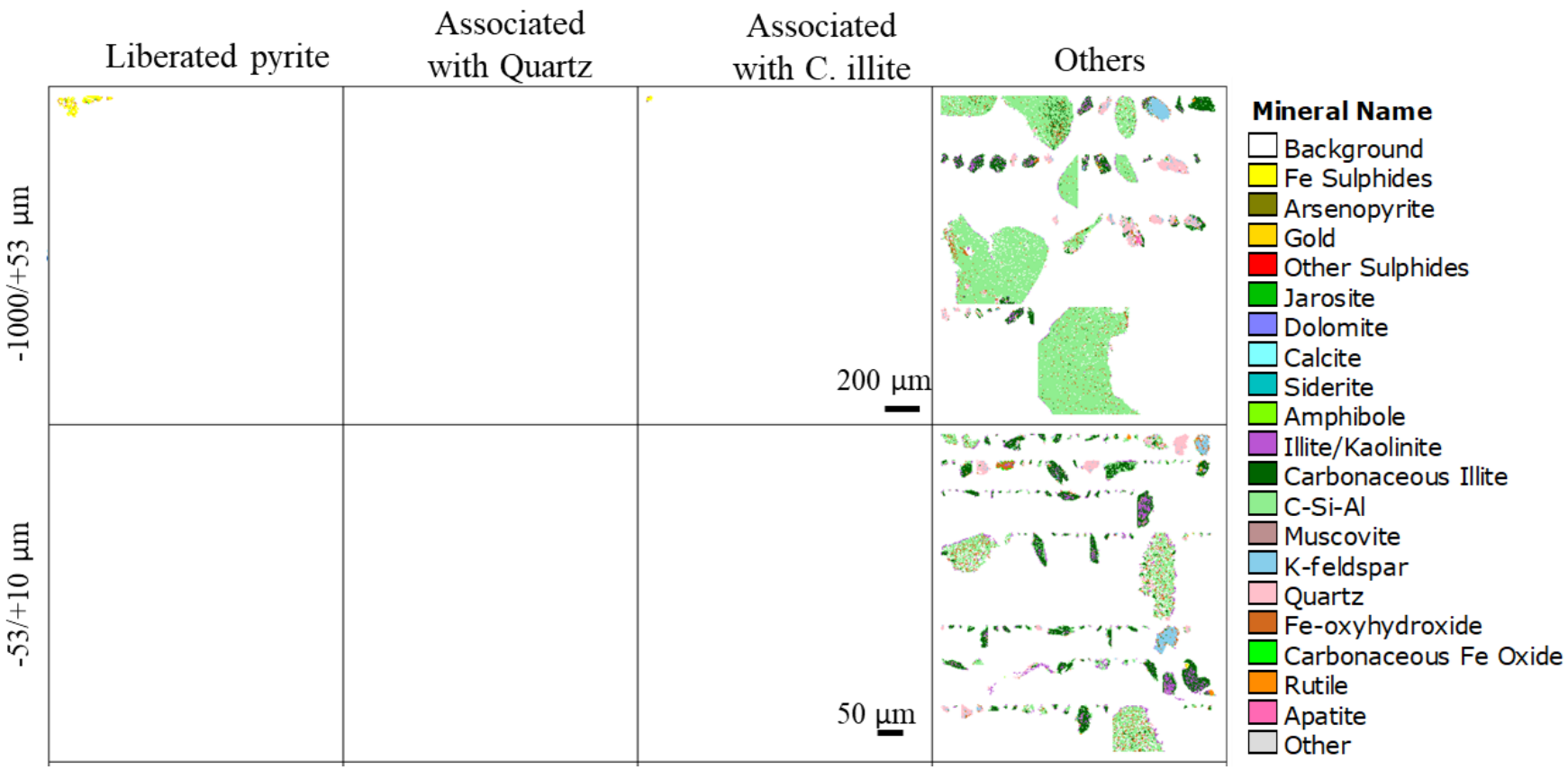

Figure 4. 10 QEMSCAN maps of liberated pyrite, pyrite associated with quartz and carbonaceous illite, and others in the solid residues after the treatment of the sample in **Fig. 4**.7 by CFSM (DAC) for 15 days depending on size fractions (µm). Scales of 200 µm and 50 µm was used for the -1000 µm /+53 µm and -53 µm/+10 µm respectively.

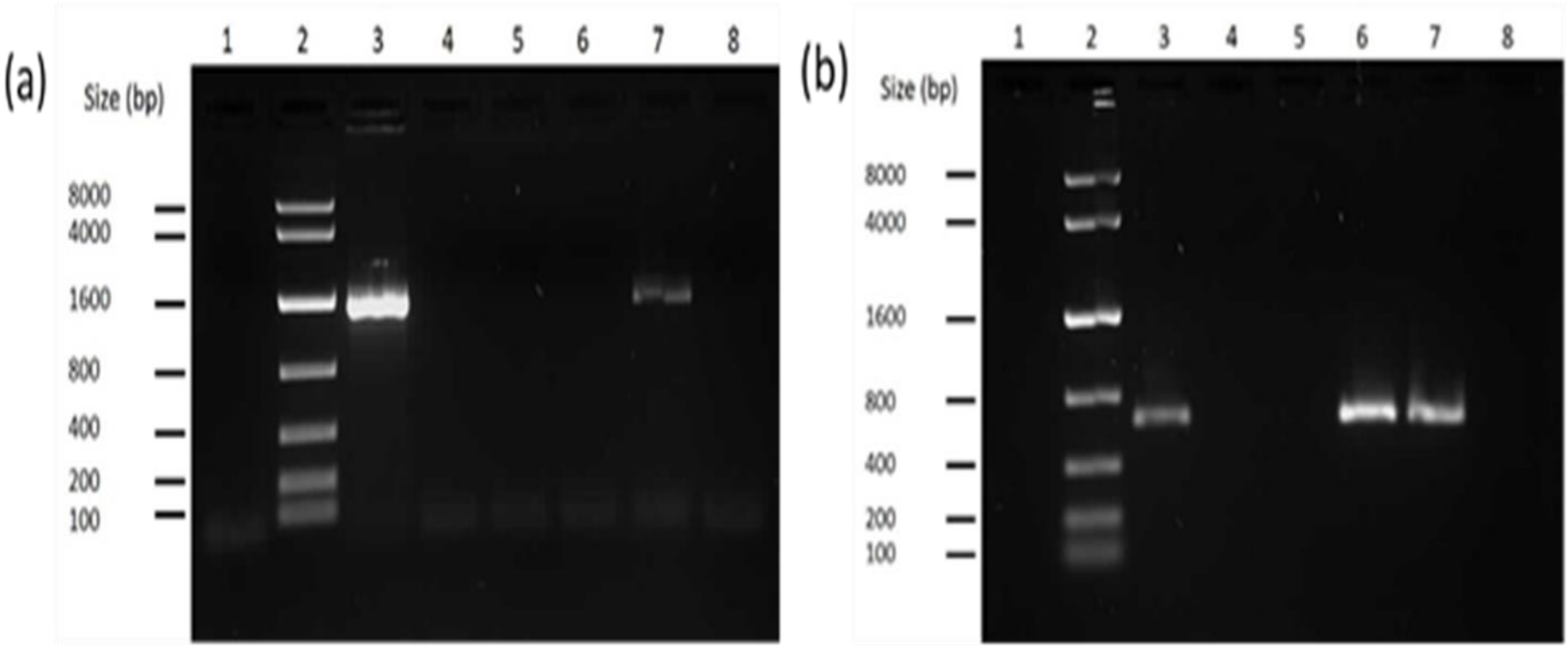

Figure 4. 11 Agarose gel electrophoresis of (a) 16S and (b) 18S rRNA PCR amplicons. Lane 1, No template (negative) control (NTC); lane 2, MW marker; lane 3, positive control; lane 4, as-received ore; lane 5, *A. brierleyi only* (DA); lane 6, CFSM only (DC); lane 7, *A. brierleyi* followed by CFSM (DAC); and lane 8, CFSM followed by *A. brierleyi* (DCA). The sizes of the molecular weight marker are indicated.

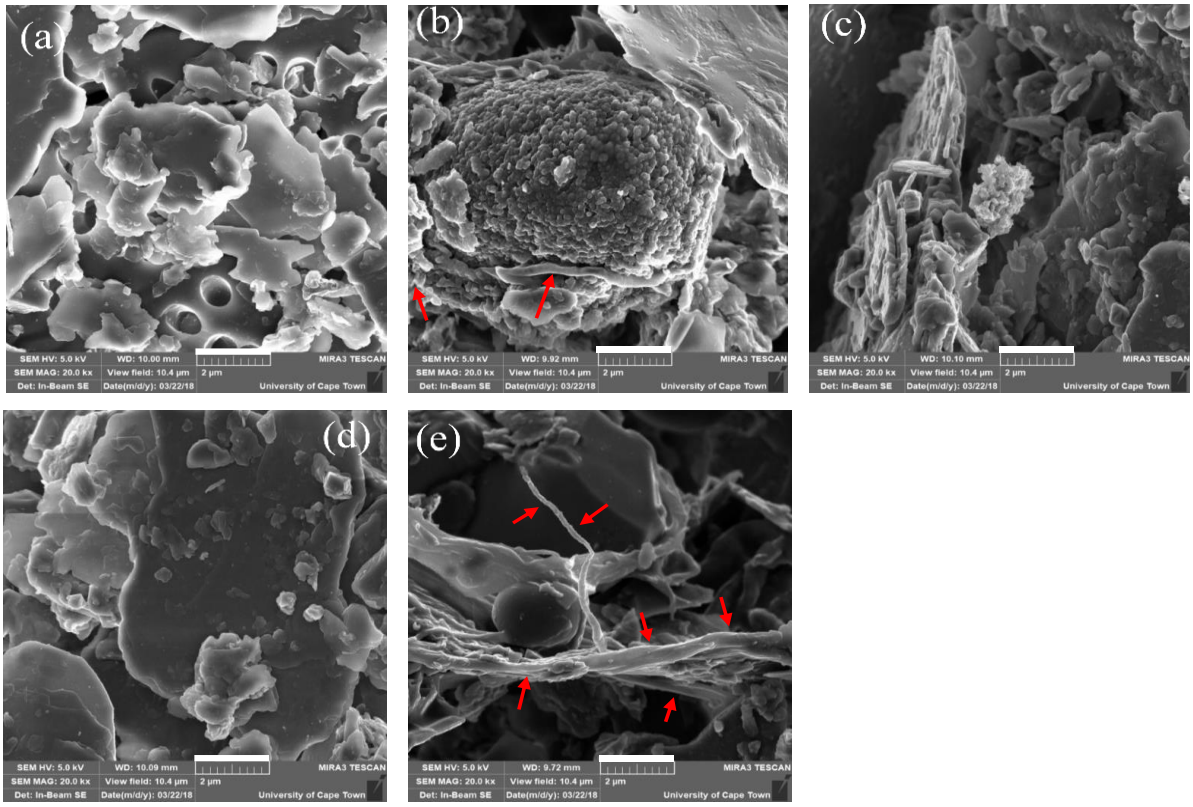

Figure 4. 12 Scanning electron micrographs of the surface of the (a) as-received ore, and the solid residues after treated by (b) CFSM (DC), (c) *A. brierleyi* (DA), (d) CFSM followed by *A. brierleyi* (DCA), and (e) *A. brierleyi* followed by CFSM (DAC). A scale 2µm was used for the analysis. Red arrows in the images clearly highlight the presence of the long thin strands of fungal biomass.

Additionally, the presence of the fungal hyphae on DC might have directly impeded the ability of the *A. brierleyi* to attach on the mineral surface or indirectly by producing bio-chemicals during its growth, which accomplished the same task. This might be the reason behind the apparent failure of the DCA sequence, although it does appear that this treatment served instead as a two-week continuous washing process and that is why neither DNA nor the biomass of the fungus was found on DCA (**Fig. 4. 12d**). Combining this finding with the previously discussed data established that the bio-treated residues had very heterogonous compositions.

4.3.5. Gold recovery

Cyanidation was applied to evaluate the effectiveness of the bio-treatments (**Fig. 4. 13**). The as-received sample yielded 24.6± 0.45% of gold after direct cyanidation which meant that the present sample was very refractory. This behavior might be caused by the inaccessibility of the gold grains to the cyanidation reagents and recovery loss through adsorption of $Au(CN)_2^-$ on components like carbonaceous matter. The gold yield in triplicate was in the order of as-received (24.6± 0.45%) < DC (37.2± 0.50%) < DCA (44.8± 0.62%) < DAC (75.1± 0.40%) ~ DA (76.7± 1.00%), although each treatment improved recovery of gold, directly employing the CFSM treatment (DC) to the fresh sample increased recovery by only 12.6%. When this was followed up with *A. brierleyi* treatment (DCA), a further 7.6% increase was obtained. This supports the findings in **Fig. 4. 2 and Table 2**, showing that this treatment pathway (DCA) was not able to significantly decompose gold-bearing sulfides in the concentrate, which left the gold encapsulated and inaccessible to the cyanide solution.

On the other hand, the results show that employing *A. brierleyi* (DA), which was responsible for a 31.5% decrease in S content, at the beginning of the sample treatment resulted in a high rise in the gold recovery from 24.6% to 76.7%. Therefore, it was expected, based on the QEMSCAN data in **Fig. 4.10** that the DAC sequence would yield the best recovery, but that was not the case as shown in **Fig. 4.13** (75.1%). This discrepancy might have been due to the presence of the fungal tissues, which were grown from fungal spores in CFSM (**Fig. 4.11**), and/or the enzymatically degraded products (**Fig. 4.10**) in the residue of DAC. This is significant because, during its growth, the fungus would be able to synthesize sugars and organic acids, which might bind the microbe to individual particles in the sample (Moreira et al., 2003). In such cases, the biomass would effectively reduce the amount of particle surface available to the lixiviant, leading to gold recovery losses. Therefore, its presence during cyanidation might have been the reason for the lower gold recovery in DAC compared with

DA despite the combined, successful efforts of *A. brierleyi* and CFSM to decompose sulfides in the sample.

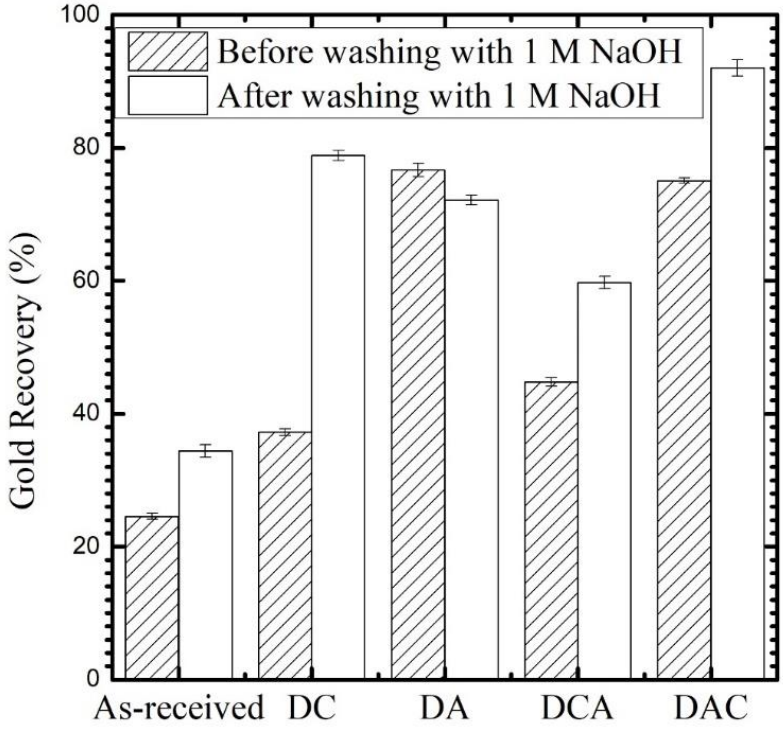

Figure 4. 13 Effect of 1 M NaOH washing on the gold recovery from the as-received ore, and the solid residues after treated by CFSM (DC), *A. brierleyi (*DA), CFSM followed by *A. brierleyi* (DCA), and *A. brierleyi* followed by CFSM (DAC) (*n* = 3).

All of the samples were washed with 1 M NaOH prior to cyanidation, and the gold recovery was compared in **Fig. 4.13**, showing that the alkaline washing improved the gold recovery for all the samples except DA. After washing DC with 1 M NaOH, the gold recovery significantly increased from 38% to 78.9%. Also, an increase of 14.9% was attained after the alkaline washing of DAC to achieve a final gold recovery of 92.0 ± 1.22% (*n* = 3). Furthermore, visual observation of the supernatant after alkaline washing of the pretreated solids showed a rising intensity of the brownish-yellow color in the order of DCA< DC < DAC, that was not observed for the as-received and DA. This implies that CFSM treatment partially altered carbonaceous matters to smaller molecules which are more easily soluble in 1 M NaOH, much like humic substances (Li et al., 2009). After bio-oxidation of sulfides in *A. brierleyi* pretreatment, tiny

grains of gold must be liberated from sulfides. The following enzymatic degradation in CFSM pretreatment degraded carbonaceous matters to smaller molecules, however, small particle sizes of aluminosilicates in DRGO were aggregated through degradable matters to produce large particles of C-Si-Al (> several hundred μm) in **Fig. 4.10**, where some tiny gold grains might have also been taken in. Although it is impossible to observe tiny gold grains (<4 μm) directly by QEMSCAN, it is speculated that alkaline washing with 1 M NaOH solubilized humic-like matters to release gold grains for cyanidation. The DAC sample possessed the largest amounts of C-Si-Al grains, and this would be the reason why the sequential bio-pretreatment (DAC) followed by alkaline washing lead the best performance during gold recovery.

This shows that the important role of CFSM in bio-mineral processing of carbonaceous gold ores is to decompose carbonaceous matter in ores into lower molecular weights of organic substances, would have clearly interfered with the cyanidation process without the addition an alkaline washing step prior to gold extraction.

4.4. Conclusions

The sequential bio-treatment of the DRGO is summarized in **Fig. 4.14**. When the DRGO was pretreated by bio-oxidation of sulfides with *A. brierleyi*, the gold recovery was improved from 24% to 77% in cyanidation. When it was followed by the enzyme degradation of carbonaceous matters by crude lignin-degrading enzymes in CFSM, derived from a white-rot fungus *Phanerochaete chrysosporium*, and alkaline washing, gold recovery was further improved to 92%. Though QEMSCAN observation and thermo-gravimetric analysis, the contribution of the enzyme treatment was found to be the degradation of refractory carbonaceous matter to smaller organic molecules like humic substances, which are easily

soluble in alkaline solutions. The bio-pretreatment process should be optimized depending on gold ore types.

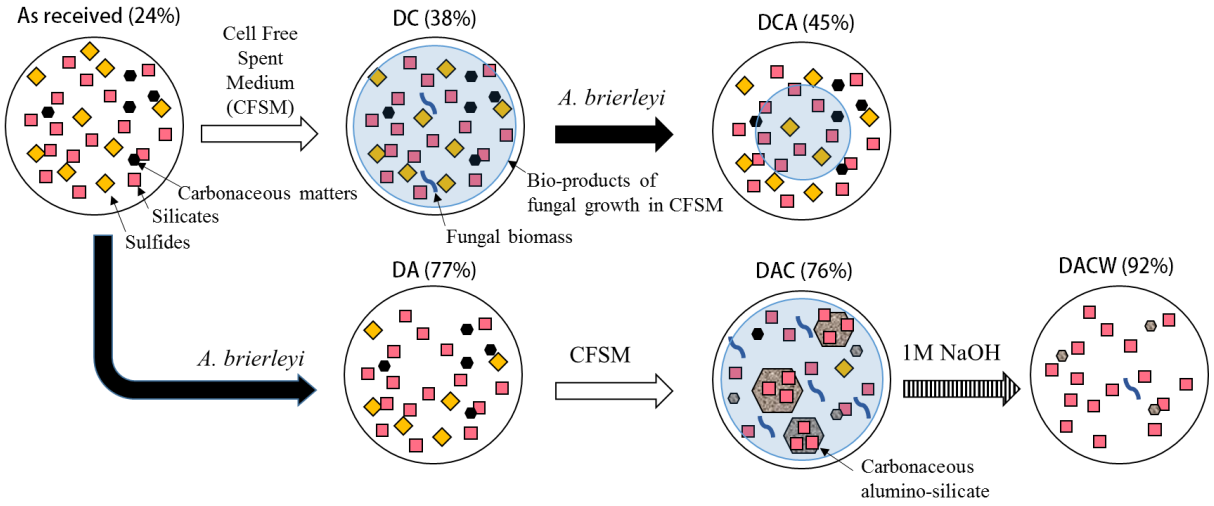

Figure 4. 14 Schematic illustration of sequential biotreatmnt and gold recovery (%) for each product.

References

Afenya, P.M., 1991. Treatment of carbonaceous refractory gold ores. *Miner. Eng*. 4, 1043-1055.

Ahn, J.H., Cho, M., Buseck, P.R., 1999. Interstratification of carbonaceous material within illite. *Am. Mineral*. 84, 1967-1970.

Baldrian, P., 2003. Interactions of heavy metals with white-rot fungi. *Enzyme Microb. Technol*. 32, 78-91.

Balek, V., Subrt, J., 1995. Thermal behaviour of iron (III) oxide hydroxides. *Pure Appl. Chem*., 67, 1839-1842.

Chen, J., Li, Y., Zhao, C., 2014. First principles study of the occurrence of gold in pyrite. *Comput. Mater. Sci*. 88, 1-6.

Cook, N.J., Chryssoulis, S.L., 1990. Concentrations of invisible gold in the common sulfides. *Can. Mineral*. 28, 1-16.

Fujian, X., Hongzhang, C., Zuohu, L., 2001. Solid-state production of lignin peroxidase (LiP) and manganese peroxidase (MnP) by *Phanerochaete chrysosporium* using steam-exploded straw as substrate. *Bioresour. Technol*. 80, 149-151.

Goodall, W.R., Scales, P.J., Butcher, A.R., 2005. The use of QEMSCAN and diagnostic leaching in the characterization of visible gold in complex ores. *Miner. Eng.* 18, 877-886.

Kersten, P.J., Kirk, T.K., 1987. Involvement of a new enzyme, glyoxal oxidase, in extracellular H2O2 production by *Phanerochaete chrysosporium*. *J. Bacteriol*. 169, 2195-2201.

Konadu, K.T., Sasaki, K., Kaneta, T., Ofori-Sarpong, G., Osseo-Asare, K., 2017. Bio modification of carbonaceous matter in gold ores: Model experiments using powdered activated carbon and cell-free spent medium of *Phanerochaete chrysosporium*. *Hydrometallurgy*, 168, 76-83.

Kudo, S., Harada, A., Kubota, H., Sasaki, K., Kaneta, T., 2017. Simultaneous determination of manganese peroxidase and lignin peroxidase by capillary electrophoresis enzyme assays. ACS Omega, 2, 7329-7333.

Larsson, L., Olsson, G., Hoist, O., Karlsson, H.T., 1993. Oxidation of pyrite by *Acidianus brierleyi*: Importance of close contact between the pyrite and the microorganisms. *Biotechnol. Lett*. 15, 99-104.

Li, H., Jin, Y., Nie, Y., 2009. Application of alkaline treatment for sludge decrement and humic acid recovery. *Bioresour. Technol*. 100, 6278-6283.

Liu, Q., Yang, H.Y., Qiao, L.L., 2013. Biotransformation of arsenopyrite by *Phanerochaete chrysosporium*. *Adv. Mat. Res*. 825, 309-313.

Lunt, D., Weeks, T., 2016. Process flowsheet selection. In Gold Ore Processing (Second Edition) 113-129.

Marsden, J., House, I., 2006. Leaching. The chemistry of gold extraction. SME, Englewood, 233-295.

Mascher, R., Lippmann, B., Holzinger, S. Bergmann, H., 2002. Arsenate toxicity: effects on oxidative stress response molecules and enzymes in red clover plants. *Plant Sci.* 163, 961-969.

Miller, P., Brown, A., 2005. Bacterial oxidation of refractory gold concentrates. *Developments in Mineral Processing*, 15, 371-402.

Moreira, M.T., Feijoo, G. and Lema, J.M., 2003. Fungal bioreactors: applications to white-rot fungi. *Rev. Environ. Sci. Biotechnol*. 2, 247-259.

Ofori-Sarpong, G., Osseo-Asare, K., Tien, M., 2011. Fungal pretreatment of sulfides in refractory gold ores. *Miner. Eng*. 24, 499-504.

Ofori-Sarpong, G., Osseo-Asare, K., Tien, M., 2013. Mycohydrometallurgy: Biotransformation of double refractory gold ores by the fungus, *Phanerochaete chrysosporium*. *Hydrometallurgy*, 137, 38-44.

Pascoe, R.D., Power, M.R. and Simpson, B., 2007. QEMSCAN analysis as a tool for improved understanding of gravity separator performance. *Miner. Eng*. 20, 487-495.

Sasaki, K., Tsunekawa, M., Tanaka, S., Konno, H., 1996. Suppression of microbially mediated dissolution of pyrite by originally isolated fulvic acids and related compounds. Colloids Surf. A. 119, 241-253.

Shvarzman, A., Kovler, K., Grader, G.S., Shter, G.E., 2003. The effect of dehydroxylation/amorphization degree on pozzolanic activity of kaolinite. *Cement. Concrete. Res.* 33, 405-416.

Thomas, K.G., 2005. Pressure oxidation overview. *Developments in Mineral Processing*, 15, 346-369.

Tien, M., Kirk, T.K., 1988. Lignin peroxidase of *Phanerochaete chrysosporium*. *Methods Enzymol*. 161, 238-249.

Wariishi, H., Valli, K., Gold, M.H., 1991. In vitro depolymerization of lignin by manganese peroxidase of *Phanerochaete chrysosporium*. *Biochem. Biophys. Res. Commun*. 176, 269-275.

Wei, D., Osseo-Asare, K., 1996. Particulate pyrite formation by the Fe^{3+} HS^{-} reaction in aqueous solutions: effects of solution composition. *Colloids Surf. A*. 118, 51-61.

Yang, H. Y., Qian, L. I. U., Song, X. L., Dong, J. K., 2013. Research status of carbonaceous matter in carbonaceous gold ores and bio-oxidation pretreatment. *Trans. Nonferrous Met. Soc. China*, 23, 3405-3411.

Yu, Q., Morioka, E., Sasaki, K., 2013. Characterization of lithium ion sieve derived from biogenic Mn oxide. *Micropor. Mesopor. Mat.* 179, 122-127.

Chapter 5:

Transformation of the carbonaceous matter in double refectory gold ore (DRGO) by crude lignin peroxidase released from white-rot fungus

5.1. Introduction

Carbonaceous matter in gold ores can competitively adsorb $Au(CN)_2^-$ complex ions during extraction, resulting in decreased gold recovery (Jha 1987; Haque 1987). As such, it is necessary to diminish the effect of the carbonaceous matter in the ore before cyanidation. Carbonaceous matter can be decomposed either chemically by high-temperature roasting or biologically using hydrolytic and lignin-degrading microbes (Jha 1987; Amakwah et al., 2005; Amankwah and Pickles, 2009, Ofori-Sarpong et al., 2013). From an environmental standpoint, the use of these microbes, while not as efficient as the roasting, can significantly improve gold yields (Ofori-Sarpong et al., 2013). Previous studies have used the white-rot fungus *Phanerochaete chrysosporium* for in vivo or in vitro treatments of several substrates because it can produce extracellular lignin-degrading enzymes like manganese peroxidase and lignin peroxidase (Tien and Kirk, 1988; Wariishi et al., 1991). These enzymes utilize hydrogen peroxide as an activator for a two-step electron transfer oxidation reaction. After activation, the enzyme Compound I and Compound II interact with the carbonaceous matter and decompose it into smaller compounds, that may have less gold adsorption ability (Tien and Kirk, 1988; Wariishi et al., 1989; Wariishi and Gold, 1990; Ofori-Sarpong et al., 2013). Also, the fungus produces carbohydrates and organic acids (Moreira et al., 2003; Flemming and Wingender, 2010), which might cover the surface of the carbonaceous matter, reducing gold recovery. Therefore, the solid residues of fungal treatment are complex products requiring extensive analysis to understand.

Carbonaceous matter often makes up less than 7% of most refractory gold ores, and has chemically and physically diverse structures depending on molecular sizes, aromaticity, functional groups, so that characterization of the original substance and products of its bio-treatments is often difficult to accomplish (Zumberge et al., 1978; Yang et al., 2013). Some

previous studies have tried to simplify the analysis by extracting the graphitic carbon using strong acids to decompose all the other components in the ore, but this process would irrevocably change the chemical properties of the carbonaceous matter from its original state (Abotsi, and Osseo-Asare, 1986; Afenya et al., 1991). Spectroscopic analytical methods like Raman and FTIR spectroscopy have been applied instead of digestion to study the preg-robbing property of some carbonaceous gold ores (Helm et al., 2009; Dimov and Hart 2017). It was proposed that there might be a linear correlation between adsorbed amounts of $Au(CN)_2^-$ and the magnitude of chemical or physical disorder in graphitic carbon. However, without an adequate understanding of the minerals associated with the carbonaceous matter; it is often difficult to determine if the sp^2 hybridized D-band is due to the chemical and physical environment around the carbonaceous matter in the sample (Ferrari, 2007; Pimenta, 2007).

Another analytical method, that has become invaluable for characterizing the mineralogy of several metal ores including gold and coal samples since the 1980s' (Butcher et al.,2000), is the Quantitative Evaluation of Minerals by Scanning Electron Microscopy (QEMSCAN) (Goodall et al., 2005; Liu et al., 2005; Pirrie et al., 2004). This technique can provide detailed information of not only the quantitative and qualitative mineralogical determination but also mineral liberation and associations. To the best of our knowledge, it has not been used for the analysis of carbonaceous matters in refractory gold ores and/or its bio-treated residues because of factors like smaller mass abundance of carbon in the ore sample and possible interference from the chemical resin used to make the pellet for analysis of powdery samples (Liu et al., 2005). This limitation of QEMSCAN can be reduced by replacing the chemical resin with carnauba wax to create a sufficient contrast between the carbonaceous matter and the wax background so that analysis of the refractory gold ore can proceed (Pirrie et al., 2004).

Therefore, the present work seeks to provide knowledge about the carbonaceous matter which is *in situ* in the double refractory gold ore (DRGO) and the bio-product formed after treatment using QEMSCAN. This will encompass; (1) analyzing the carbonaceous matter in its original state in the gold ore sample to understand its association with the other minerals, (2) determining the changes that occur during its decomposition by lignin peroxidase and the related enzymes, which are released from white-rot fungus, in the cell-free spent medium (CFSM) and (3) using this information to aid in the understanding of results collected from Raman spectroscopy and three-dimensional fluorescence spectrometry. This knowledge will improve the understanding of the beneficiation of carbonaceous matter in refractory gold ores.

5.2. Experimental

5.2.1. Sample preparation and characterization

The concentrate after sulfide flotation of the as-received sample (DRGO) and the product after decomposition of sulfides in the concentrate by a thermophilic, iron-oxidizing archaeon *Acidianus brierleyi* (DA) were prepared in similar conditions to those shown in section 4.2.2. After preparation, both solids (as-received sample and DA) were collected by filtration, dried under vacuum at ambient temperature and then provided for the CFSM treatment. The mineral phases in the original and bio-treated samples were determined by QEMSCAN (FEI 650F; 25 kV, 10 nA and field step of 0.5 -4 µm). Major elemental compositions were determined by X-ray fluorescence spectroscopy (Rigaku, ZSX Primus II), Carbon Hydrogen Nitrogen (CHN) analysis (Yanaco CHN MT-5) and induced coupled plasma-optical emission spectrometry (ICP-OES, Perkin Elmer Optima 8300) after acid digestion. Minor elemental

compositions, including gold contents, were determined by induced coupled plasma-mass spectrometry (ICP-MS, MS, Agilent 7500c) after digestion.

5.2.2. Phanerochaete chrysosporium *cultivation and enzyme assay*

Cultures of *P. chrysosporium* were prepared for CFSM production with the following media composition as in section 2.1.1; 10 g glucose, 1.18 g succinic acid, 0.2 g ammonium tartrate, 10 mg thiamine, 10 mg 2,6-dimethoxyphenol, 2 g KH_2PO_4, 0.5 g $MgSO_4.7H_2O$ and 0.1 g $CaCl_2.2H_2O$ per 1 L in addition to 70 mL trace element solution (3 g $MgSO_4 \cdot 7H_2O$, 1 g NaCl, 0.5 g $MnSO_4 \cdot 5H_2O$, 0.1 g $FeSO_4 \cdot 7H_2O$, 0.1 g $CuSO_4 \cdot 5H_2O$, 10 mg boric acid per 1 L) (Tien and Kirk, 1988). This fungus was grown in 500 mL of the above medium at the initial pH 4.0 ± 0.1 in a 2 L-flask. All flasks were covered by porous plugs to allow for aeration and incubated at 37°C under stationary conditions. After three days of fungal growth, CFSM was aseptically recovered from the fungal cells and spores by filtration using a sterilized 0.22 µm SteriCup® filter unit.

The activities of the enzymes manganese peroxidase (MnP) and lignin peroxidase (LiP) were determined by UV spectrometry. The peroxidase enzymes in 12 mL of the CFSM was concentrated by a 10 kDa molecular weight cut-off filter (Amicon Ultra-15, MWCO 10 kDa) (Zeng et al., 2013) for 15 min at 5000G and room temperature. The activity of lignin peroxidase and manganese peroxidase were determined using veratryl alcohol and Mn^{2+} as the respective substrates. The assay methods were based on previous work by Wariishi et al. (1992) and Tien and Kirk (1988). It can be briefly described as follows; the MnP assay was conducted in a reaction volume of 1 mL containing 50 mM malonate (pH 4.5), 2 mM Mn^{2+}, 0.4 mM H_2O_2 and 0.5 mL of MWCO concentrate. The Mn^{3+}-malonate complex was determined by spectrometry at 270 nm (extinction coefficient 11590 $M^{-1}cm^{-1}$). The LiP assay

was conducted under similar conditions as for the MnP, with the final volume containing 50 mM succinate (pH 2.5) and 2 mM veratryl alcohol. The veratryl aldehyde concentration was determined by spectrometry at 308 nm (extinction coefficient 9300 $M^{-1}cm^{-1}$). The activities of LiP and MnP in the CFSM was calculated from the results for the MWCO concentrate.

5.2.3. CFSM treatment

A 25 g sample of the original DRGO and 12.5 g of DA sample, were suspended to 500 mL and 250 mL of CFSM at pH 4.0 in four 2 L-flasks and 1 L-flasks, separately. The flasks were covered by porous plugs and shaken at 30°C and 128 rpm for three days. After that, the solids were collected by centrifugation before being re-suspended in a fresh batch of CFSM. This process was repeated five times to degrade the aromatic carbons. After the final step, the solid residues were collected and washed with ultra-pure water before being dried under vacuum. The CFSM treated residues of the as-received sample and DA sample were labelled as DC and DAC, respectively. For comparison, the DC sample was subjected to sulfide oxidation by *A. brierleyi*. The solid residue was named as DCA.

5.2.4. Characterization of carbonaceous matter residue

The flotation concentrate (DRGO) and all of the bio-treated residues were washed with 1 M NaOH to characterize the extracted decomposed carbonaceous matter after treated by CFSM treatment. A 0.4 g of the as-received ore and treated residues were suspended in 8.5 mL of 1 M NaOH. The washing was conducted by shaking for 24 h at 120 rpm and room temperature. Afterwards, the solid mass was collected, washed three times with ultrapure water prior to drying under vacuum for overnight. To observe the effect of the washing on the carbonaceous matter, the solid residues were analyzed by Raman spectroscopy (Thermo

Scientific DXR Smart Raman; 532 nm, 10 mW) and QEMSCAN, and the supernatant was characterized by three-dimensional fluorescence spectrometry (JASCO FP-6600). Raman spectra were analyzed by using the PeakFit software for drawing backgrounds and peak separation.

5.3. Results and Discussion

5.3.1. Carbonaceous matter identification in flotation concentrate

The mineralogical composition of the as-received sample has already been provided in **Table 4.1** and discussed in detail in in section 4.3.3. The discussion was mostly focused on the identification of the major silicate and sulfide phases. However, in this section, the main focus is on the carbonaceous matter. The carbon content in the as-received sample was determined by CHN to be 5.86%, which may include both organic and inorganic forms, due to the existence of small amounts of carbonates in the mineralogical analysis **(Table 4.2)**. Comparatively, the QEMSCAN analysis was only able to detect about a 10% of the carbon in the size fraction of -1000 µm/10 µm, which corresponds to approximately 48.7% of the total mass of the flotation concentrate (**Table 4.1**). The difference between the two results for CHN and QEMSCAN indicates that the carbonaceous matter was most likely concentrated in the -10 µm size fraction (Afenya, 1991). This fraction could not be adequately analyzed due to excessive aggregation by QEMSCAN. Meanwhile, the data shows that the amounts of Fe, As, and S in the flotation concentrate were in good agreement between acid digestion and QEMSCAN results for the as-received sample. Based on both results, it is most likely that the majority of the Fe-sulfides were in the -1000 µm/+10 µm size fraction. This finding suggests that there might be a limited association between the carbonaceous matter and the sulfides.

The mineralogical analysis of the -1000 µm/+10 µm size fraction in as-received ore by QEMSCAN identified the principal silicates and clay minerals as illite ($(K, H_3O)(Al, Mg, Fe)_2(Si, Al)_4O_{10}[(OH)_2, (H_2O)]$), kaolinite ($Al_2Si_2O_5(OH)_4$) and quartz ($SiO_2$) (**Table 4.2**). Surprisingly, the QEMSCAN analysis showed two different types of illite, with the main difference between the two types being the presence or absence of carbon. Ahn et al., (1991) reported that during the crystallization of illite in environments containing carbonaceous matter, the carbonaceous matter could be incorporated into the structure of illite to form a modified illite mineral with mixed silicate and carbonaceous matter phases. Therefore, illite particles containing carbon were labelled as carbonaceous illite. Additionally, the sample contained minute amounts of inorganic carbonate, calcite ($CaCO_3$) and dolomite ($CaMg(CO_3)_2$). This suggests that the carbonaceous illite might have the majority of the carbon in the present carbonaceous gold ore.

Figure 5.1 shows the distribution of the carbonaceous illite throughout the flotation concentrate (DRGO). The carbonaceous illite was mostly liberated in the ore with small amounts being associated with illite, quartz, pyrite, carbonaceous alumino-silicate (C-Si-Al) and others. This mineral was found in each size fraction of the as-received sample, indicating that carbonaceous illite might be the primary host for the organic carbon. The carbon content in the carbonaceous illite grains appeared to fluctuate, which affected the mineral's texture as observed in **Fig. 5.2**, with carbon-poor carbonaceous illite (**Fig. 5.2a**) and carbon-rich carbonaceous illite (**Fig. 5.2b**). A mineral classified as carbonaceous alumino-silicate (C-Si-Al), which is also a carbon bearing mineral, is discussed further in context by comparing with the solid residues after the CFSM treatment. Finally, the QEMSCAN results showed that the significant sulfide phases consist of 15.04% Fe sulfides and 2.45% arsenopyrite (FeAsS) in DRGO by QEMSCAN (**Table 4.2**).

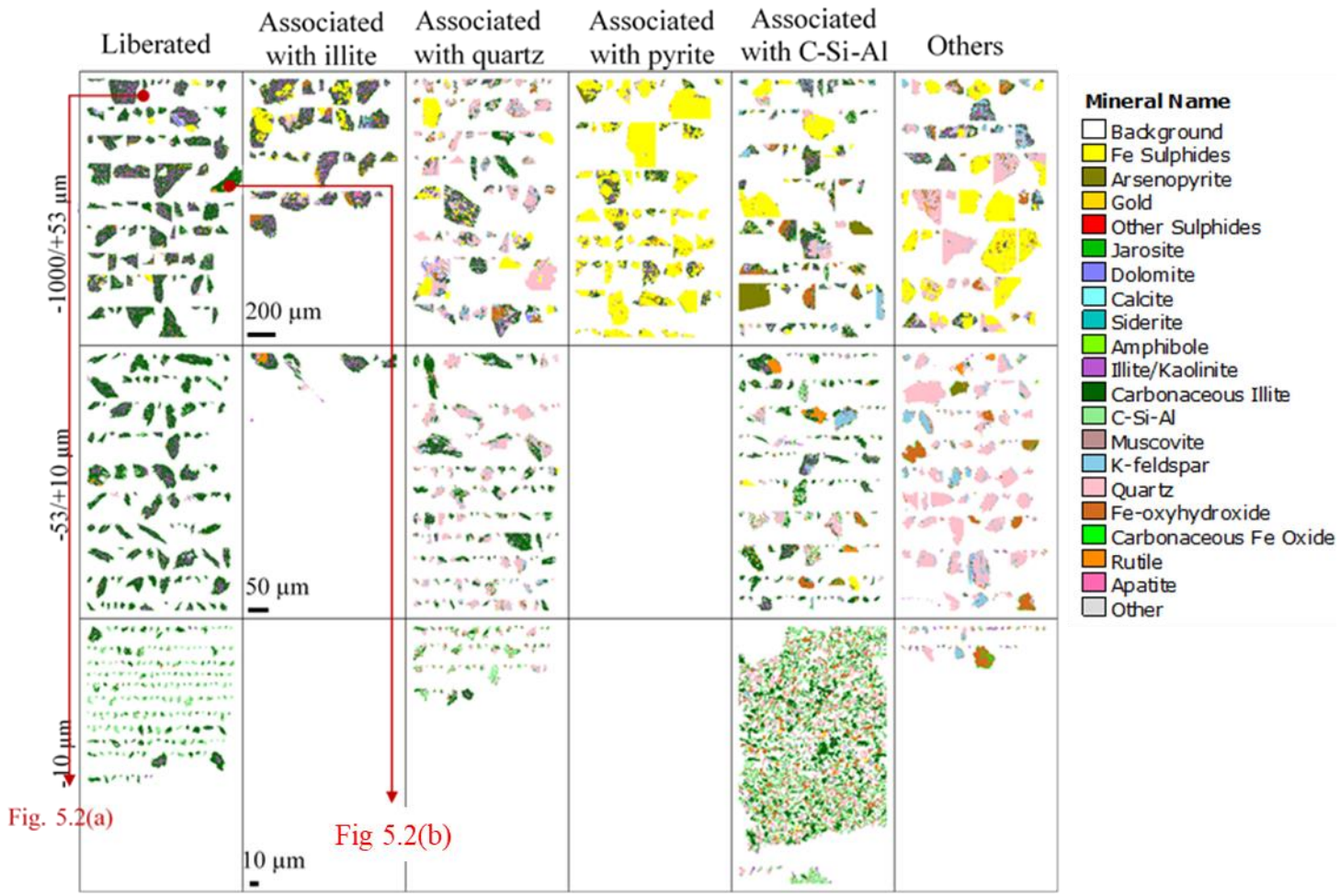

Figure 5. 1 QEMSCAN maps of liberated carbonaceous illite, carbonaceous illite associated with illite, quartz, pyrite, C-Si-Al and others in the as-received ore depending on size fractions (µm). Severe agglomeration in the -10 µm /+0 µm range made the results in the region inconclusive. Scales of 200 µm, 50 µm and 10 µm was used for the -1000 µm /+53 µm and -53 µm/+10 µm and -10 µm respectively.

The effect of carbonaceous matter on the texture of illite is illustrated in **Figure 5.2a** and **5.2b**. Illite particles typically have a flaky texture (Williams and Haydel, 2010) which is evident in both images. However, Figure **5.2a** shows the mixture of small grains of illite and carbonaceous illite, while Figure **5.2b** shows mostly carbonaceous illite. It can also be observed that the carbon content had an impact on the porosity of the particle, with Fig. **5.2b**, which was made up almost entirely of carbonaceous illite, having the more porous texture. Previous studies have reported that the inclusion of organic matter in the illite structure might cause the formation of separate silicate and carbonaceous matter phases in the mineral. This might have resulted in the increased porosity observed for the carbonaceous illite (Ahn et al., 1991, Tian et al., 1998a, Tian et al., 1998b). Further analysis failed to show any other mineral phases containing significant amounts of organic carbonaceous matter, including particles made entirely or mostly of organic carbon. Therefore, it is most likely that all of the organic carbon in the mixture exist as the carbonaceous illite.

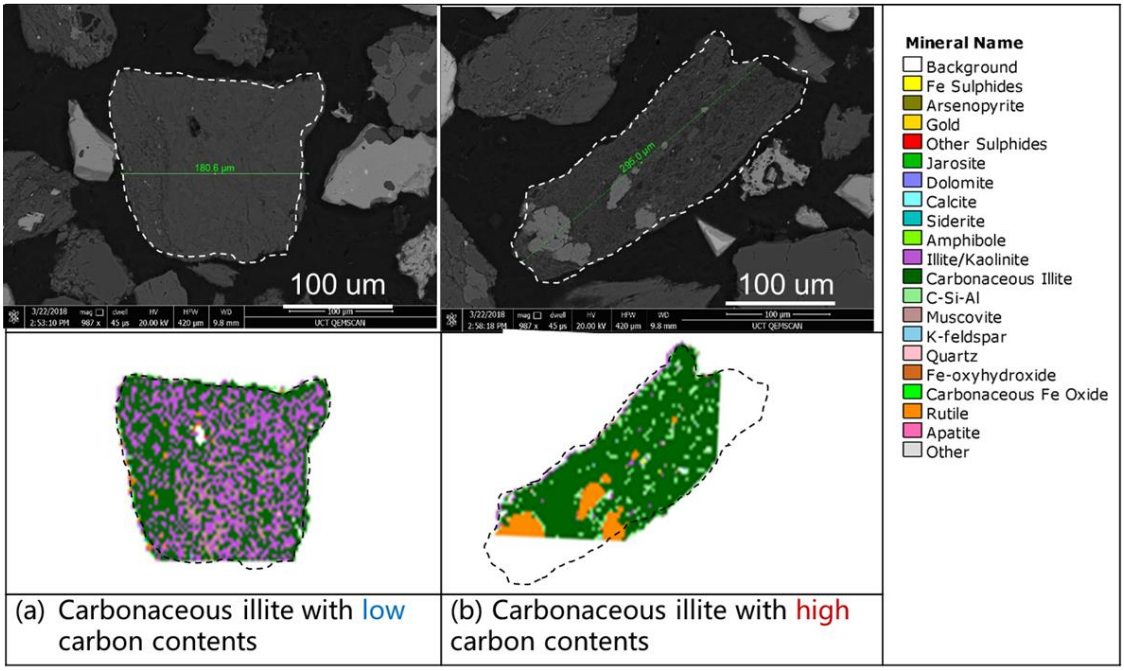

Figure 5. 2 Cross-sectional QEMSCAN images showing the textures of illite particles containing (a) a mixture of carbonaceous illite and illite (b) mostly carbonaceous illite in the as-received ore.

5.3.2. Bio-oxidation of carbonaceous matters by CFSM

The peroxidases in the cell-free spent medium (CFSM) of *P. chrysosporium* were used to decompose the carbonaceous matter in two samples; the flotation concentrate, and after preliminary oxidation of the sulfides by *A. brierleyi* (DA). The resultant samples were named as DC and DAC, respectively. These enzymes, LiP and MnP in the CFSM, had been previously determined using capillary electrophoresis (Harada et al., 2016; Kudo et al., 2017). Therefore, UV spectrometry was applied to determine enzyme activity in the CFSM before it was used on the carbonaceous matter. Slightly purifying the enzymes with the MWCO revealed LiP and MnP activities of 23.0 ±3.8 U/L and 424.3 ± 25.6 U/L in the concentrate, which translated to approximately 1.1 ± 0.2 U/L and 20.6 ± 1.2 U/L of enzymes in the CFSM every 3 days of fungal growth. These enzymes have been shown to decompose carbonaceous matter into smaller organic molecules with the aid of hydrogen peroxide (Wariishi et al., 1991; Liu et al., 2019). Although the enzymatic decomposition mechanism could not be monitored directly due to factors like the sample heterogeneity, it can be expected that the aromatic carbon would serve as the primary substrate for enzymes and thus ensuring its decomposition (Konadu et al., 2017). The effect of the enzymatic treatment was determined by the characterization of the solid residue by QEMSCAN analysis.

The solid residue which was produced after only CFSM treatment of the flotation concentrate (DC), was targeted at decomposing carbonaceous matter (Arora et al., 2002), appears to have resulted in the formation of some unknown by-products as shown by QEMSCAN in **Figure 5.3**. It can be readily observed that the average grain size of the carbonaceous illite, which is the major organic carbon carrier, became smaller after the CFSM treatment. This reduction in grain size was the general case for all size fractions and all the different mineral associations, especially for the liberated carbonaceous illite and those

associations with quartz. Therefore, the relative increase in the amount of quartz and pyrite, and the relative decrease in carbonaceous illite was expected; however, the amount of carbonaceous alumino-silicate (C-Si-Al) relatively increased instead of decreasing (**Table 4.2).** This unexpected finding was due to the formation of new particles with textures unlike the grains previously classified as C-Si-Al in the as-received sample. QEMSCAN observation of the new particles in DC showed that it appeared to have different morphologies from the original C-Si-Al grains in the as received (**Fig. 5.3**). Therefore, to distinguish this new type of C-Si-Al found in the DC residue from that in the original flotation concentrate, parameters like the accepted EDS intensity range for carbon and aluminum in C-Si-Al and carbonaceous illite were modified (**Fig. 2.1**) and all the sample were reclassified. Notably, the major differences between the C-Si-Al in DC and the carbonaceous illite in the as-received sample were that the C-Si-Al had relatively higher C content, 50-158.5 arbitrary unit (a.u.), and lower Al content, 40-192 a.u., compared to carbonaceous illite, C content, 10- 50 a.u., Al content 196- 400 a.u.

Furthermore, the C-Si-Al in DC could be distinguished from the as-received sample based on morphology. The C-Si-Al in DC resembled agglomerated sediments while the C-Si-Al in the as-received ore appeared like the carbonaceous illite in **Fig. 5.2** except for having slightly higher carbon content. This higher carbon content might have been partly derived from overestimation occurring at the interface between the edge carbonaceous illite particle and the wax background. Based on this result, it is likely that the new carbonaceous alumino-silicate (C-Si-Al) with the highly porous structure is the by-product of the CFSM decomposition of the carbonaceous matter containing illite.

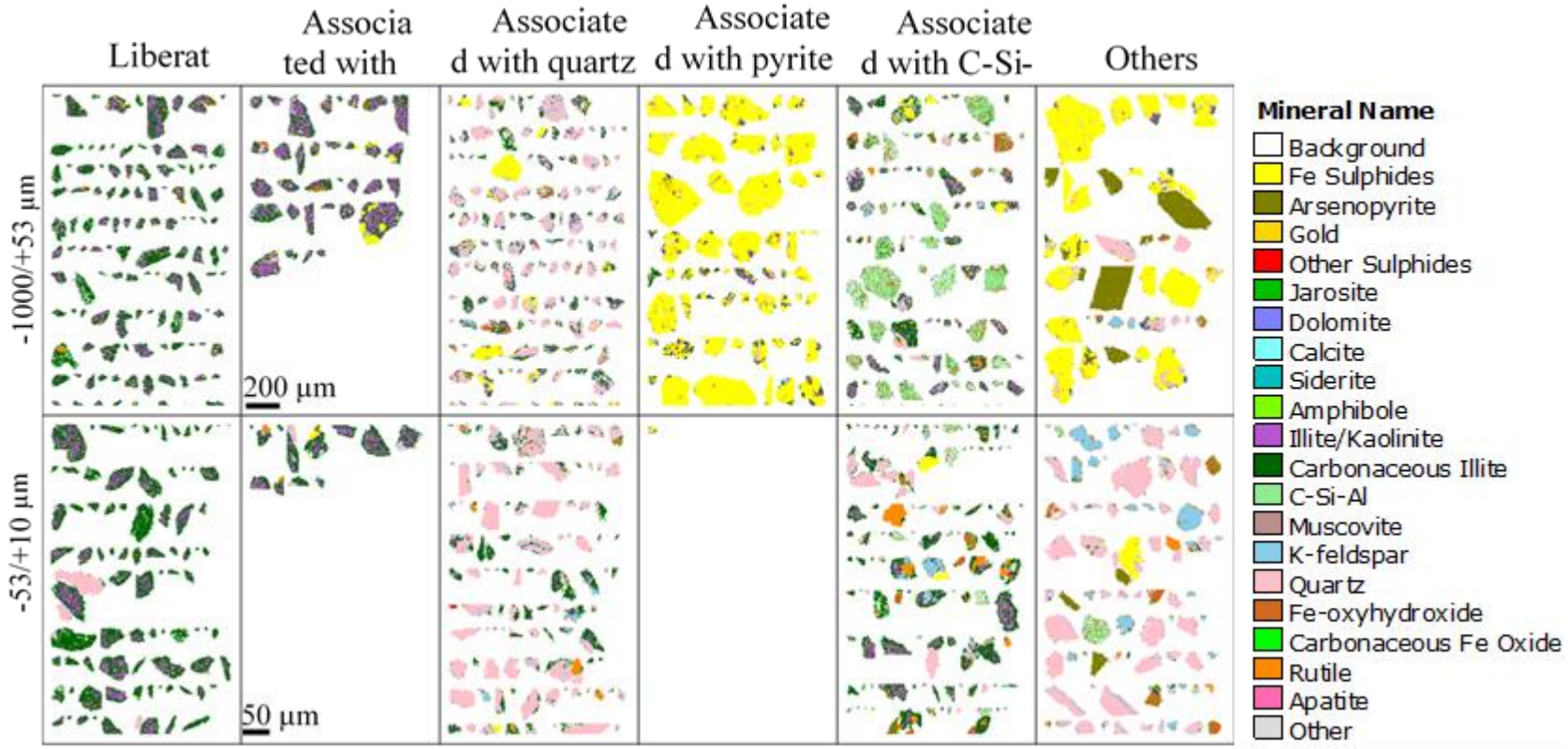

Figure 5. 3 QEMSCAN maps of liberated carbonaceous illite, carbonaceous illite associated with illite, quartz, pyrite, C-Si-Al and others in the solid residue of DRGO after 15 days-treated by CFSM (DC) depending on size fractions (µm). Scales of 200 µm, 50 µm and 10 µm was used for the -1000 µm /+53 µm and -53 µm/+10 µm and -10 µm respectively.

The effect of the peroxidase enzymes on the carbonaceous matter in the DAC system is illustrated by **Figures 5.4**. This treatment sequence ensured a very significant decrease in sulfides, from 13.5% to 0.77% for Fe sulfide and 0.77% to 0.02% for arsenopyrite. Additionally, the carbonaceous matter in carbonaceous illite was oxidized and converted into smaller molecules, resulting in the formation of large particles of C-Si-Al. **Fig 5.5** shows that the amount of C-Si-Al significantly increased from 2.78% in DA to 19.48% in DAC. This relative increase might have also been seen due to the almost complete dissolution of Fe sulfides and arsenopyrite in DAC by mostly *A. brierleyi* and to a limited extent by the CFSM (Ofori-Sarpong et al., 2013; Mahmoud et al., 2017). The relatively higher amount of the C-Si-Al in the DAC compared to the DC sample indicated that the enzymatic decomposition appeared to have been much more active after the sulfide decomposition in the previous step. The successful enzymatic reaction in the DAC system might have been due to the decrease in arsenic contents caused by oxidative dissolution of arsenopyrite by *A. brierleyi* in the 1st step (**Table 4.1**). It leads to a decrease in the inhibitory effect of arsenic on the enzymatic activity of LiP and MnP in CFSM (Mascher et al., 2002).

The possible order, through which the C-Si-Al was formed by the CFSM treatment of carbonaceous illite in the DAC sequence, is illustrated in **Fig. 5.6** using an observed QEMSCAN view field. The image shows that the carbonaceous illite originally had either a non-porous or a slightly porous nature based on carbon contents (**Fig. 5.6a**). The LiP and MnP attacked the carbonaceous matter in carbonaceous illite, and upon its oxidation, the porosity of the carbonaceous illite grains increased until the texture changed to resemble the agglomerated sediments (**Fig 5.6b-c**).

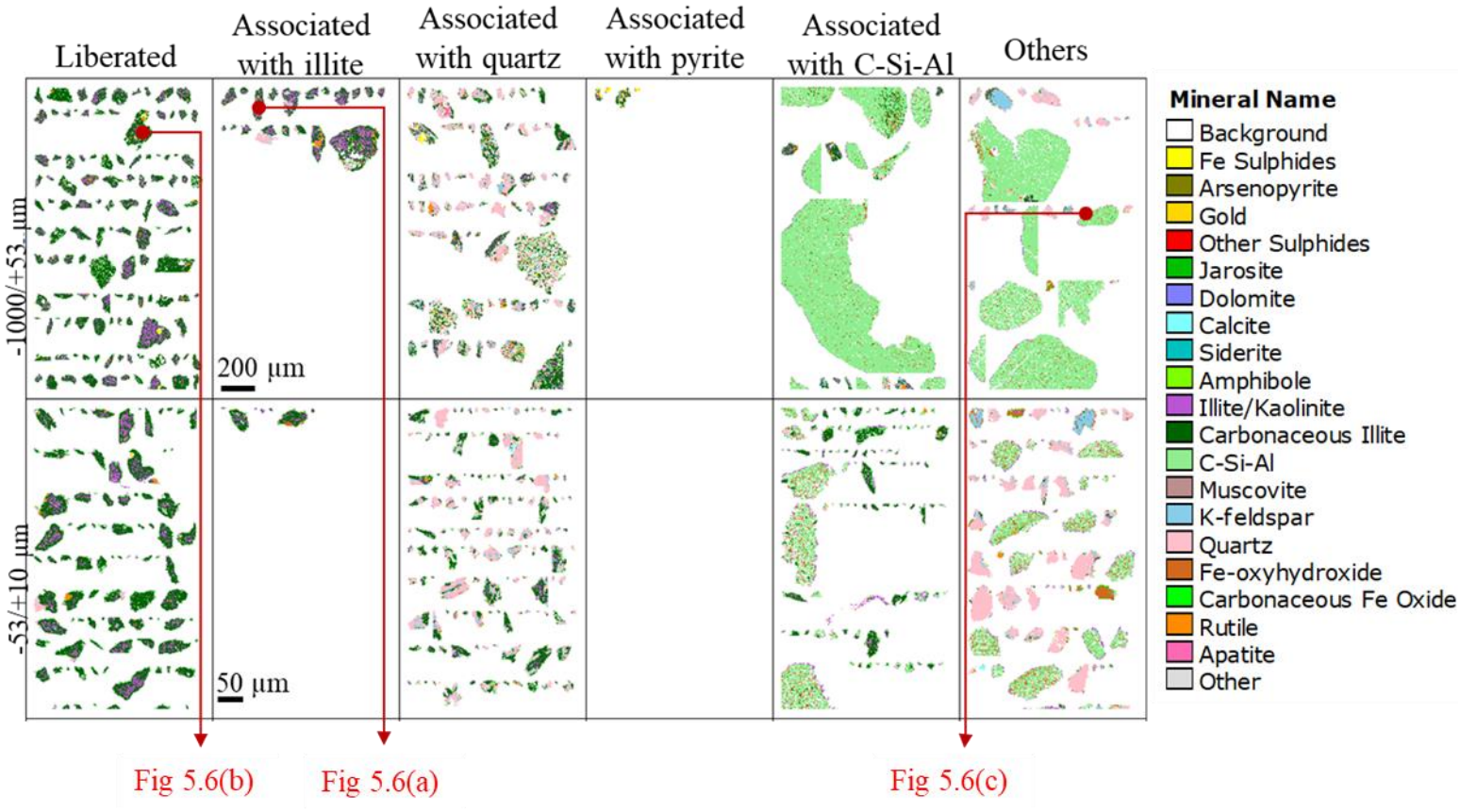

Figure 5. 4 QEMSCAN maps of liberated carbonaceous illite, carbonaceous illite associated with illite, quartz, pyrite, C-Si-Al and others in the solid residues after the treatment of DAC depending on size fractions (µm). Scales of 200 µm, 50 µm and 10 µm was used for the -1000 µm /+53 µm and -53 µm/+10 µm and -10 µm respectively.

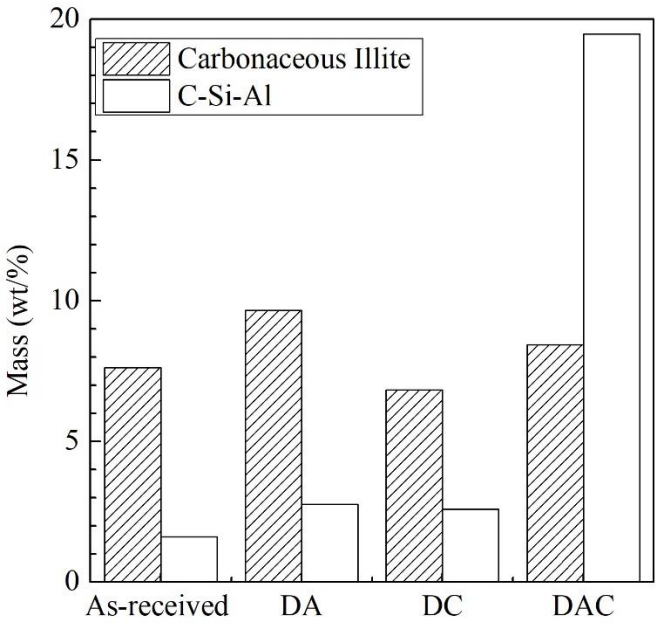

Figure 5. 5 QEMSCAN quantification of the carbonaceous matter bearing minerals in the as-received sample and the bio-treated residues.

Thus, it suggests that the newly formed organic carbon might have been distributed among smaller grains of illite (Ahn et al., 1999) and after decomposition of organic carbon in carbonaceous illite by the enzyme treatment, the C-Si-Al particle appeared to have become overly porous relative to the carbonaceous illite. The large size of the C-Si-Al relative to the carbonaceous illite points out that either the CFSM or the enzymatic decomposition of the carbonaceous matter produced binding agents that aided in the agglomeration of the silicates to form such large structures. These binding agents from the CFSM might include polysaccharides, and organic acids (Moreira et al., 2003; Flemming and Wingender, 2010) used to cultivate the fungus or produced by the fungus itself during its growth in the culturing and treatment steps as reported by DNA analysis (**Fig 4.11**). On the other hand, the product of enzymatic decomposition of the carbonaceous matter was characterized by Raman spectroscopy and fluorescence analysis to identify some of its properties.

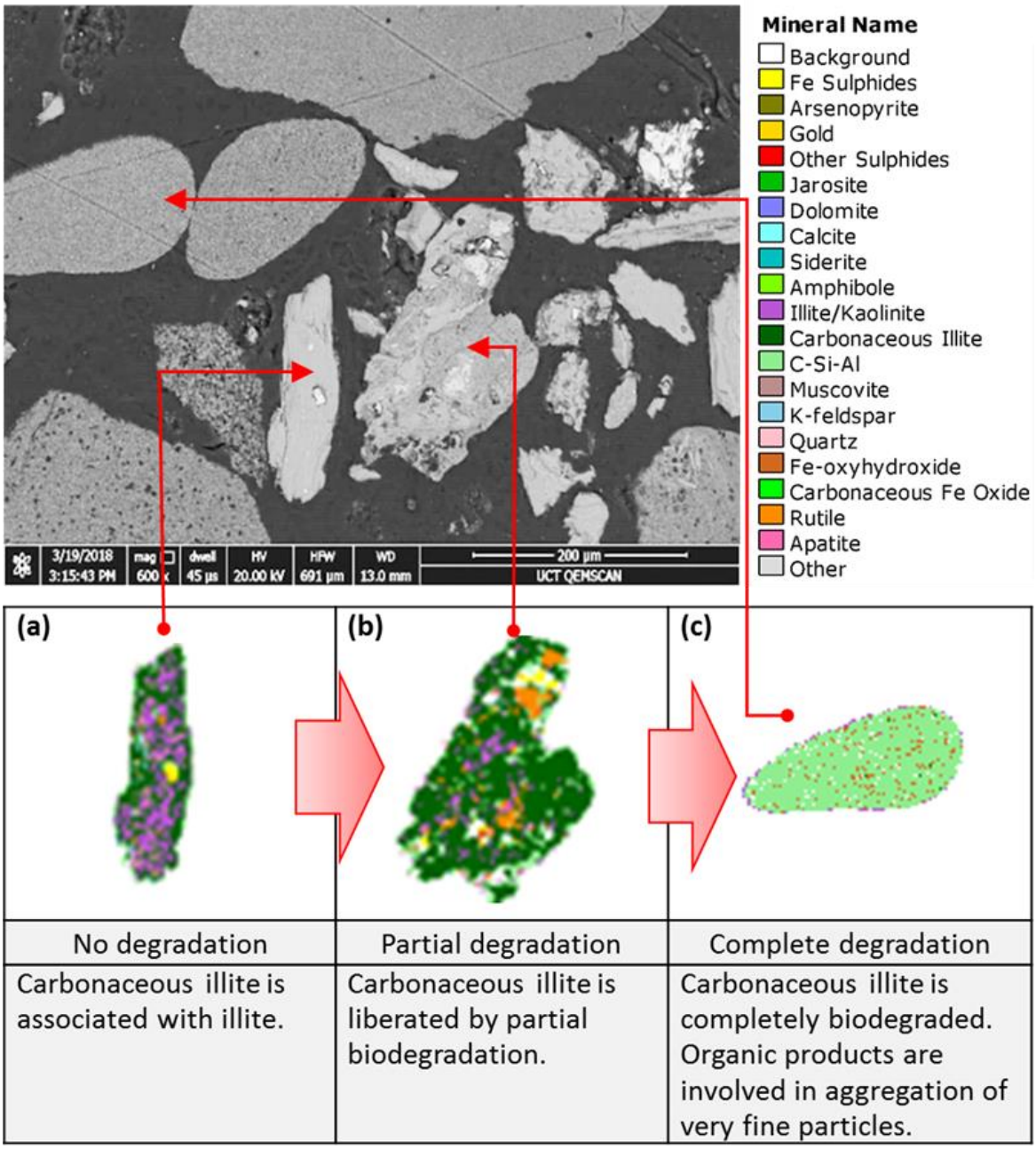

Figure 5. 6 Cross-sectional QEMSCAN images showing the conversion of carbonaceous illite into a carbonaceous alumino-silicate in solid residues after DAC treatment.

5.3.3. Chemical characterization of the solid residues

Figure 5.7a and 5.7b show the Raman spectra of all samples before and after the alkaline washing. Raman spectrum in a region from 1800 to 1200 cm^{-1} is often used to evaluate the

completeness of sp^2 orbital of aromatic carbon in graphite (Ferrari et al., 2007). The spectra had a low S/N ratio because the aromatic/graphitic carbon in as-received makes up less than 6wt% of the ore (Table 4.1), suggesting that it is not in a physically or chemically homogenous in the sample (Pimenta et al., 2007). The as-received sample showed two clear bands at 1341 cm^{-1} and 1582 cm^{-1} and one small band around 1460 cm^{-1}. Two clear bands can be assigned to the graphitic carbon (G-band) at 1582 cm^{-1} and the defect (D-band) at 1350 cm^{-1} (Sonibare et al., 2010; Dimov and Hart, 2017). After peak separation for each spectrum, the relative intensity of I_D/I_G was calculated using the peak areas and summarized in **Figure 5.7c** to evaluate the biodegradation characteristics.

After the CFSM treatment only, the relative intensity of I_D/I_G decreased compared with the as-received (**Fig. 5.7c**). The same trend can also be observed from DA to DAC. These results indicate that the enzymatic treatment was much more effective in decomposition of defect-bearing C=C bonds in the chemically and physically defective sites, i.e. sp^2 carbons close to other functional groups, cracks and edges (Pimenta et al., 2007; Russier et al., 2011), because G-band type of carbons are too stable to degrade enzymatically. Such physical defects would have increased the area of graphitic carbon available to the enzymes while the chemical heterogeneity could have made it easier for the cleavage of the aromatic rings to occur (Kirk and Farrell, 1987). This trend was never observed in the transformation from as-received to DA, and from DC to DCA. It is evident that bio-oxidation of sulfides by *A. brierleyi* had a minimal effect on the relative intensities of I_D/I_G for DA and DCA, and this might be due to the limited association between sulfides and carbonaceous illite (**Table 4.1**).

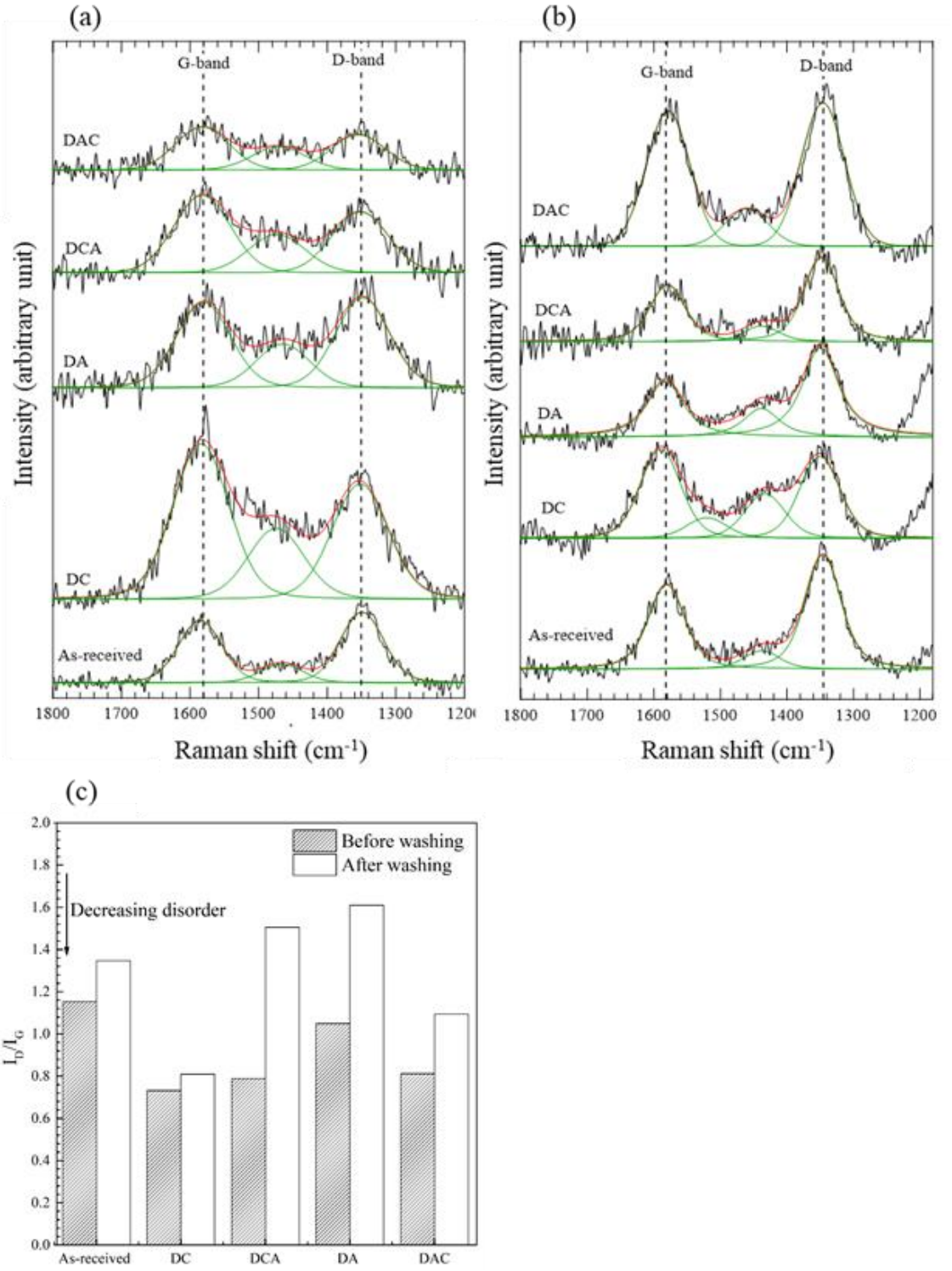

Figure 5. 7 Raman spectra (a) before and (b) after 1 M NaOH washing of the as-received ore, and the solid residues after treated by CFSM (DC), *A. brierleyi (*DA), CFSM followed by *A. brierleyi* (DCA), and *A. brierleyi* followed by CFSM. (c) the intensity ratio (I_D/I_G) for the relative quantity of the defect in all samples with graphitic structures.

Next, it can be observed that alkaline washing with 1 M NaOH tended to convert G-band type of carbons into D-band type of carbon in as-received, so the relative intensity of I_D/I_G increased. This trend is common in all other samples in **Fig. 5.7a-c**. After washing the DAC sample with 1 M NaOH, the extracted solution was brownish, suggesting that humic-like substances were extracted (Sasaki et al., 1996) and that G-band type of carbons were partially decomposed to dissolve into soluble humic-like substances. To characterize the extracted solution, the three-dimensional fluorescence spectrometry was applied, which is known to show the characteristic "fluorescence fingerprint" of aromatic compounds.

Figure 5.8a shows that the three-dimensional fluorescence peak position for alkaline washing extract of DAC is located at 355 nm of the excitation wavelength (E_x) and 458 nm of the emission wavelength (E_m). The maximum E_x and E_m values for the present substance fall within the range for humic substances determined by previous researchers (Senesi et al., 1991; Plaza et al., 2006; Zhang et al., 2013). This result suggests that the organic by-products like humic substances were formed by oxidative decomposition of the carbonaceous matter in CFSM treatment of DRGO and then retained in the solid residue. It is reported that humic substances have pK_a ranging from 2.9 to 5.5 (Stumm and Morgan,1996) and illite has approximately 2.5-3.0 of pH_{zpc} (Stumm and Morgan,1996; Cappuyns, and Swennen, 2008). As such, electrostatic complexes may form between the clay and humic substances at pH 4.0 used for the CFSM reaction if the humic substances are protonated. Meanwhile, if the carboxylic groups in humic substances are dissociated, they are negatively charged and would not interact electrostatically with the illite at pH 4.0. In such a case, the presence of dissolved metallic ions like Fe^{3+}, released by oxidative dissolution of Fe sulfides, and other ions like Mg^{2+} which exist in the CFSM, might aid in the formation and stabilization of the humic-like substances in the silicate aggregate (**Fig 5.9**). This might be responsible for the formation of large particles labelled as C-Si-Al.

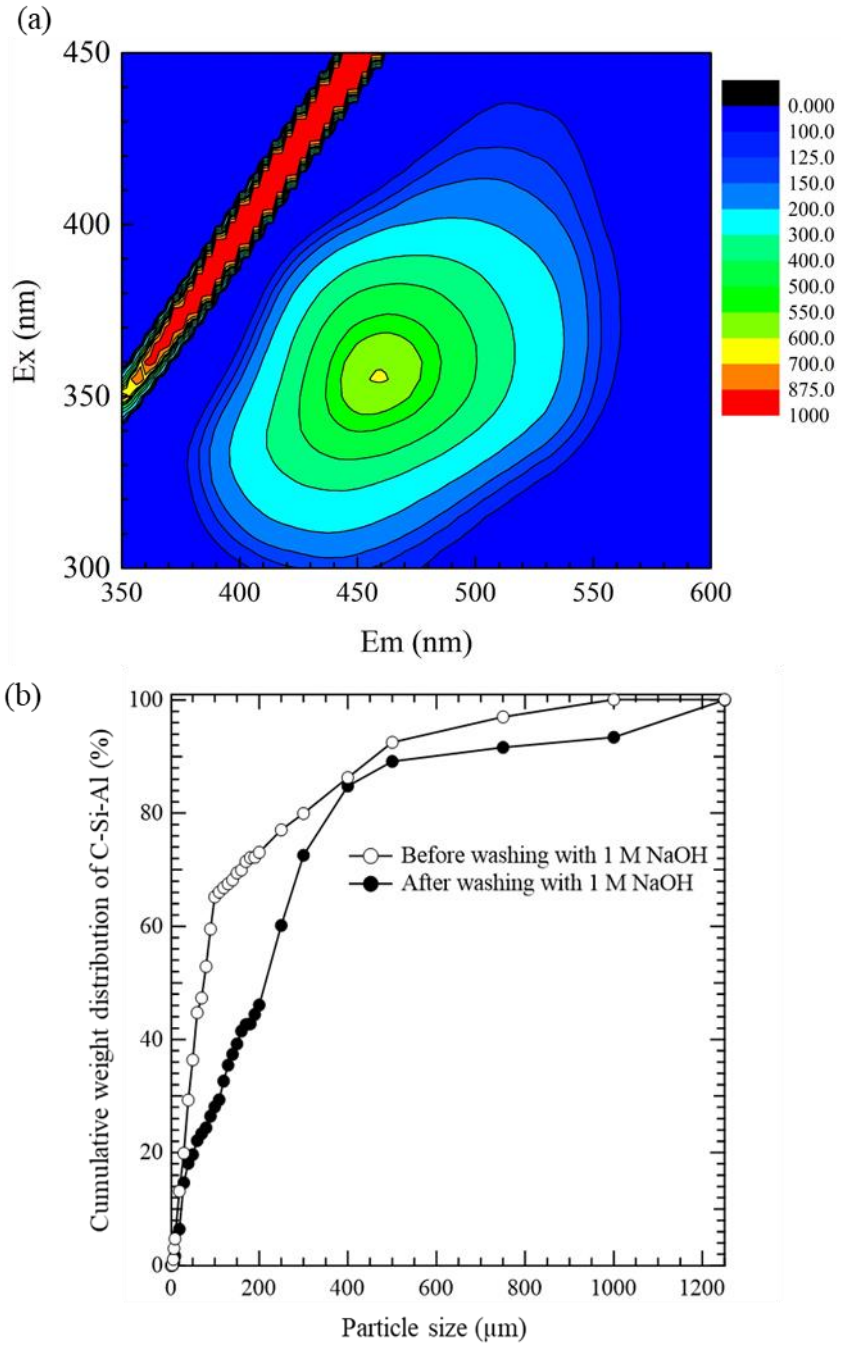

Figure 5. 8 (a) Three-dimensional fluorescence spectrum for the supernatant after 1 M NaOH washing of DAC and (b) cumulative particle size distribution of C-Si-Al using QEMSCAN to compare the solid residue of DAC before and after 1 M NaOH washing.

After washing the solid residue of DAC with 1 M NaOH, the grain size distribution of C-Al-Si particles was analyzed by QEMSCAN in **Fig. 5.8b**. The relative abundance of the C-Al-Si

particles in the size fraction of 50 ~ 400 μm decreased during alkaline washing of DAC. This suggests that the newly formed large particles include an easily dissolved organic fraction in alkaline solution. However, the dissolution of the humic-like substances appears to have shrunk rather than destroying the C-Si-Al structure because the amount of C-Si-Al in the DAC before and after washing was 19.48wt% and 17.74wt% respectively. Therefore, the C-Si-Al might contain other binding or bridging agents in addition to the humic-like substances. Alkaline-insoluble substances like polysaccharides, organic acids and proteins, which are among the substances released extracellularly by the fungus (Flemming, and Wingender, 2010) might be involved in the aggregation of fine aluminosilicates as these "bridges".

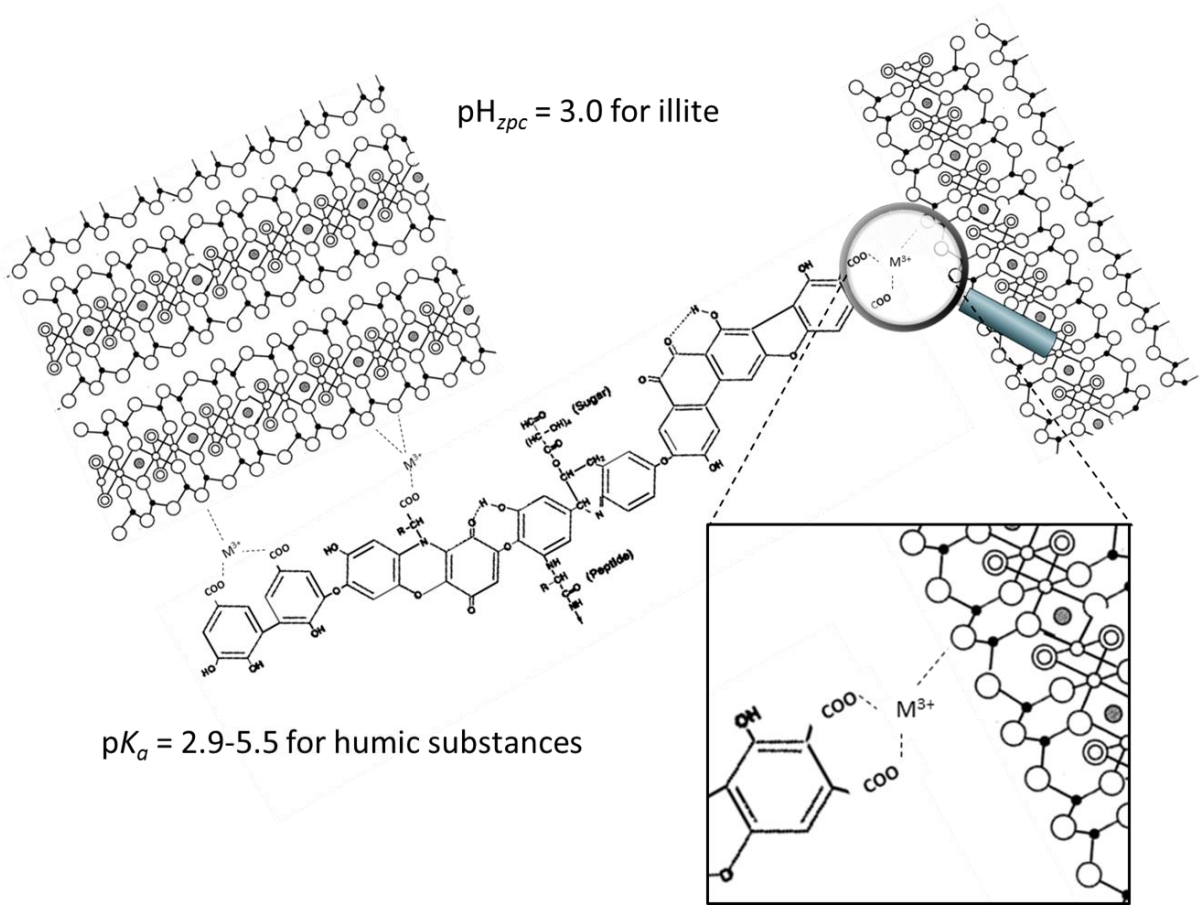

Figure 5. 9 Schematic representation of the formation of carbonaceous aluminosilicate (C-Si-Al) from the decomposition of carbonaceous matter by the CFSM.

5.4. Conclusions

This study applied QEMSCAN analysis to identify the carbonaceous matter in a DRGO sample in its initial state and also characterize the product after enzymatic treatment. It was discovered that the carbonaceous matter was associated with illite and the porosity of the ensuring carbonaceous illite mineral was dependent on the amount of carbon in the structure. It was concluded that the CFSM treatment was able to decompose the carbonaceous matter into humic-like substances by attacking the graphitic carbon with some physical or chemical defects. The product after the CFSM treatment seems to be humic-like substances, which are involved in the formation of a sediment-like carbonaceous alumino-silicate (C-Si-Al), indicating that CFSM treatment altered the refractory carbonaceous matters into easily decomposable compounds by alkaline washing. The treatment sequence consisting of (1) microbiological sulfide decomposition and (2) enzymatic decomposition of carbonaceous matter, (3) alkaline washing yielded the greatest Au(0) recovery without any harsh chemical conditions. This process opens up the possibility for bio-mineral processing of carbonaceous precious metal ores, which are sometimes not developed for economic reasons.

References

Abotsi, G.M., Osseo-Asare, K., 1986. Surface chemistry of carbonaceous gold ores I. Characterization of the carbonaceous matter and adsorption behavior in aurocyanide solution. *Inter. J. Miner. Process.* 18, 217-236.

Afenya, P.M., 1991. Treatment of carbonaceous refractory gold ores. *Miner. Eng*. 4, 1043-1055.

Ahn, J.H., Cho, M., Buseck, P.R., 1999. Interstratification of carbonaceous material within illite. *Am. Mineral*. 84, 1967-1970.

Amankwah, R.K., Pickles, C.A., 2009. Microwave roasting of a carbonaceous sulphidic gold concentrate. *Miner. Eng*. 22, 1095-1101.

Amankwah, R.K., Yen, W.T., Ramsay, J.A., 2005. A two-stage bacterial pretreatment process for double refractory gold ores. *Miner. Eng*. 18, 103-108.

Arora, D.S., Chander, M., Gill, P.K., 2002. Involvement of lignin peroxidase, manganese peroxidase and laccase in degradation and selective ligninolysis of wheat straw. *Inter. Biodeter. Biodegrad.* 50, 115-120.

Butcher, A.R., Helms, T.A., Gottlieb, P., Bateman, R., Ellis, S., Johnson, N.W., 2000, October. Advances in the quantification of gold deportment by QEMSCAN. In *Seventh Mill Operators Conference, Kalgoorlie, WA, AusIMM* , 267-271.

Cappuyns, V., Swennen, R., 2008. The use of leaching tests to study the potential mobilization of heavy metals from soils and sediments: a comparison. *Water Air Soil Pollut*. 191, 95-111.

Dimov, S.S., Hart, B.R., 2017. Applications of microbeam analytical techniques in gold deportment studies and characterization of losses during the gold recovery process. *Surf. Interface Anal*. 49, 1404-1415.

Ferrari, A.C., 2007. Raman spectroscopy of graphene and graphite: disorder, electron–phonon coupling, doping and nonadiabatic effects. Solid State Commun. 143, 47-57.

Flemming, H.C., Wingender, J., 2010. The biofilm matrix. Nat. Rev. Microbiol. 8, 623-633.

Goodall, W.R., Scales, P.J., Butcher, A.R., 2005. The use of QEMSCAN and diagnostic leaching in the characterization of visible gold in complex ores. *Miner. Eng*. 18, 877-886.

Haque, K.E., 1987. Gold leaching from refractory ores—literature survey. *Miner. Process Extr M*. 2, 235-253.

Harada, A., Sasaki, K., Kaneta, T., 2016. Direct determination of lignin peroxidase released from *Phanerochaete chrysosporium* by in-capillary enzyme assay using micellar electrokinetic chromatography. *J. Chromatogr. A*, 1440,145-149.

Helm, M., Vaughan, J., Staunton, W.P., Avraamides, J., 2009. An investigation of the carbonaceous component of preg-robbing gold ores. In World gold conference, 139-144.

Jha, M.C., 1987. Refractoriness of Certain Gold OrestoCyanidation: Probable Causes and Possible Solutions. *Miner. Process Extr M*. 2, 331-352.

Kirk, T.K., Farrell, R.L., 1987. Enzymatic" combustion": the microbial degradation of lignin. *Annu. Rev. Microbiol.* 41, 465-501.

Konadu, K.T., Sasaki, K., Kaneta, T., Ofori-Sarpong, G., Osseo-Asare, K., 2017. Bio-modification of carbonaceous matter in gold ores: Model experiments using powdered activated carbon and cell-free spent medium of *Phanerochaete chrysosporium*. *Hydrometallurgy*, 168, 76-83.

Kudo, S., Harada, A., Kubota, H., Sasaki, K., Kaneta, T., 2017. Simultaneous determination of manganese peroxidase and lignin peroxidase by capillary electrophoresis enzyme assays. *ACS Omega*, 2, 7329-7333.

Liu, J., Zhang, S., Shi, Q., Wang, L., Kong, W., Yu, H., Ma, F., 2019. Highly efficient oxidation of synthetic and natural lignin-related compounds by *Physisporinus vitreus* versatile peroxidase. *Inter. Biodeter. Biodegrad*. 136, 41-48.

Liu, Y., Gupta, R., Sharma, A., Wall, T., Butcher, A., Miller, G., Gottlieb, P., French, D., 2005. Mineral matter–organic matter association characterisation by QEMSCAN and applications in coal utilisation. *Fuel,* 84, 1259-1267.

Mahmoud, A., Cezac, P., Hoadley, A.F., Contamine, F., D'Hugues, P., 2017. A review of sulfide minerals microbially assisted leaching in stirred tank reactors. *Inter. Biodeter. Biodegrad*. 119, 118-146.

Mascher, R., Lippmann, B., Holzinger, S. Bergmann, H., 2002. Arsenate toxicity: effects on oxidative stress response molecules and enzymes in red clover plants. *Plant Sci.* 163, 961-969.

Moreira, M.T., Feijoo, G. and Lema, J.M., 2003. Fungal bioreactors: applications to white-rot fungi. *Rev. Environ. Sci. Biotechnol.* 2, 247-259.

Ofori-Sarpong, G., Osseo-Asare, K., Tien, M., 2013. Mycohydrometallurgy: Biotransformation of double refractory gold ores by the fungus, *Phanerochaete chrysosporium*. *Hydrometallurgy*, 137, 38-44.

Pimenta, M.A., Dresselhaus, G., Dresselhaus, M.S., Cancado, L.G., Jorio, A., Saito, R., 2007. Studying disorder in graphite-based systems by Raman spectroscopy. *Phys. Chem. Chem. Phys*. 9, 1276-1290.

Pirrie, D., Butcher, A.R., Power, M.R., Gottlieb, P., Miller, G.L., 2004. Rapid quantitative mineral and phase analysis using automated scanning electron microscopy (QemSCAN); potential applications in forensic geoscience. *Geol. Soc*. 232, 123-136.

Plaza, C., Brunetti, G., Senesi, N., Polo, A., 2006. Fluorescence characterization of metal ion–humic acid interactions in soils amended with composted municipal solid wastes. *Anal. Bioanal. Chem*. 386, 2133-2140.

Russier, J., Ménard-Moyon, C., Venturelli, E., Gravel, E., Marcolongo, G., Meneghetti, M., Doris, E., Bianco, A., 2011. Oxidative biodegradation of single-and multi-walled carbon nanotubes. *Nanoscale*, 3, 893-896.

Sasaki, K., Tsunekawa, M., Tanaka, S., Konno, H., 1996. Suppression of microbially mediated dissolution of pyrite by originally isolated fulvic acids and related compounds. *Colloids and Surfaces A: Physicochemical and Engineering Aspects* 119 (1996) 241-253.

Senesi, N., Miano, T.M., Provenzano, M.R., Brunetti, G., 1991. Characterization, differentiation, and classification of humic substances by fluorescence spectroscopy. *Soil Sci.* 152, 259-271.

Sonibare, O.O., Haeger, T., Foley, S.F., 2010. Structural characterization of Nigerian coals by X-ray diffraction, Raman and FTIR spectroscopy. *Energy*, 35, 5347-5353.

Stumm, W, and Morgan, J.J, 2012. Aquatic Chemistry: Chemical equilibria and rates in natural waters. John Wiley & Sons.

Tien, M., Kirk, T.K., 1988. Lignin peroxidase *of Phanerochaete chrysosporium*. *Meth. Enzymol.* 161, 238-249.

Wariishi, H., Dunford, H.B., MacDonald, I.D., Gold, M.H., 1989. Manganese peroxidase from the lignin-degrading basidiomycete *Phanerochaete chrysosporium*. Transient state kinetics and reaction mechanism. *J. Biol. Chem*. 264, 3335-3340.

Wariishi, H., Gold, M.H., 1990. Lignin peroxidase compound III. Mechanism of formation and decomposition. *J. Biol. Chem*. 265, 2070-2077.

Wariishi, H., Valli, K., Gold, M.H., 1991. In vitro depolymerization of lignin by manganese peroxidase of *Phanerochaete chrysosporium*. *Biochem. Biophys. Res Commun*. 176, 269-275.

Zeng, G.M., Zhao, M.H., Huang, D.L., Lai, C., Huang, C., Wei, Z., Xu, P., Li, N.J., Zhang, C., Li, F.L., Cheng, M., 2013. Purification and biochemical characterization of two extracellular peroxidases from *Phanerochaete chrysosporium* responsible for lignin biodegradation. *Inter. Biodeter. Biodegrad*. 85, 166-172.

Zhang, Y., Liu, X., Osburn, C.L., Wang, M., Qin, B., Zhou, Y., 2013. Photobleaching response of different sources of chromophoric dissolved organic matter exposed to natural solar radiation using absorption and excitation–emission matrix spectra. PLoS One, 8, 77515-77528.

Zumberge, J.E., Sigleo, A.C., Nagy, B., 1978. Molecular and elemental analyses of the carbonaceous matter in the gold and uranium bearing Vaal Reef carbon seams, Witwatersrand sequence. *Miner. Sci. Eng*. 10, 223-246.

Chapter 6:

Fungal mediated decomposition of carbonaceous matter in carbonaceous metallic sulfide ores: Preliminary study using DRGO as a surrogate for sulfidic ore

6.1. Introduction

The ubiquity of carbonaceous matter in the environment means that it has been found to not only associate with gold hosting pyrite and arsenopyrite but also with other important sulfides like chalcopyrite, Molybdenite, Vaesite and others (Cailteux et al., 2005; Wang and Wang 2010). The presence of the carbonaceous matter in these sulfide ores introduces two main issues that would affect the recovery of these metals. Firstly, the distribution of carbonaceous matter throughout the ore would affect its surface charge and thus its adsorptive properties. If the carbonaceous matter has the same distribution pattern as observed in QEMSCAN for DRGO (Chapter 5), then its interaction with the silicates would result in a relatively more negative surface charge compared to the pristine carbonaceous matter only (Hussain et al.,1996; Zhou et al., 2014). Such a change in the surface potential of the carbonaceous matter while it still retains its structure might increase its ability to adsorb Cu^{2+} and Ni^{2+} ions from solution at the relatively low pH used for bio-oxidation treatments (Kadirvelu et al., 2001; Chen et al., 2003).

Secondly, the presence of carbonaceous matter in the sulfidic copper sulfide or nickel sulfide ore appears to have two diverging effects on bioleaching; (i) improving bio-oxidation by serving as a catalyst and (ii) competitively adsorbing the microbial cells and thus decreasing the leaching efficiency (Nakazawa et al., 1998; Liang et al., 2010; Liu et al., 2015). The positive electro-catalytic effect of the only occurs through direct contact between the carbonaceous matter and the sulfidic mineral (Liang et al., 2010). Such direct contact might be limited in the natural ore, especially if the carbonaceous matter is not hosted by the sulfides. In which case, the competitive adsorption of the microbial cells would be predominant. For these reasons, it important to investigate the possible application of the fungal treatment to a carbonaceous sulfide ore to minimize these negative impacts. This preliminary investigation will focus on using DRGO as a surrogate for a carbonaceous copper sulfide or nickel sulfide ore.

Carbonaceous matter in the DRGO is known to be one of the primary cause of gold recovery

loss. A sequential treatment procedure was employed in the previous work to liberate the gold from the sulfide and prevent preg-robbing by using *Acidianus brierleyi,* and fungal cell-free spent medium (CFSM) from *Phanerochaete chrysosporium* respectively (Chapter 4). DRGO was treated by CFSM then followed by *A. brierleyi* and vice versa. The results from both experiments showed that the second sequence (*A. brierleyi* then CFSM) was successful, and while the first sequence (CFSM then *A. brierleyi*) failed (Chapter 4). It was concluded that the first sequence failed because some of the by-products of the CFSM treatment might have hindered *A. brierleyi* from directly or indirectly attacking the sulfide minerals. However, due to necessity, the bio-treatment sequence to recovery copper or nickel would have to follow the sequence of CFSM treatment before *A. brierleyi* treatment. Therefore, it important to determine the main factor responsible for the inhibition of the sulfide oxidation by *A. brierleyi*.

6.2. Experimental

6.2.1. Sample preparation and washing procedure

The flotation concentrate was subjected to the CFSM only treatment procedure that has already been explained in sections **2.1 and 4.2.2**. The DRGO-treated solid was then washed with 0.1 M HCl, 0.1-1 M NaOH and 2-propanol. 12 g of dried CFSM-treated DRGO were suspended in 250 ml of washing solution for 24 h at 120 rpm and room temperature. Afterwards, the solid was collected, washed three times with ultrapure water before been dried under vacuum overnight. Then, the solid products were analyzed using X-ray powder diffraction (XRD) scanning electron microscope (SEM), Raman spectroscopy, fluorescent in situ hybridization, thermo-gravimetric differential thermal analysis (TG/DTA) and QEMSCAN using similar conditions to those already outlined in section 2.3 except for the QEMSCAN sample preparation. The test was aimed to quantify the amount of agglomerates in the CFSM

treated DRGO before and after washing. To avoid mechanical destruction of these agglomerates, the screening before analysis was conducted using only 10 µm cloth filter.

6.2.2. A. brierleyi *treatment of washed DRGO-CFSM*

4 g of DRGO was added to 80 mL of the HBS medium including 0.04% yeast extract and 5 mM of $FeSO_4.7H_2O$ at pH 1.2 in 200 mL Erlenmeyer flasks, where 10^7 cell/ml of *A. brierleyi* was inoculated. The flasks were shaken at 70°C and 120 rpm for 14 days and supernatants were regularly taken to monitor pH, Eh (vs SHE), total Fe concentrations and cell density. The pH, Eh and dissolved iron and arsenic concentrations were determined, respectively by electrodes and ICP-OES.

6.2.3. Effect of fungal biomass on sulfide oxidation by A. brierleyi

The effect of the fungal biomass on sulfide oxidation by *A. brierleyi* was determined by mixing 0-2% of oven dried, 60°C, *P. chrysosporium* biomass with the as-received sample to simulate the DRGO_CFSM sample after chemical washing. The pyrite oxidation conditions were the same as listed above except for the solid to the liquid to solid ratio, which was 2 g to 100 mL in a 300 mL flask.

6.3. Results and discussion

6.3.1 *CFSM treatment of DRGO*

The flotation concentrate was treated with the CFSM of *P. chrysosporium* to decompose the carbonaceous matter in the sample. The pH and Eh vs SHE rose slightly from 4.03 to 4.49 and 419 mV to 463.7 mV respectively in the first 6 days, after which, it reduced to 4.26 and 418.7 mV and remained virtually constant. The initial increase in pH can be attributed to the

decomposition of some acid depleting minerals in the flotation concentrate, while the slight increase in EH vs SHE cannot be accounted for presently. The total arsenic and iron solubilized by the CFSM were 0.319 mM and 0.095 mM, respectively (**Fig 6.1a**). This accounted for 3% and 0.1% of the arsenic and iron in the sample. Therefore, the data confirms the previous finding that the CFSM treatment was not very effective for the oxidation of sulfides (Chapter 4). The changes in the morphology of the mineral grains over the treatment period were monitored by SEM observation (**Fig. 6.1b-1e**). The SEM observation in **Fig. 6.1b** shows that all of the particles in the as-received sample were virtually liberated from each other before the CFSM treatment. After 3 days of CFSM treatment, particle agglomeration appeared to have occurred as can be seen from the center of the red square in **Fig. 6.1c**. The agglomeration of particle appeared very early in the CFSM treatment, i.e. after 3 days of treatment, and further observation of the solid residues as treatment time progressed showed that it persisted throughout the bio-treatment.

Additionally, the surface of some larger particles were covered by fungal biofilms after the 9th day of treatment (**Fig. 6.1d**). Of these two new features in the bio-residues, particle agglomeration and biofilm formation, it appears that the aggregation formation preceded the biofilm formation on the surface of the mineral grains. The SEM observation was unable to detect the fungal hyphae, but the presence of the biofilm indicates that the *P. chrysosporium* growth might have started by day 9. Particle agglomeration appears to have preceded the formation of the biofilm, indicating that the binding agents were in the CFSM. Although these binding agents do not appear to have been extensively classified, they are most likely some carbohydrates that were synthesized by the *P. chrysosporium* from the glucose that was added to the growth medium (Pigman, 1972; Adams, 2004; Bowman and Free, 2006; Latgé, 2007).

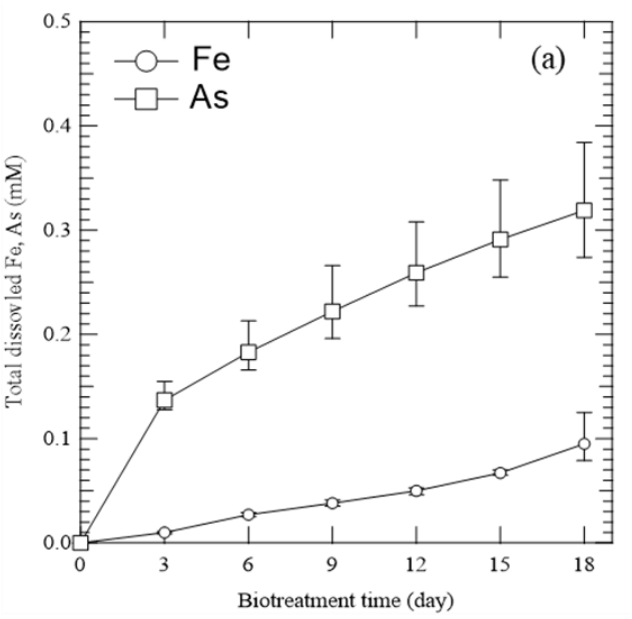

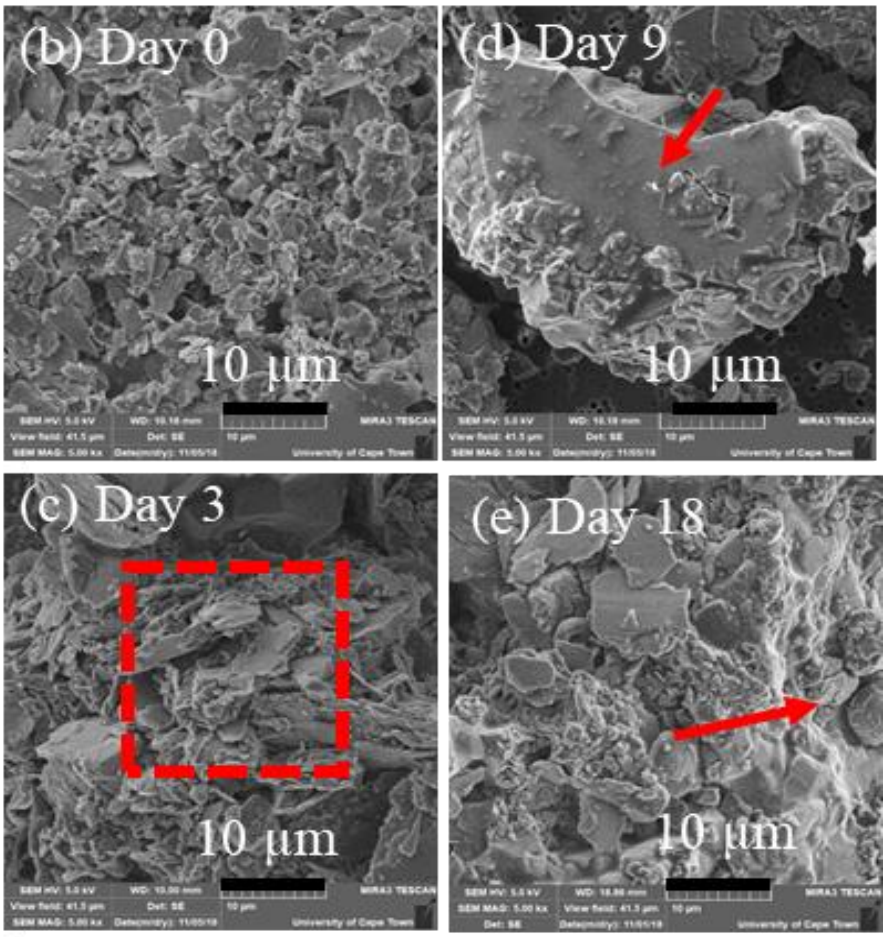

Figure 6. 1 (a) Effect of treatment time on total Fe and As released during CFSM bio-treatment; **(b)-(e)** Effect of CFSM treatment time on morphology of the as-received sample and DRGO_CFSM as observed by SEM. Scale of 10 µm, was used for SEM observation. The

square box in Fig 6.1c shows the increased agglomeration of particles whilst the arrows in Fig 6.1 d and e point to the biofilm formed during the latter part of the experiment.

These two new features in the bio-residue might have been the reason behind the inhibition of the *A. brierleyi.* DNA analysis (**Fig 4.10b**) of the DCA sample showed that although the *A. brierleyi* treatment of the CFSM product was unsuccessful, it appeared to remove the signal for the fungal DNA, indicating that the binding agents and biofilm might be soluble under acidic conditions. Therefore, the CFSM product in this study was washed with various concentrations of HCl. Furthermore, the 3D fluorescence analysis in **Fig 5.8** indicated that the carbonaceous matter was converted to humic substances. The possible effect of this by-product on sulfide oxidation by *A. brierleyi* was determined by introduction NaOH washing before the iron oxidizer. Finally, isopropanol, an organic solvent, was also used on the DRGO_CFSM to solubilize some of the organic by-products of the CFSM treatment. The impacts of the bio-treatments are discussed in the next section.

6.3.2 Effect of washing on the DRGO_CFSM sample

6.3.2.1 HCl

The effect of acidic washing was assessed by SEM observation of the biofilm (**Fig. 6.2**) and QEMSCAN analysis of the larger agglomerates (**Fig 6.3 and 6.4**) formed during the CFSM treatment. A biofilm appeared to form during the CFSM treatment of the DRGO (**6.2a**), and it appears to have been retained even after washing with 0.1 M HCl, above 0.1 M however, the biofilm appeared to disappear from the observed particles (**Fig. 6.2**). This indicates that some of the biomolecules produced by the CFSM treatment are acid soluble (Zhang and Cremer 2006). Therefore, it could be expected that the acidic washing might have a significant effect on particulate agglomeration by dissolving the binding agents.

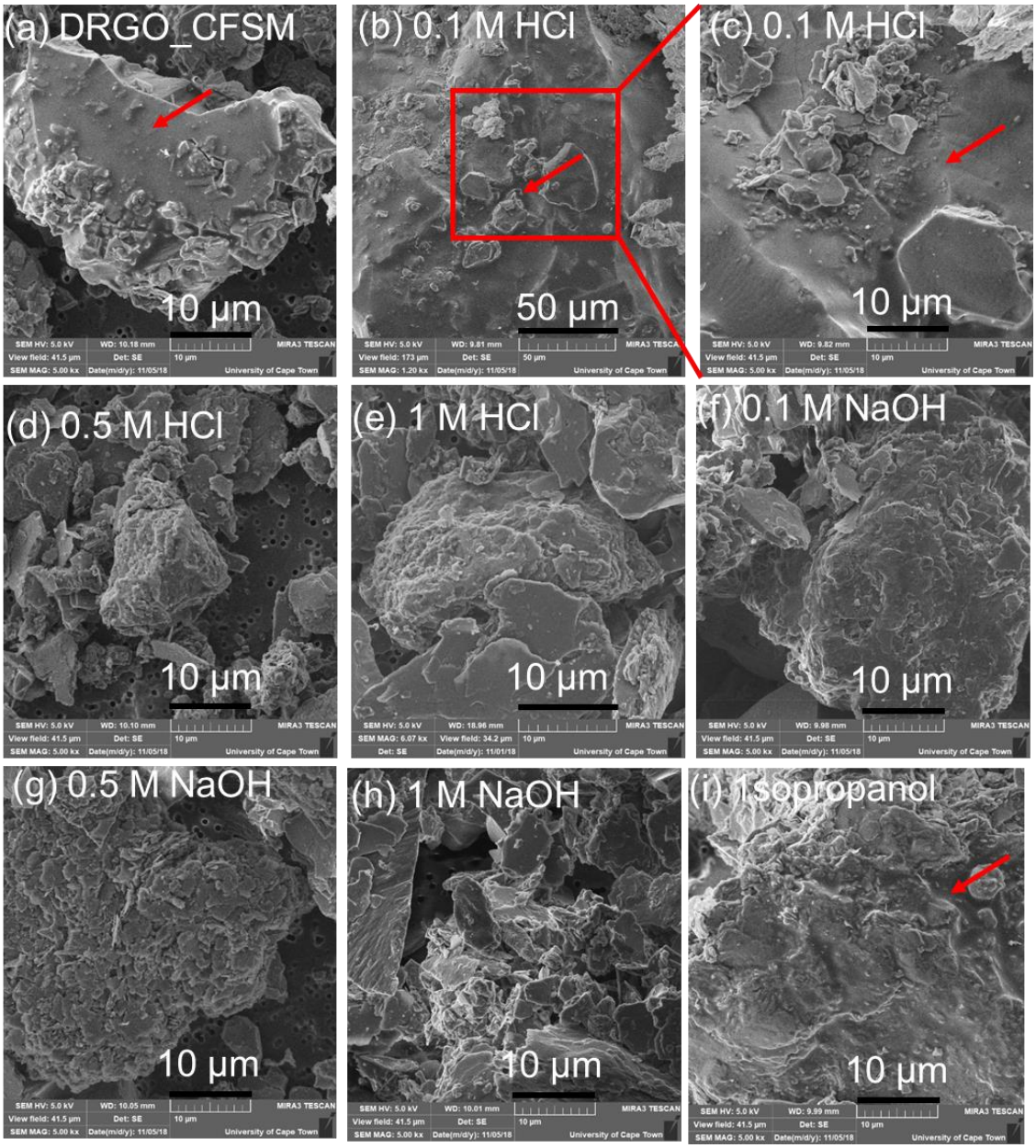

Figure 6. 2 SEM observation of the fungal biofilm in the (a) DRGO_CFSM sample and after it had been subjected to washing with (b), (c) 0.1 M HCl; (d) 0.5 M HCl; (e) 1 M HCl; (f) 0.1 M NaOH; (g) 0.5 M NaOH; (h) 1 M NaOH and (i) isopropanol. Scales of 50 µm and 10 µm were used for SEM observation. The arrows in Fig 6.2a-c and 6.2i point to the biofilm in the individual samples.

The impact of chemically washing the DRGO_CFSM sample on particulate agglomeration was determined by QEMSCAN analysis of the solid. However, it is important to note that the definition of agglomerated particles in this chapter is different from the C-Si-Al in **chapter 5**.

In previous chapters, all the samples for QEMSCAN analysis were screen vigorously using a laboratory scale vibrating screen to obtain +53 µm and – 53 µm products. The – 53 µm products were then subjected to ultra-sonic assisted screening through a 10 µm cloth filter. Therefore, to be able to study the effect of agglomeration in CFSM only treated DRGO using QEMSCAN, only the 10 µm cloth filter was used in this case. Due to altering the screening method, the wt% of the +10 µm fraction increased from 49.3% in **Table 4.2** to 60.5% for this sample. The higher amount of materials in the +10 µm fraction including agglomerates prevented the CFSM only treated DRGO from being analyzed determined because the canuba wax blocks could not maintain a smooth surface after polishing on numerous occasions.

However, the results for the DRGO-CFSM can be intuited from the result for the 2-propanol washed sample, which was analyzed by QEMSCAN, because the large aggregated made up at least 15.9wt%. This means that there was at least 15.9wt% of agglomerates in the DRGO-CFSM sample. This is much larger than the 2.6wt% of C-Si-Al found in the DC samples in chapter 5 (**Table 4.1**). Additionally, agglomerates in the two samples, CFSM only treated DRGO prepared with both vibrating and ultra-sonication screening and only ultrasonic screening, looked very different as shown in **Fig 6.3**. Therefore, it can be summarized that the agglomerated particles described in this chapter is very different from the C-Si-Al produced by carbonaceous matter decomposition.

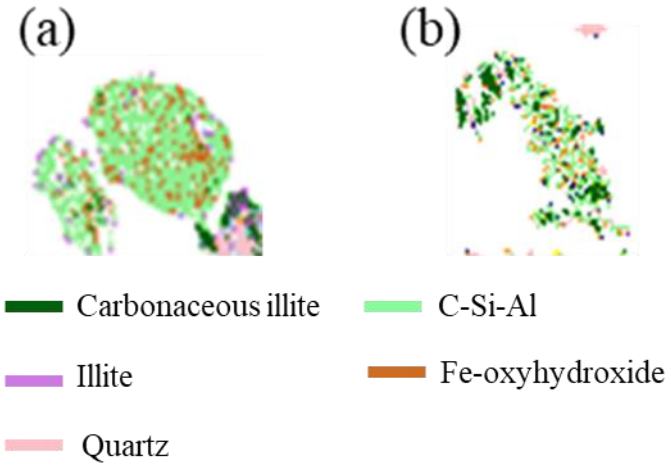

Figure 6. 3 Two types of aggregates produced CFSM only treated DRGO prepared for QEMSCAN analysis using (a) vibrating screening to produce +53 µm and – 53 µm products, followed by ultrasonic-assisted filtering of the – 53 µm products through a 10 µm sieve and (b) only ultrasonic-assisted filtering of the whole sample through a 10 µm sieve.

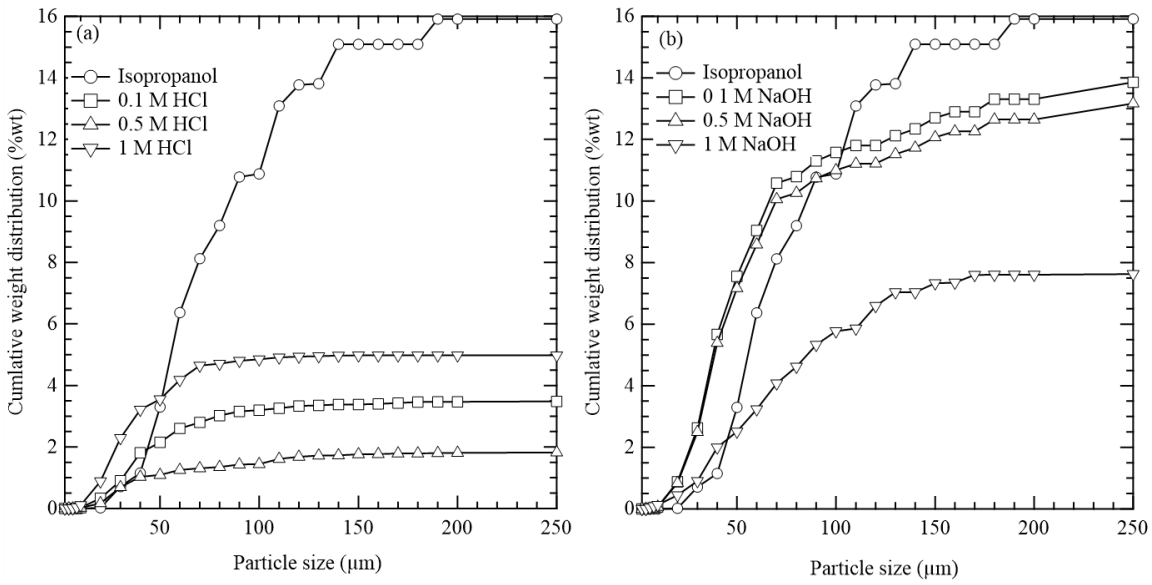

Figure 6. 4 QEMSCAN analysis of the cumulative particle size distribution of larger agglomerates in (a) isopropanol and HCl washed DRGO_CFSM and (b) isopropanol and NAOH washed DRGO_CFSM.

The effect of isopropanol and HCl washing on the number of large aggregates (**Fig. 6.3b**) in the DRGO_CFSM sample was analyzed by QEMSCAN analysis, and the data is shown in **Fig 6. 4a**. Comparatively, it can be observed that the isopropanol washing fared worse at breaking down agglomerated compared with the other chemical agents. This indicates that the binding agents in the solids might have had a high polarity and thus have very low solubility in isopropanol (Bouchard et a., 2007; Montañés et al., 2007). While the HCl washing was very effective at breaking down these aggregate, with the 0.5 M concentration preformation best. Assuming the DRGO_CFSM contained at least 15.9%wt of aggregates, using 0.1 M, 0.5 M and 1 M HCl reduced the number of aggregates by 4.6, 8.7 and 3.2 times respectively. Using the highest concentration of acid appear to have led to the reformation of smaller aggregates sized ≤ 80 μm. This change might be due to the precipitation rather than the solubilisation of the binding agents at the higher Cl^- and ionic strength (Zhang and Cremer 2006). These binding agents are usually carbohydrates and protein produced by *P. chrysosporium* and other white rot fungi to enable their attachment to surfaces (Pigman, 1972). Therefore, it likely that the lower concentration of Cl^- (0.1 M and 0.5 M) help to improve the solubility while 1 M Cl^- produced adverse effects. The HCl washing decreased both the biofilm and aggregations, which should theoretically decrease the inhibition of the *A. brierleyi* by increasing direct/indirect assess to the sulfide minerals.

6.3.2.2 NaOH

The performance of the alkaline washing appears to residue midway between the isopropanol treatment and the HCl treatment (**Fig 6.4b**), indicating that the humic-like substances were removed by increasing the concentration of the NaOH (Kipton et al., 1992). However, the opposite result was observed for the CHN analysis of the solid residues (**Table**

6.1) shows that the NaOH washing might have outperformed the HCl washing. The results show the carbon content in the DRGO_CFSM sample was higher than that of the as-received sample, which is to be expected due to the presence of the fungal binding agents like carbohydrates, humic-like substances and biofilm. After alkaline washing to extract humic-like substances (**Fig 5.8**), the biofilm appears to have disappeared (**Fig 6.2 f-h**). The removal of the biofilm might be due to the hydrolysis-assisted dissolution of some of the carbohydrates that were in the DRGO_CFSM (Chen et al., 2007). The dissolution and removal carbohydrates in addition to the humic substances might be the reason why the 1 M NaOH washed DRGO_CFSM sample had the lowest carbon content of 5.95%.

6.3.3 A. brierleyi *treatment of washed DRGO_CFSM*

The effectiveness of the washing at reducing the inhibition of *A. brierleyi* determined for the DRGO_CFSM sample and the washed solid residues (**Fig. 6.5**). The pH was relatively steady throughout the experiment while the Eh vs SHE for the all the samples except for the 1 M HCl decreased in the first day after which it became steady (**Fig. 6.5a-b**). The initial decrease in Eh vs SHE was most likely due to the dissolution of some $Fe^{(III)}$-oxides, releasing ferric ions into solution, and the subsequent reduction of the ferric ions (Garrels and Thompson 1960). This is the reason why the highest initial Eh vs SHE was observed for the 1 M NaOH sample while the 1 M HCl sample saw a gradual increase until it reached a steady state. **Fig. 6.5c-d** shows that the release of arsenic and iron followed the same trend regardless of the sample or the washing condition. Generally, arsenic was released until the 8-10th day after which the reaction attained equilibrium. On the other hand, the iron dissolution reaction was completed in 4 days. Due to the unique conditions under which each sample was prepared, a direct assessment of the Fe sulfide and arsenopyrite dissolution cannot be made, therefore, the total iron and arsenic

released in the three stages of the bio-oxidation (1: CFSM treatment, 2: washing and 3: *A. brierleyi*) were computed and present in **Fig 6. 6**.

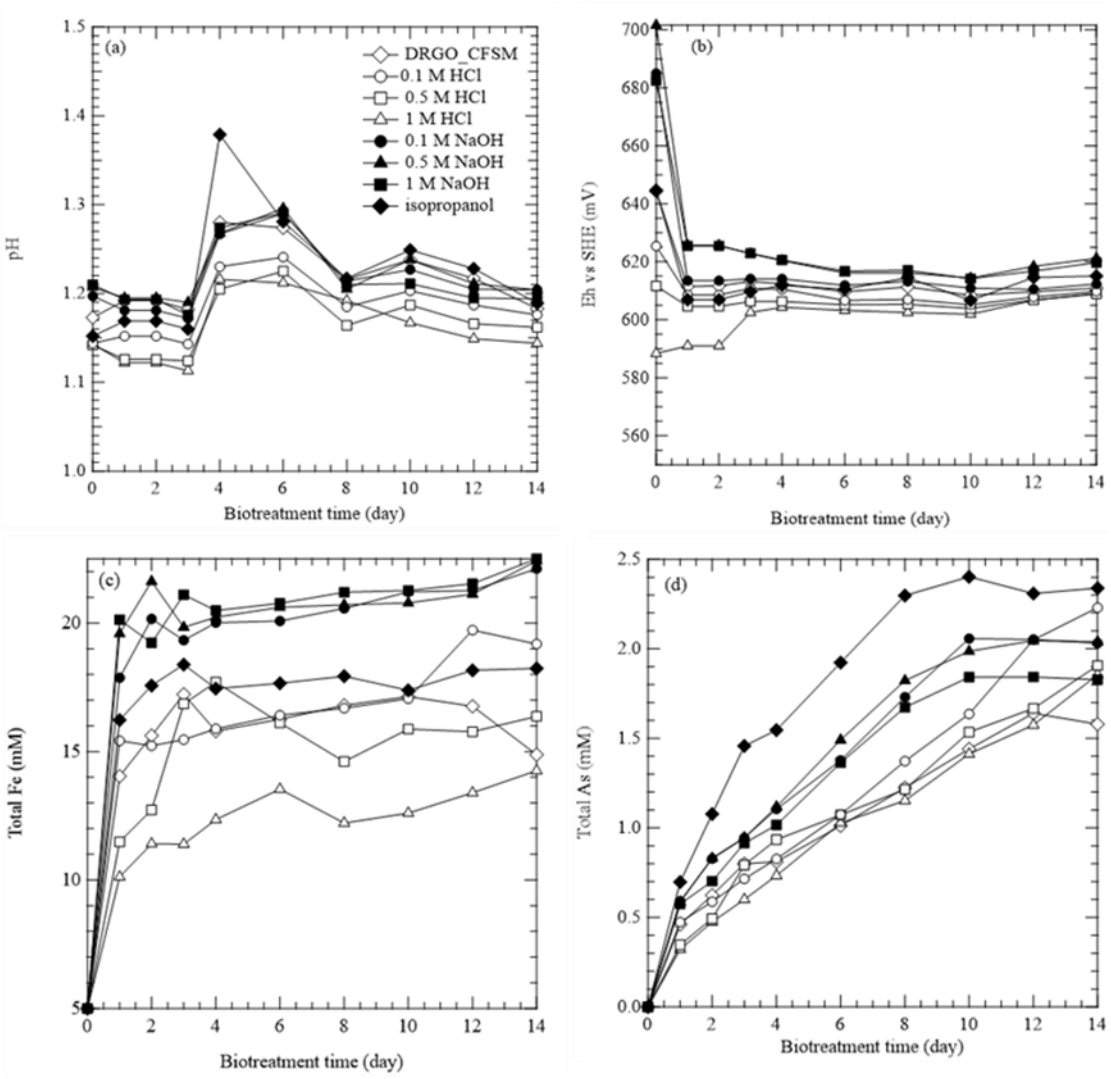

Figure 6. 5 Changes in (a) pH, (b) Eh vs SHE, (c) Fe concentrations, and (d) As concentrations with time of bio-oxidation by *A. brierleyi*. Symbols: ◊, DRGO_CFSM; ○, 0.1 M HCl; □, 0.5 M HCl; △, 1 M HCl; ●, 0.1 M NaOH; ■ ,0.1 M NaOH; ▲, 1 M NaOH and ♦, isopropanol.

Table 6. 1 CHN analysis of the as-received sample, only CFSM treatment and both CFSM and chemical washing.

Sample	C (%)	H (%)	N (%)
As-received	5.86	0.42	0.2
DRGO-CFSM	11.63	1.57	0.59
1.0 M HCl	7.93	0.84	0.39
0.5 M HCl	8.07	0.85	0.41
0.1 M HCl	8.21	0.68	0.42
1.0 M NaOH	5.95	0.64	0.22
0.5 M NaOH	6.71	0.67	0.25
0.1 M NaOH	6.35	0.66	0.27
isopropanol	7.08	0.77	0.39

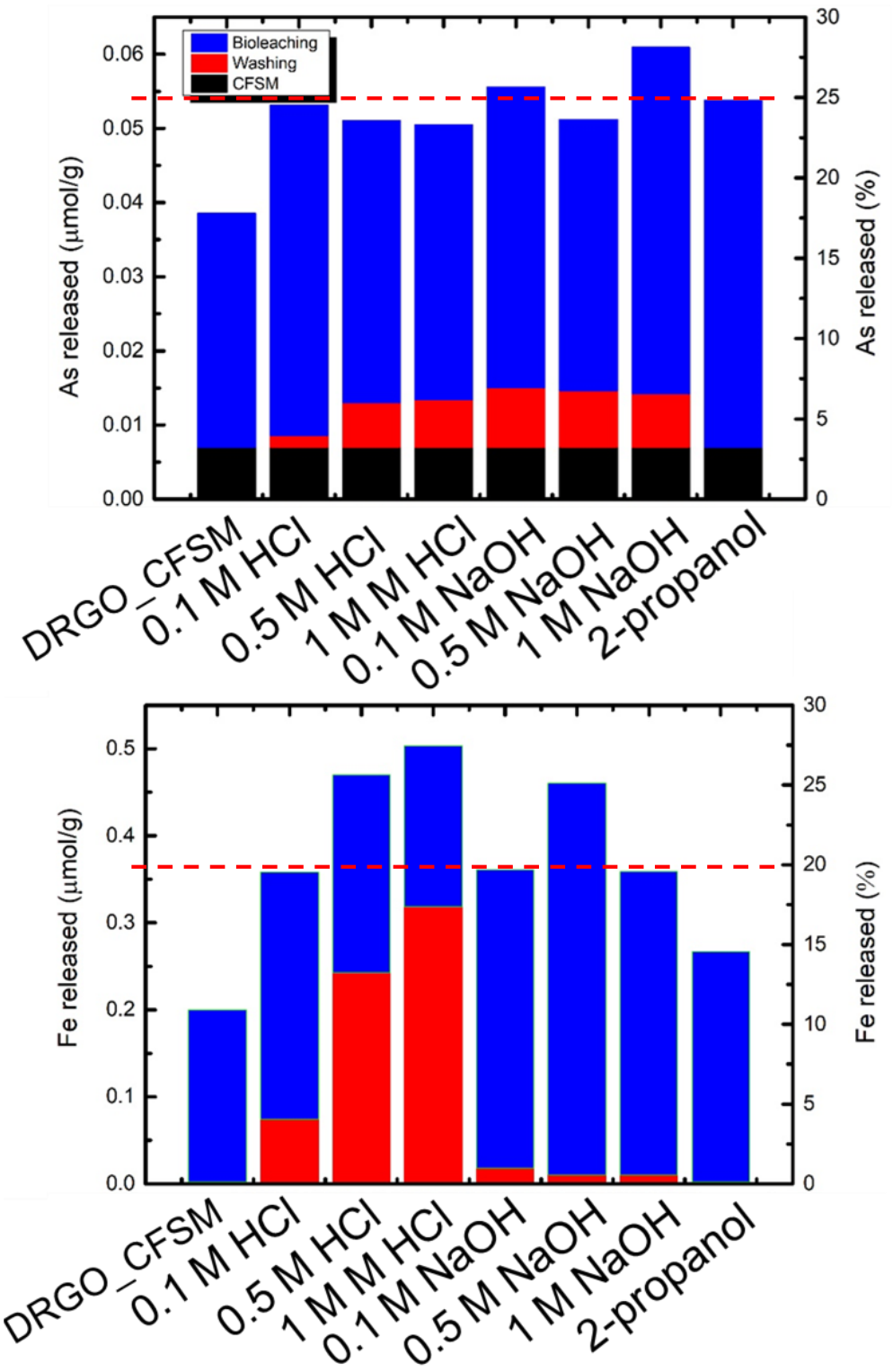

Figure 6. 6 The aggregated released As and Fe from CFSM treatment, chemical washing and bio-oxidation by *A. brierleyi*.

The results of the aggregated released Fe and As can be considered using HCl 0.1 M as a standard for comparison because the pH during acidic washing was around 1.0 which is the

most similar out of all the other samples to the pH condition used for the *A. brierleyi* treatment. As such, this condition gives the closest approximation of the pH conditions for both the washing and sulfide bio-oxidation. The total arsenic released for all three steps was very similar for all the washed sample, with the total amount varying between 23% to 28%. On the other hand, iron release for the acid and alkaline washed sample was between 20%-26%. The varying in both total dissolved Fe and As was mostly due to the chemical dissolution of Fe-oxides and some sulfides by pyrite and the alkaline precipitation of Fe-oxides from pyrite and arsenopyrite (Thomas, 2005). This result coupled with the Eh vs SHE indicates that the inhibition of *A. brierleyi* that was previously encountered for a CFSM treated sample was still in effect. This illustrates that the fungal biofilm and particulate agglomeration might not be the main factors responsible for the inhibition of *A. brierleyi*.

6.3.4 Fungal biomass inhibition of A. brierleyi

The findings in **Fig 6.6** showed that the *A. brierleyi* was still inhibited from oxidising sulfides despite the removal of some of the biofilm (**Fig 6.2)** and the decrease in particulate aggregation by the alkaline and acidic washing (**Fig 6.4**). This indicated that the most likely cause of the *A. brierleyi* inhibition was the fungal biomass which was previously identified in **Chapter 4** by TG-DTA analysis (Yu et al., 2013). While the biomass was not wholly removed by chemical washing (**Fig 6.7**), it was reduced by about 45% by the 1 M NaOH washing. However, it appears that that reduction was not enough to allow for the oxidation of the sulfides. Having determined that the biomass was the most likely cause of the ineffective sulfide oxidation by *A. brierleyi*, fluorescence in situ hybridization microscopy was used to locate the fungus DNA in relation to the ore particles (**Fig. 6.8**). The results show that the fungi specific DNA dye (fluorescein isothiocyanate) shows that the fungal biomass was spread almost uniformly

throughout the observed particles, indicating the biomass attachment was ubiquitous in all three samples. From this result, it could be concluded that the physical attachment to the mineral surface rendered the *A. brierleyi* oxidising ability obsolete similar to how sulfide oxidation efficiency decreases with the formation of secondary phase like jarosite (Sasaki et al., 1998).

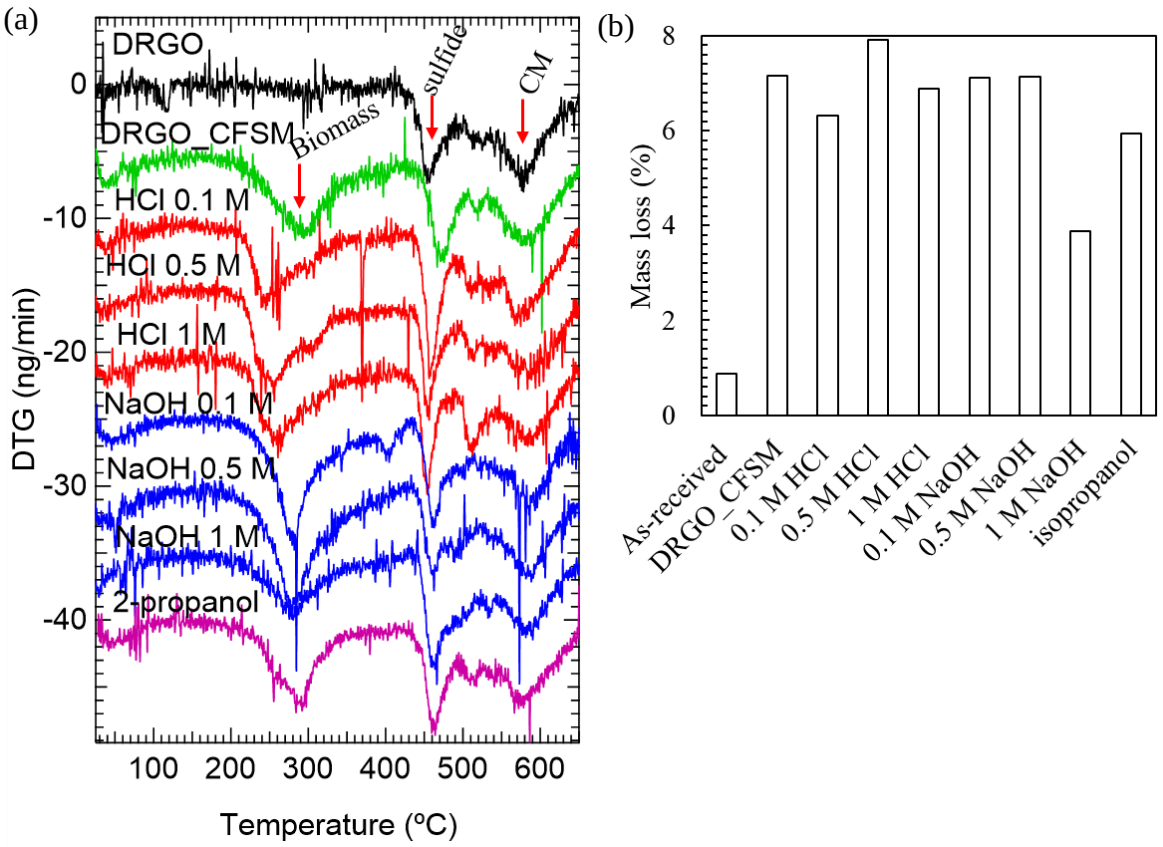

Figure 6. 7 Thermal decomposition characteristics of the as-received sample and DRGO_CFSM and washed residues showing (a) DTG and (b) mass loss between 220°C to 434°C.

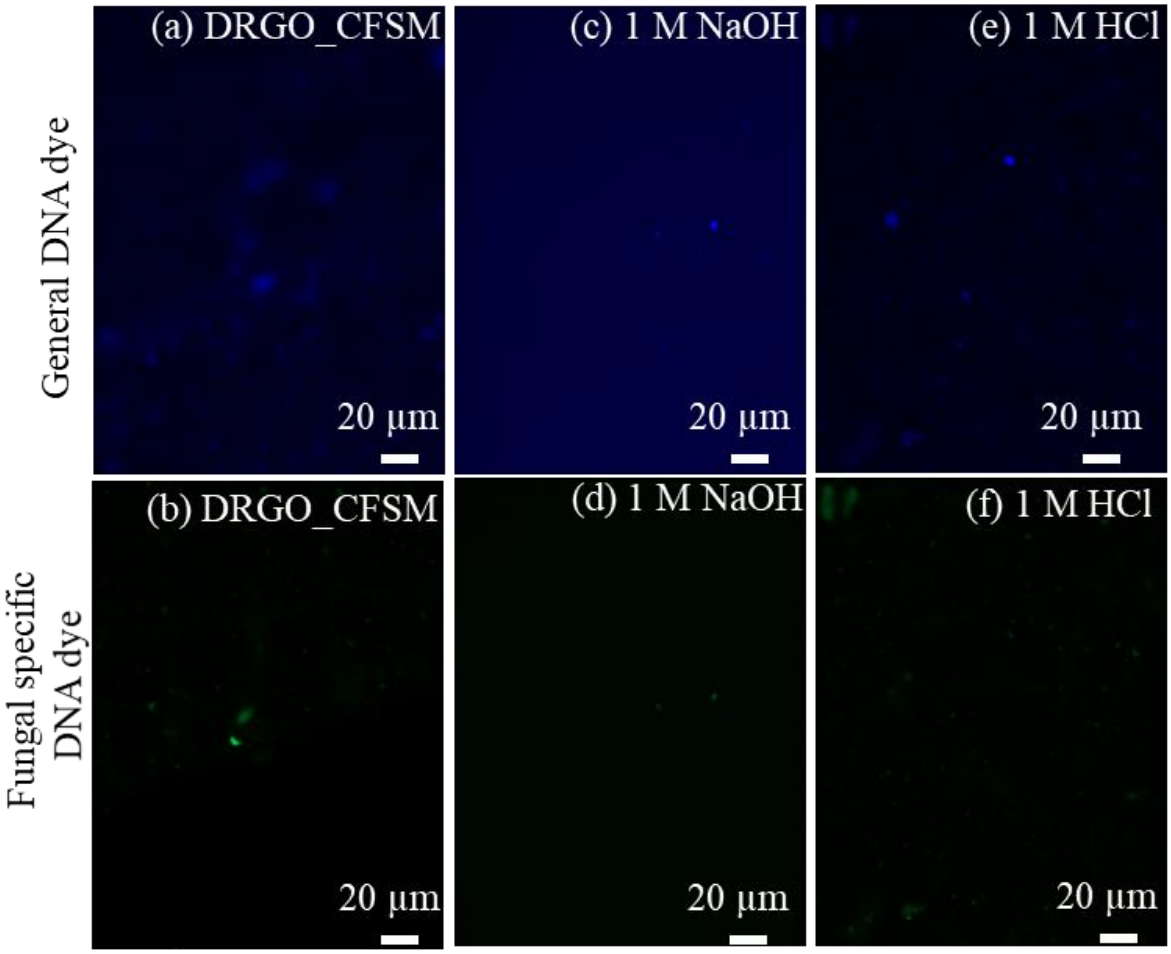

Figure 6. 8 Fluorescence microscopic observation of the fungal DNA in the (a-b) DRGO_CFSM, (c-d) I M NaOH washed solid and (e-f) I M HCl washed solid. 4',6-diamidino-2-phenylindole (DAPI) staining was used to generate the a, c and e micrographs while 18S rRNA probe staining was used to generate b, d and f. The scale bar indicates 20 µm.

The impact of only the biomass was determined by simulating the DRGO_CFSM sample through physically mixing the dry, powered biomass with the as-received sample and then pyrite oxidation was undertaken (**Fig. 6.9**). The amount of biomass in the sample varied from 0-2wt% of the added ore. The results for the pH, Eh and cell density shows that the inhibitory effect of the fungal biomass was evident above 1 wt%. It can be expected that due to the surface charge of the fungal biomass and pyrite at pH 4.0 where DRGO_CFSM was produced and the pH 1.2-1.4 where simulated DRGO_CFSM was used, the binding between the fungal biomass and the solid surface would be weaker in the simulated DRGO_CFSM (Gopal et al., 2002;

Reyes-Bozo et al., 2015). Despite this, sulfide oxidation was inhibited above 1wt% of the biomass. This finding illustrates that the fungi biomass, which is less dense compared to minerals like pyrite and arsenopyrite, was able to settle on the surface of the denser particles and restrict *A. brierleyi* access to those particles. This surrogate experiment gives an accurate view of the effect of the biomass in the real DRGO_CFSM sample because the attachment to the pyrite surface would occur in a much shorter time while the *A. brierleyi* is still acclimatising itself to the ore. Based on this result, the next goal of this work would be to decrease the fungal biomass about below 1 wt%. Although the 1 M NaOH washing was unable to decrease the biomass amount beneath this level, it shows some promise to reduce the biomass amount, and by optimising the washing conditions, the application of the CFSM treatment before sulfide bioleaching to recover Cu and Ni might be viable.

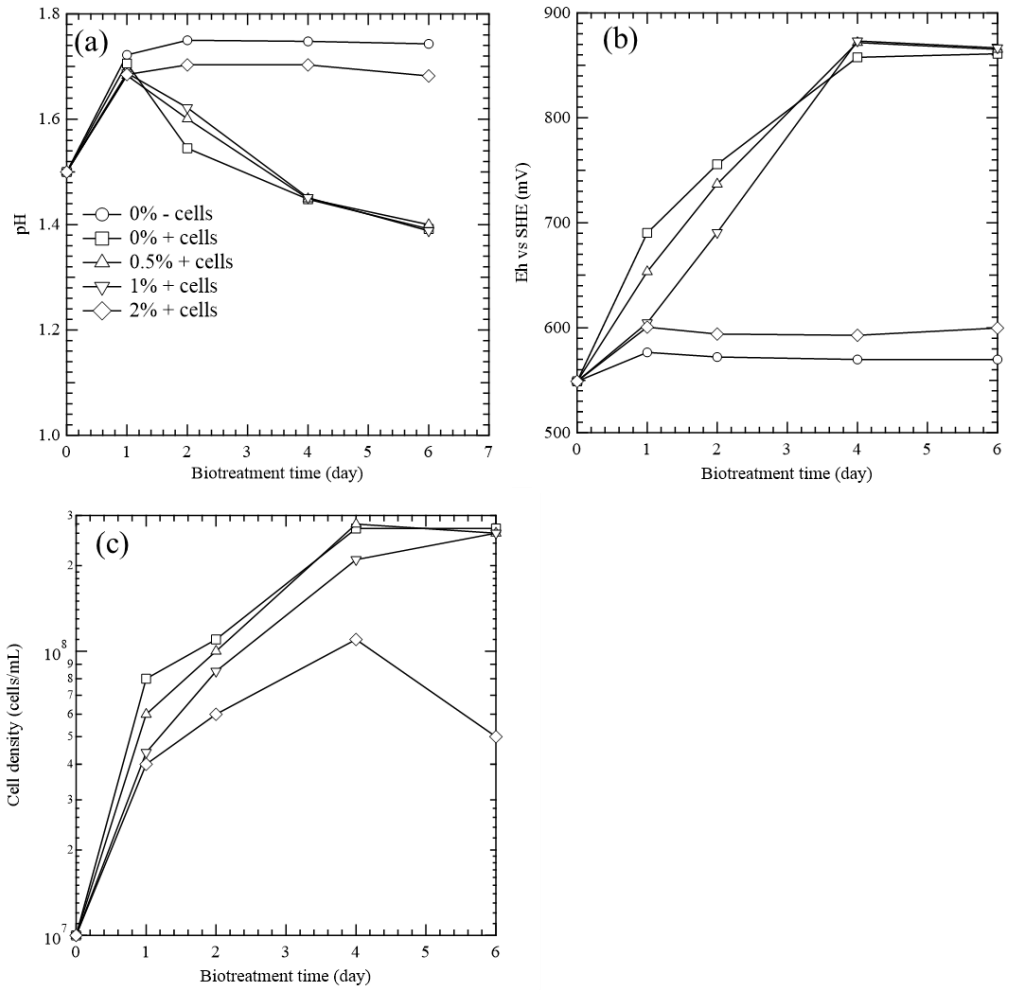

Figure 6. 9 Effect of 0-2% physically mixed *P. chrysosporium* biomass with as-received DRGO on (a) pH, (b) Eh vs SHE, and (c) cell density during bio- oxidation with *A. brierleyi*. Symbols: DRGO_CFSM; ○, 0% biomass without cell (chemical control); □, 0% biomass with cell △, 0.5% biomass with cell; ▽, 1% biomass with cell; ◊, 2% biomass with cell.

6.4 Conclusion

Chemical washing was implemented after CFSM was used to treat the carbonaceous matter in DRGO to determine the major impediment to using *A. brierleyi* to decompose the sulfides in the DRGO_CFSM residue. The results show that each treatment reduced the carbon content in the DRGO_CFSM however, the substance extracted depended on the solvent. It most likely that the NaOH removed the humic substances and hydrolysed some carbohydrates while the HCl targeted the carbohydrates, leaving behind the fungal biomass. Based on how similar the trends are for iron and arsenic dissolution despite the washing method used, it can be concluded that the major source of the impediment to the archaeon treatment is the fungal biomass. *A. brierleyi* treatment of a simulated DRGO_CFSM showed that sulfide oxidation could occur ≤ 1wt% biomass. Out of all the reagents used for washing, only 1 M NaOH reduce the biomass amount significantly, but it was not enough to get below the 1% threshold. Further study is needed to remove this component to allow for successful sequential treatment of the DRGO with CFSM and *A. brierleyi*.

References

Adams, D.J., 2004. Fungal cell wall chitinases and glucanases. *Microbiol*. 150, 2029-2035.

Bouchard, A., Hofland, G.W., Witkamp, G.J., 2007. Properties of sugar, polyol, and polysaccharide water− ethanol solutions. *J. Chem. Eng. Data*, 52, 1838-1842.

Bowman, S.M., Free, S.J., 2006. The structure and synthesis of the fungal cell wall. *Bioessays*, *28*, 799-808.

Cailteux, J.L.H., Kampunzu, A.B., Lerouge, C., Kaputo, A.K., Milesi, J.P., 2005. Genesis of sediment-hosted stratiform copper–cobalt deposits, central African Copperbelt. *J. Afr. Earth Sci.* 42,134-158.

Chen, Y., Jiang, S., Yuan, H., Zhou, Q., Gu, G., 2007. Hydrolysis and acidification of waste activated sludge at different pHs. *Water Res*. 4, 683-689.

Garrels, R.M., Thompson, M.E., 1960. Oxidation of pyrite by iron sulfate solutions. Ame. J. Sci. 258, 57-67.

Gopal, M., Pakshirajan, K., Swaminathan, T., 2002. Heavy metal removal by biosorption using *Phanerochaete chrysosporium*. *Appl. Biochem. Biotechnol*. 102, 227-237.

Hussain, S.A., Demirci, Ş., Özbayoğlu, G., 1996. Zeta potential measurements on three clays from Turkey and effects of clays on coal flotation. *J. Coll. Interf. Sci.* 184, 535-541.

Kadirvelu, K., Thamaraiselvi, K., Namasivayam, C., 2001. Adsorption of nickel (II) from aqueous solution onto activated carbon prepared from coirpith. *Sep. Purif. Technol.* 24, 497-50.

Kipton, H., Powell, J., Town, R.M., 1992. Solubility and fractionation of humic acid; effect of pH and ionic medium. *Anal. Chim. Acta*, 267, 47-54.

Latgé, J.P., 2007. The cell wall: a carbohydrate armour for the fungal cell. *Mol. Microbial.* 66, 279-290.

Liang, C.L., Xia, J.L., Zhao, X.J., Yang, Y., Gong, S.Q., Nie, Z.Y., Ma, C.Y., Zheng, L., Zhao, Y.D., Qiu, G.Z., 2010. Effect of activated carbon on chalcopyrite bioleaching with extreme thermophile *Acidianus manzaensis*. *Hydrometallurgy*, 105, 179-185.

Liu, W., Yang, H.Y., Song, Y., Tong, L.L., 2015. Catalytic effects of activated carbon and surfactants on bioleaching of cobalt ore. *Hydrometallurgy*, 152, 69-75.

Montañés, F., Olano, A., Ibáñez, E., Fornari, T., 2007. Modeling solubilities of sugars in alcohols based on original experimental data. AIChE J. 53, 2411-2418.

Nakazawa, H., Fujisawa, H., Sato, H., 1998. Effect of activated carbon on the bioleaching of chalcopyrite concentrate. *Int. J. Miner. Proc*. 55, 87-94.

Pigman, W., 1972. The carbohydrates: chemistry and biochemistry. Academic Press, 2nd ed, 569-587.

Reyes-Bozo, L., Escudey, M., Vyhmeister, E., Higueras, P., Godoy-Faúndez, A., Salazar, J.L., Valdés-González, H., Wolf-Sepúlveda, G., Herrera-Urbina, R., 2015. Adsorption of biosolids and their main components on chalcopyrite, molybdenite and pyrite: Zeta potential and FTIR spectroscopy studies. *Miner. Eng.* 78, 128-135.

Sasaki, K., Tanaike, O. and Konno, H., 1998. Distinction of Jarosite-Group Compounds by Raman Spectroscopy. *Can. Mineral*, 36, 1225-1235.

Thomas, K.G., 2005. Pressure oxidation overview. *Developments in Mineral Processing*, 15, 346-369.

Wang, M., Wang, X., 2010. Extraction of molybdenum and nickel from carbonaceous shale by oxidation roasting, sulphation roasting and water leaching. *Hydrometallurgy*, 102, 50-54.

Yu, Q., Morioka, E., Sasaki, K., 2013. Characterization of lithium ion sieve derived from biogenic Mn oxide. *Micropor. Mesopor. Mat*. 179, 122-127.

Zhang, Y., Cremer, P.S., 2006. Interactions between macromolecules and ions: the Hofmeister series. *Curr Opin. Chem. Boil.* 10, 658-663.

Zhou, Y., Zhang, Y., Li, P., Li, G., Jiang, T., 2014. Comparative study on the adsorption interactions of humic acid onto natural magnetite, hematite and quartz: effect of initial HA concentration. *Powder Technol*. 251, 1-8.

Chapter 7:

Conclusions

The implementation of a pre-treatment procedure before cyanidation has become a necessity when treating double refractory gold ores (DRGO) due to the presence of sulfides and carbonaceous matter in the ore. The difficulty encountered during the processing of DRGO results from losses due to the encapsulation of gold by sulfides and preg-robbing of the leached aurocyanide by carbonaceous matter. Therefore, pre-treatment is needed to liberate the gold from the sulfides and decrease the preg-robbing ability of the carbonaceous matter to aid in the better recovery of gold. The pre-treatment of sulfides to liberate gold has already been established and industrialized. Therefore, and attention has shifted to the pre-treatment of carbonaceous matter. One of the methods that have been researched recently is the bio-oxidative treatment of the carbonaceous matter using lignin-degrading enzymes secreted by the white-rot fungus *P. chrysosporium*. In most cases where this fungus has been applied to the treatment of DRGO recently, the effectiveness of the enzymatic approach was determined based only on the gold recovery rather than direct analysis of the carbonaceous matter transformation. Therefore, to improve the understanding of the carbonaceous matter transformation, the cell-free spent medium (CFSM) of *P. chrysosporium* was used to treat DRGO sequentially, and the alteration in the carbonaceous matter is elucidated in this thesis.

Before the CFSM could be used to oxidize the carbonaceous matter in DRGO, it was necessary to determine its effectiveness at decomposing only the carbonaceous matter in the absence of other minerals like sulfides and silicates, that are part of the DRGO. **In Chapter 3**, powdered activated carbon (PAC) was used as a surrogate for the carbonaceous matter due to its aromaticity and gold absorption ability. The CFSM treatment of PAC occurred over 14 days and TOC, FTIR and ^{13}C-NMR analysis of the liquid and solid residues found that the enzymatic treatment decomposed the aromatic C=C bonds in the PAC, resulting in the formation of smaller water-soluble organic substances. This lead to a significant decrease in the specific surface area and an increase in the number of large micron-sized pores in the bio-treated PAC.

Due to these changes in the bio-treated PAC, its gold adsorption ability decreased by 58% in 3-7 days. Between 7-14 days, a further 16% decrease was observed due to the passivation of the surface of the treated PAC by biomolecules secreted into the CFSM by the *P. chrysosporium*. Due to these two factors, the gold uptake decreased 74% in 14 days, implying that the CFSM treatment might be able to use the aromatic carbon in the DRGO as a solid substrate.

The DRGO was bio-treated sequentially with the iron-oxidizing archaea *A. brierleyi* to dissolve sulfide minerals like pyrite and arsenopyrite and the lignin-degrading enzymes in the CFSM to decompose the carbonaceous matter. In **Chapter 4**, two sequences were explored, using the *A. brierleyi* before CFSM (DAC) and vice versa (DCA), to determine which one achieved the higher gold recovery. Each sequence was evaluated using a combination of water chemistry, QEMSCAN, TG-DTA, SEM, DNA extraction and cyanidation. Pre-treating the DRGO with only *A. brierleyi* (DA) and only CFSM (DC) increased gold recovery from 24% to 77% and 38%, respectively. This was due to the inability of the CFSM to effectively breakdown the sulfides, which were the major gold-bearing minerals. When *A. brierleyi* was followed by the CFSM (DAC) and vice versa (DCA), the gold recovery was 76% and 45% respectively. The DCA sequence was judged to have been unsuccessful due to the inhibition of the *A. brierleyi* by some unspecified component of the earlier CFSM treatment. On the other hand, the CFSM step in the DAC sequence had converted the carbonaceous matter into an alkaline soluble substance which had to be removed because it was interfering in the gold leaching procedure. After 1 M NaOH washing, the gold recovery for DAC was 92%, while 60% was observed for DCA. This result indicates that the sequence utilizing the iron-oxidizing microbe before the CFSM was the ideal way to pre-treat the DRGO.

In **Chapter 5**, the transformation of the carbonaceous matter during the DAC sequence was investigated using QEMSCAN analysis. It was found that the carbonaceous matter was closely

associated with illite, and therefore, the term carbonaceous illite was coined. Additionally, it was discovered that higher carbon contents increase the porosity of the carbonaceous illite because the carbonaceous matter and illite existed as separate entities inside the mineral. The enzymatic oxidation of the carbonaceous matter in the DRGO was more extensive, if the sample had undergone a prior treatment to dissolve Fe sulfides and arsenopyrite. This is because the enzymes are susceptible to arsenic poisoning, and therefore, the dissolution of arsenopyrite improved the enzymatic reaction.

Additionally, the oxidative dissolution of the Fe sulfides and arsenopyrite in the DA step probably reduced the consumption of biogenic hydrogen peroxide in the CFSM for Fenton-like reactions. Due to this, the competition for biogenic hydrogen peroxide the between the lignin-degrading enzymes and the sulfide minerals reduced, which benefited the carbonaceous matter oxidation. Raman spectroscopy showed that the lignin-degrading enzymes preferentially attacked the defects in the graphitic structure of carbonaceous matter and in the process, produced some humic-like substances. These humic-like substances served as one of the binding agents in the formation of the carbonaceous aluminosilicate residue (C-Si-Al). This new C-Si-Al appeared to be the main product of the carbonaceous illite decomposition, and its retention of the humic substances explains why the alkaline washing step was needed to improve gold recovery from DAC from 76% to 92%. Based on the information provided in **Chapters 4** and **5**, a schematic representation of the bio-treatment procedure for the DRGO was proposed in **Fig.7.1**. The bio-treatment would follow the DAC sequence with an alkaline washing step before cyanidation. The system can be optimized by improving the enzyme production yield to increase the efficiency of the bio-treatment and investigating the possibility of using the chemically extracted humic substances as a growth substrate for the fungus. Finally, the DAC system could be applied to carbonaceous gold ores from several mining regions in the world to determine the universality of this approach to gold ore pre-treatment.

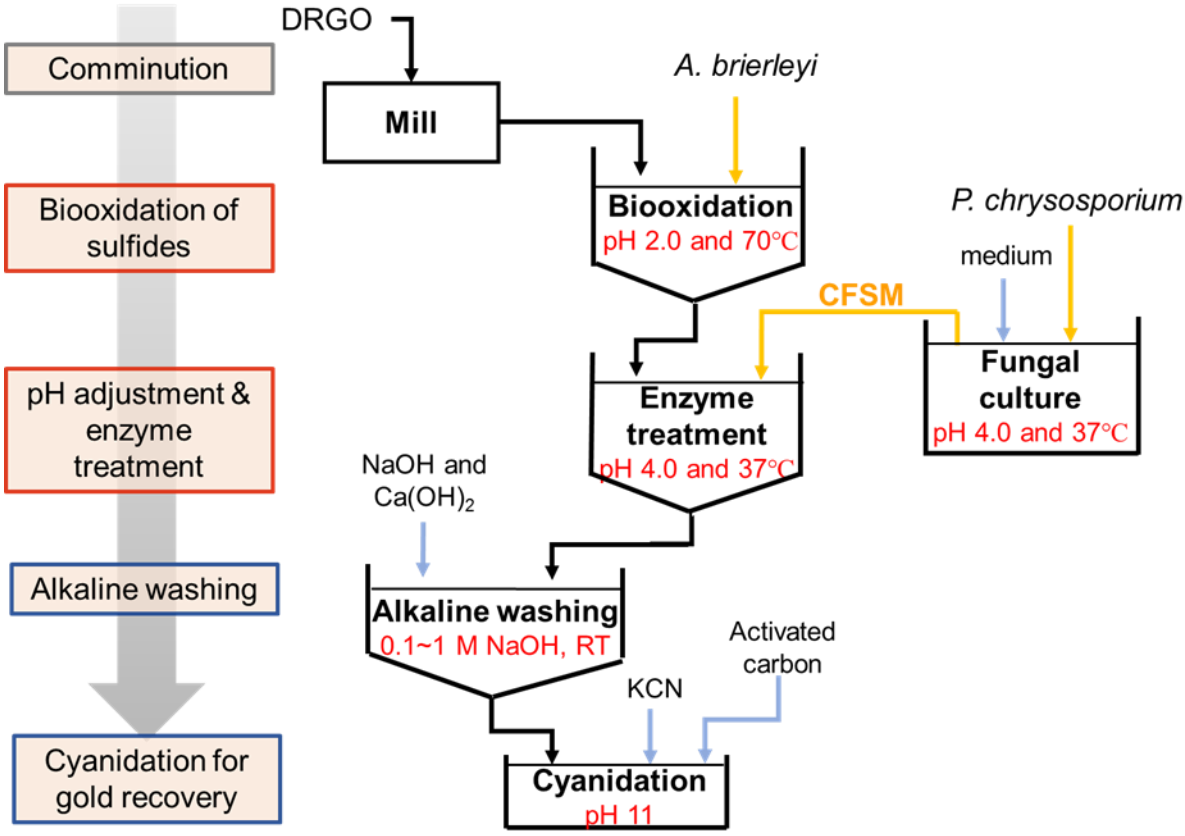

Figure 7. 1 Proposed sequential bio-treatment process for DRGO.

In **Chapter 4,** it was discovered that *A. brierleyi* was incapable of oxidizing the pyrite and arsenopyrite if it was applied after the CFSM treatment (DCA). Therefore, in **Chapter 6**, the CFSM only treated DRGO was examined to determine the main factor responsible for the inhibition of the *A. brierleyi* as a preliminary investigation into applying the enzymatic treatment to some carbonaceous base metal ores like copper or nickel sulfides. The three possible impediments to the *A. brierleyi* that were identified after the CFSM only treatment of DRGO (DC) were; (1) humic-like substances from the decomposition of the carbonaceous illite, (2) biomolecules like carbohydrates and organic acids which aided in the formation of biofilms and large agglomerates, and (3) the fungal biomass. The DC residue was chemical-washed using 0.1-1 M HCl and NaOH for 24 hrs and the solid residues of each washing solution was

analyzed by QEMSCAN and fluorescence in situ hybridization (FISH) imaging and SEM. It was discovered that washing the CFSM-treated solids with 0.1-1 M HCl or 0.1-1 M NaOH removed biofilms, broke down the aggregates and extracted the humic acids, but sulfide oxidation by *A. brierleyi* was still impeded. FISH imaging showed that the fungal biomass was still attached to some of the mineral grains in the DC sample, even after the chemical washing (alkaline and acidic). Therefore, it was concluded that the fungal biomass was the reason for the insignificant sulfide oxidation when *A. brierleyi* was used on the DC sample.

Furthermore, it was found that physically mixing more than 1wt% of biomass with the DRGO completely stopped the *A. brierleyi* from working. This indicates that the biomass was the main impediment to the *A. brierleyi*. Based on this information, the application of the DCA treatment to the carbonaceous base metal ores would not be successful without significantly reducing the amount of fungal biomass before bioleaching with *A. brierleyi*.

In the last chapter, this work is concluded. It was discovered that the CFSM treatment might be a viable way of pre-treating the DRGO to improve gold recovery. However, the sequence used for bio-treatment was critical since the fungal biomass could inhibit sulfide oxidation by *A. brierleyi*. Additionally, it provided *in situ* characterization showing the transformation of the carbonaceous matter; but, more research is needed to both optimize this pre-treatment process and further analyze its products in both the liquid and solid phases.

Acknowledgements

Firstly, I would like to express my most profound gratitude and thanks to Prof. Keiko Sasaki for all her support and advice during my five-year stay at Kyushu University. I am very happy and honored to have been her student because this opportunity has allowed me to evolve into a better researcher and individual. Through her encouragement and advice, I was introduced to the bioprocessing of double refractory gold ores. The practicality of the biohydrometallurgy and the skills, approaches and knowledge that Prof. Sasaki willing shared with me will continue to shape my life far into the future. I am also grateful for the patience and tolerance that Prof. Sasaki showed to help me adapt to my study at Kyushu University. I am eternally thankful that I have been able to study from her and will continue to apply the knowledge I gained in all applicable parts of my life.

Next, I want to express my sincere thanks to the members of my thesis committee: Prof. Hiroaka Nakano (Department of Materials Science and Engineering), Assoc. Prof. Naoko Okibe and Assoc. Prof. Hajime Miki. I am grateful for your discerning commentary about my dissertation, which helped me to improve it.

Furthermore, I would like to profoundly thank Prof. Kwadwo Osseo-Asare (Penn State University) for all the help that he freely provided to me. I am very grateful that he helped to advocate for the opportunity that brought me to Japan and then continued to mentor me after I arrived in Kyushu University. I am most grateful for all your valuable suggestions that have and will continue to influence my life. I am also grateful to Prof. Tysyoshi Hirajima for all the insightful advice that helped to improve the experience in and out of the university. To Prof. Sue Harrison (University of Cape Town), I would like to thank you and your laboratory members for being perfect hosts and collaborators in my research and showing me the sights in Cape Town. I want to thank Assit. Prof. Moriyasu Nonaka for helping with my research.

To Ms. Makiko Semba, Ms. Miwa Hirashima and Ms. Minako Matsue, I would like to thank you for all your profound help. You three helped me to settle in Japan and through your actions and consideration, I was able to conduct my research and live without being overwhelmed. I thank you very much.

Additionally, I would like to thank all the members of the mineral processing, recycling and environmental remediation laboratory past and present, who have helped and supported me and enriched my life with their friendship. These include Dr. Yusei Masaki, Dr. Masahito Tanaka, Dr. Wuhui Luo, Dr. Xiangchun Liu, Dr. Gde Pandhe Wisnu Suyantara, Dr. Paulmanickam Koilraj, Dr. Binglin GUO, Dr. Muthu Prabhu, Dr. Srinivasarao Kancharla, Dr. Intan Nurul Rizki, Dr. Santisak Kitjanukit, Dr. Chitiphon Chuaicham, Dr. Karthikeyan Sekar, Kenta Toshiyuki, Yu Takaki, Shugo Nagato, Yuta Era, Keishi Oyama, Tsubasa Oji, Quanzhi Tian, Niko Dian Pahlevi, Yoshikazu Hayashi, Yuta Kamura, Kyohei Takamatsu, Yusuke Hotta, Li Zhang, Shingou Nakama, Shunsuke Imamura, Ryohei Nishi, Haruki Noguchi, Yuta Orii, Yu Tanaka, Diego Moizes Mendoza Flores and Ryotora Sakai.

To my family, thank you for all the support and prayers that have guided me here.

Finally, I would like to thank the Green Asia Program and the JSPS DC2 (18J10835) for all the scholarship that was provided to me.